การพัฒนาอิมมูโนแอสเสย์บนอุปกรณ์ของไหลจุลภาคฐานกระดาษสำหรับการตรวจวัดแรกโทพา
มีน แอลฟาฟีโตโปรตีน ฮอร์โมนกระตุ้นต่อมไทรอยด์มนุษย์

นางสาวภัทรชยา ปรีชาเกษตรกิจ

วิทยานิพนธ์นี้เป็นส่วนหนึ่งของการศึกษาตามหลักสูตรปริญญาวิทยาศาสตรดุษฎีบัณฑิต
สาขาวิชาเทคโนโลยีชีวภาพ
คณะวิทยาศาสตร์ จุฬาลงกรณ์มหาวิทยาลัย
ปีการศึกษา 2560

DEVELOPMENT OF IMMUNOASSAY ON PAPER-BASED MICROFLUIDIC DEVICES FOR DETERMINATION OF RACTOPAMINE, ALPHA-FETOPROTEIN, HUMAN THYROID STIMULATING HORMONE

Miss Pattarachaya Preechakasedkit

A Dissertation Submitted in Partial Fulfillment of the Requirements
for the Degree of Doctor of Philosophy Program in Biotechnology
Faculty of Science
Chulalongkorn University
Academic Year 2017

Thesis Title	DEVELOPMENT OF IMMUNOASSAY ON PAPER-BASED MICROFLUIDIC DEVICES FOR DETERMINATION OF RACTOPAMINE, ALPHA-FETOPROTEIN, HUMAN THYROID STIMULATING HORMONE
By	Miss Pattarachaya Preechakasedkit
Field of Study	Biotechnology
Thesis Advisor	Professor Dr.Orawon Chailapakul
Thesis Co-Advisor	Associate Professor Dr.Nattaya Ngamrojanavanich
	Assistant Professor Dr.Nanthika Khongchareonporn

Accepted by the Faculty of Science, Chulalongkorn University in Partial Fulfillment of the Requirements for the Doctoral Degree

.....Dean of the Faculty of Science
(Associate Professor Dr.Polkit Sangvanich)

THESIS COMMITTEE

.....Chairman
(Associate Professor Dr.Vudhichai Parasuk)

.....Thesis Advisor
(Professor Dr.Orawon Chailapakul)

.....Thesis Co-Advisor
(Associate Professor Dr.Nattaya Ngamrojanavanich)

.....Thesis Co-Advisor
(Assistant Professor Dr.Nanthika Khongchareonporn)

.....Examiner
(Associate Professor Dr.Kittinan Komolpis)

.....Examiner
(Associate Professor Dr.Polkit Sangvanich)

.....External Examiner
(Associate Professor Dr.Weena Siangproh)

ภัทรชยา ปรีชาเกษตรกิจ : การพัฒนาอิมมูโนแอสเสย์บนอุปกรณ์ของไหลจุลภาคฐานกระดาษสำหรับการตรวจวัดแรกโทพามีน แอลฟาฟีโตโปรตีน ฮอร์โมนกระตุ้นต่อมไทรอยด์มนุษย์ (DEVELOPMENT OF IMMUNOASSAY ON PAPER-BASED MICROFLUIDIC DEVICES FOR DETERMINATION OF RACTOPAMINE, ALPHA-FETOPROTEIN, HUMAN THYROID STIMULATING HORMONE) อ.ที่ปรึกษาวิทยานิพนธ์หลัก: ศ. ดร.อรวรรณ ชัยลภากุล, อ.ที่ปรึกษาวิทยานิพนธ์ร่วม: รศ. ดร.นาตยา งามโรจนวณิชย์, ผศ. ดร.นันทิกา คงเจริญพร, 118 หน้า.

วิทยานิพนธ์นี้เป็นการพัฒนาอิมมูโนแอสเสย์บนอุปกรณ์ของไหลจุลภาคฐานกระดาษโดยใช้ตัวติดฉลากต่างชนิดสำหรับการประยุกต์ที่หลากหลายในด้านความปลอดภัยทางการเกษตรและการวินิจฉัยโรค ซึ่งสามารถแบ่งได้เป็น 3 ส่วน ส่วนแรกเป็นการพัฒนาวิธีการเชื่อมต่อระหว่างแรกโทพามีนกับพาหะโปรตีนเพื่อใช้สร้างแถบทดสอบแบบไหลตามแนวราบฐานกระดาษของแรกโทพามีนโดยใช้อนุภาคนาโนทองคำเป็นตัวติดฉลาก วิธีการเชื่อมต่อที่พัฒนาขึ้นเป็นวิธีที่ง่ายและขั้นตอนเดียว ใช้สารเคมีน้อย แถบทดสอบสำหรับตรวจวัดแรกโทพามีนในอาหารสัตว์ให้ค่าความเป็นเส้นตรงที่ 0.075-0.750 นาโนกรัมต่อกรัม และให้ขีดจำกัดการตรวจวัดที่ 0.1 นาโนกรัมต่อกรัม ในส่วนที่สองเป็นการพัฒนาอุปกรณ์แบบไหลตามแนวราบฐานกระดาษที่พิมพ์แวกซ์โดยใช้เอนไซม์เป็นตัวติดฉลากสำหรับการตรวจวัดแอลฟาฟีโตโปรตีนในซีรัมมนุษย์โดยการหยอดตัวอย่างเพียงครั้งเดียว อุปกรณ์ที่เสนอภายใต้ภาวะที่เหมาะสมสามารถใช้ตรวจวิเคราะห์แอลฟาฟีโตโปรตีนด้วยขีดจำกัดการตรวจวัดที่ 1 นาโนกรัมต่อมิลลิลิตร และค่าความเป็นเส้นตรงที่ 1-100 นาโนกรัมต่อมิลลิลิตร ในส่วนที่สามเป็นการพัฒนาอิมมูโนแอสเสย์แบบไหลตามแนวราบสำหรับฮอร์โมนกระตุ้นต่อมไทรอยด์มนุษย์โดยใช้ตัวติดฉลากเรืองแสงชนิดใหม่ ไฮบริดนาโนคอมโพสิตของทองอนุภาคนาโนเมตรและสารเรืองแสงยูโรเปียมโดปซิลิกาถูกสังเคราะห์และใช้เป็นตัวติดฉลากเรืองแสงชนิดใหม่ที่ให้การอ่านสัญญาณสองแบบผ่านสัญญาณเชิงสีและสัญญาณเรืองแสง ขีดจำกัดการตรวจวัดที่ 0.1 ไมโครยูนิตต่อมิลลิลิตรของสัญญาณเรืองแสงด้วยช่วงความเป็นเส้นตรงที่ 0.05-50 ไมโครยูนิตต่อมิลลิลิตรให้ขีดจำกัดการตรวจวัดต่ำกว่าสัญญาณเชิงสี (5 ไมโครยูนิตต่อมิลลิลิตร) 50 เท่า ซึ่งสามารถใช้ในการคัดกรองทั้งภาวะไทรอยด์ฮอร์โมนต่ำและภาวะไทรอยด์ฮอร์โมนสูงในซีรัมมนุษย์ได้ ผลการศึกษาข้างต้นอธิบายได้ว่าอุปกรณ์ที่นำเสนอโดยใช้ตัวติดฉลากต่างชนิดกันนั้นให้การตรวจวิเคราะห์ที่ง่ายและรวดเร็ว พกพาได้ มีความไวและความจำเพาะสูง แม่นยำ ทำซ้ำได้ และราคาถูก

สาขาวิชา เทคโนโลยีชีวภาพ ลายมือชื่อนิสิต .....

ปีการศึกษา 2560 ลายมือชื่อ อ.ที่ปรึกษาหลัก .....

ลายมือชื่อ อ.ที่ปรึกษาร่วม .....

ลายมือชื่อ อ.ที่ปรึกษาร่วม .....

5572851423 : MAJOR BIOTECHNOLOGY

KEYWORDS: IMMUNOASSAY / PAPER-BASED MICROFLUIDIC DEVICES / RACTOPAMINE / ALPHA-FETOPROTEIN / HUMAN THYROID STIMULATING HORMONE

PATTARACHAYA PREECHAKASEDKIT: DEVELOPMENT OF IMMUNOASSAY ON PAPER-BASED MICROFLUIDIC DEVICES FOR DETERMINATION OF RACTOPAMINE, ALPHA-FETOPROTEIN, HUMAN THYROID STIMULATING HORMONE. ADVISOR: PROF. DR.ORAWON CHAILAPAKUL, CO-ADVISOR: ASSOC. PROF. DR.NATTAYA NGAMROJANAVANICH, ASST. PROF. DR.NANTHIKA KHONGCHAREONPORN, 118 pp.

In this dissertation, immunoassays on paper-based microfluidic devices have been developed using different types of label for various applications in agriculture safety and medical diagnosis, which can be divided into three parts. In the first part, the conjugation method of ractopamine (RAC) and protein carrier is developed for fabricating paper-based lateral flow strip test of RAC using gold nanoparticles (AuNPs) as a label. The developed conjugation method provided a simple and one-step method with the use of less chemicals. The strip test for RAC determination in animal feed offers a linearity of 0.075-0.750 ng g^{-1} and a limit of detection (LOD) of 0.1 ng g^{-1}. In the second part, a wax-printed paper-based lateral flow device using enzyme label is developed to determine alpha-fetoprotein (AFP) in human serum by one-step sample loading. The proposed devices under the optimal conditions can be used for the AFP determination with the LOD of 1 ng mL^{-1} and a linearity of 1-100 ng mL^{-1}. In the third part, the lateral flow immunoassay of human thyroid stimulating hormone (hTSH) is developed using a novel fluorescent label. The hybrid nanocomposite of the AuNPs and fluorophores of europium (III) doped silica (AuNPs@SiO_2-Eu^{3+}) was synthesized and used as the novel fluorescent label with dual signal readout through a colorimetric and a fluorescent signals. The LOD of 0.1 μIU mL^{-1} of the fluorescent signal with a linear range of 0.05-50 μIU mL^{-1} provided 50-fold lower than the LOD of colorimetric signal (5 μIU mL^{-1}), which could be used for screening both hypothyroidism and hyperthyroidism in human serum. The above results demonstrate that the proposed devices using different types of label provide simple and rapid analysis, portability, high sensitivity and specificity, precision, reproducibility and low cost.

Field of Study: Biotechnology

Academic Year: 2017

Student's Signature .....

Advisor's Signature .....

Co-Advisor's Signature .....

Co-Advisor's Signature .....

ACKNOWLEDGEMENTS

Firstly, I would like to sincerely acknowledge to my advisor, Professor Dr. Orawon Chailapakul. This dissertation would not be possible without her advice, support, kind encouragement and motivation. Under her guidance, I could successfully overcome many difficulties and receive various experiences during Ph.D. program. It has been an honor to be her Ph.D. student.

I am also sincerely thankful to my co-advisor, Associate Professor Dr. Nattaya Ngamrojnavanich for providing important advice and always giving the kind encouragement. My deepest acknowledgement goes to my co-advisor, Assistant Professor Dr. Nanthika Khongchareonporn, who has generally offered her time and encouragement in guiding me through the research process and revising my manuscript.

I am truly grateful to Professor Dr. Kwanwoo Shin and Professor Dr. Oh-Sun Kwon from Sogang University for giving me the internship opportunities and excellent experience throughout 4 months in South Korea. I also sincerely acknowledge Professor Dr. Koji Suzuki and Professor Dr. Daniel Citterio from Keio University for leading me to work on the exciting projects, revising my manuscript and giving me the great opportunities during 9 months in Japan.

I especially would like to thank my dissertation examination committees, Associate Professor Dr. Vudhichai Parasuk, Associate Professor Dr. Polkit Sangvanich and Associate Professor Dr. Kittinan Komolpis, who gave helpful comments and advice in this dissertation. My sincere appreciation is also extended to the external committee member, Associate Professor Dr. Weena Siangproh, for her suggestions and manuscript revision.

I gratefully acknowledge the financial support from the Thailand Research Fund (TRF) through the International Research Network (PHD58W0001) and the 90th Anniversary of Chulalongkorn University Fund (Ratchadaphiseksomphot Endowment Fund).

CONTENTS

Page

Page

Page

Page

Page

LIST OF TABLES

LIST OF FIGURES

LIST OF ABBREVIATIONS

µg	microgram
µIU	microunit
µL	microliter
1°Ab	primary antibody
2 °Ab	secondary antibody
Ab	antibody
AFP	alpha-fetoprotein
Ag	antigen
ALP	alkaline phosphatase
APTES	(3-aminopropyl)triethoxysilane
AuNPs	gold nanoparticles
BCIP	5-bromo-4-chloro-3'-indolyphosphate
BSA	bovine serum albumin
BTBCT	4'-Bis(1",1",1"-trifluoro-2",4"-butanedione-6"-yl)-chlorosulfo-o-terphenyl
C	control
CF	cellulose fiber
CLB	clenbuterol
CMYK	cyan, magenta, yellow and black
DLS	dynamic light scattering
DNA	deoxyribonucleic acid
EDC	1-ethyl-3-(3-dimethylaminopropyl)-carbodiimide
ELISA	enzyme-linked immunosorbent assay
eq	equation

Eu^{3+}	europium (III)
g	g-force
g	gram
GAM	goat-antimouse IgG
GC-MS	gas chromatography-mass spectrometry
GF	glass fiber
h	hour
HPLC	high performance liquid chromatography
HRP	horseradish peroxidase
hTSH	human thyroid stimulating hormone
IgG	immunoglobulin G
K	equilibrium constant
LFIA	lateral flow immunoassay
LOD	limit of detection
LOQ	limit of quantitation
LSPR	localized surface plasmon resonance
M	molar
mAb	monoclonal antibody
MeOH	methanol
MES	2-(N-morpholino)ethanesulfonic acid
mg	milligram
min	minute
mL	milliliter
mM	millimolar
mm	millimeter
m-PEG-SH	O-[2-(3-mercaptopropionyl-amino)ethyl]-O'-methylpolyethylene glycol

MRL	maximum residue limit
NaCl	sodium chloride
NBT	nitro-blue tetrazolium
NCM	nitrocellulose membrane
NE	norepinephrine
ng	nanogram
NHS	N-hydroxysuccinimide
nm	nanometer
°C	degree Celsius
OVA	ovalbumin
pAb	polyclonal antibody
PBS	phosphate buffer saline
PHE	phenylephrine
p-NPP	*p*-nitrophenyl phosphate
R^2	coefficient
RAC	ractopamine
RBG	red, blue and green
RNA	ribonucleic acid
rpm	round per minute
RSD	relative standard deviation
SAL	salbutamol
SD	standard deviation
SER	surface-enhanced Raman scattering
SiO_2	silica
T	test
TEM	transmission electron microscopy
TEOH	tetraethyl orthosilicate (TEOS)

TER	terbutaline
THPMP	3-(trihydroxysilyl)propylmethyl phosphonate
TMB	3,3’,5,5’-tetramethylbenzidine
UV-vis	UV-visible
v/v	volume by volume
w/v	weight by volume

CHAPTER I

INTRODUCTION

1.1 Introduction

In the past decades, the global risks for worldwide mortality have been significantly occurred from agriculture and food contaminants, human diseases and environmental pollutions. The analytical techniques, that can rapidly and easily determine contaminants and/or biomarkers, are an essential and important approach for agriculture and food safety, medical diagnosis and environmental monitoring. Normally, the analytical techniques can be divided into confirmation methods such as high performance liquid chromatography (HPLC) [1] and gas chromatography-mass spectrometry (GC-MS) [2], and a screening method such as an immunoassay [3, 4]. Unfortunately, the confirmation methods exhibit the drawbacks in long analysis time, expensive instruments, high volume of chemicals and the requirement of highly qualified personnel. The immunoassay as the screening method is an alternative approach for the detection of contaminants and/or biomarkers.

The immunoassay is an analytical technique based on the specific binding reaction between an antibody and an analyte called an antigen. The immunoassay has been widely applied in agriculture and food safety, medical diagnosis and environmental monitoring due to its high sensitivity and selectivity. Typically, a traditional immunoassay called the enzyme-linked immunosorbent assay (ELISA) is the measurement of the analyte in a 96-microwell plate requiring a multistep procedure of mixing, washing, and incubation. This technique has some disadvantages including complicated steps, long analysis time and the use of instrument for data analysis [5]. The combination of the immunoassay and the paper-based microfluidic devices for

reducing complicated steps and analysis time is an interesting method to overcome the limitations of the conventional ELISA [6].

Currently, the paper-based microfluidic devices have attractively become as analytical tools for various applications due to their rapid test, ease of use, low consumption of reagent and sample, portability, disposability, instrument free, low cost and on-site measurement. For the fabrication of patterns on the paper-based materials, various fabrication methods have been reported including photolithograpy [7], inkjet printing [8], wax printing [9] and wax-screen printing [10]. Among the fabrication methods, wax printing displays an attractive method due to the rapid and simple fabrication. In addition, the pattern can be easily designed through computer software. In the selection of the paper-based material, the NCM has popularly used as the material in the immunoassay application due to its high protein-binding capability, smooth surface, and uniform pore size. The detection method of the immunoassay on the paper-based microfluidic devices is commonly based on a colorimetric assay using metal, enzyme or fluorescent labels.

The immunoassay on the paper-based microfluidic devices was originally prepared using the most popular metal label of gold nanoparticles (AuNPs) [11]. The use of AuNPs as label has advantages in term of instrument-free measurement and long-term stability. In addition, various sizes of the AuNPs have been attracted for several applications. However, the use of AuNPs has a limitation of low sensitivity compared to the other labels. In case of the enzyme label, there are two popular types including alkaline phosphatase (ALP) [12] and horseradish peroxidase (HRP) [13]. Although the use of the enzyme label provides the advantage of high sensitivity, the colorimetric signal of the enzyme label cannot be exported itself. The addition of a substrate solution is also required, for instance, 5-bromo-4-chloro-3'-indolyphosphate and nitro-blue tetrazolium (BCIP/NBT) [6] for the ALP and 3,3',5,5'-tetramethylbenzidine (TMB) [14] for the HRP. Consequently, the paper-based

microfluidic devices using the enzyme label still require complicated steps of a sample loading on the device until the reaction completion, a washing step for removing the unbounded substances, and the device immersion in the substrate solution for the colorimetric signal evaluation. Therefore, the development of an automated paper-based microfluidic devices using the enzyme label is an interesting approach to be easy to use and fast analysis. Beside the metal and the enzyme labels, the fluorescent label has presently been popular in many immunoassay applications because of its attractive advantage of very low sensitivity which is suitable for the early stage monitoring of contaminants and biomarkers. The various fluorescent labels called fluorophores have been reported to be used in the immunoassay, for example, a quantum dot [15], a europium [16] and a lanthanide [17]. To use the fluorescent label, the emission fluorescent signal can be easily evaluated by the excitation light using a low-cost UV lamp.

Normally, the colorimetric and fluorescent signals of the immunoassay on the paper-based microfluidic devices can be respectively identified by the naked eyes and through the low-cost UV lamp indicating only yes/no response in a qualitative analysis. To improve capability of the colorimetric and fluorescent assays, a quantitative analysis is required for the assessment of the acute amount of the analyte in the sample. The quantitative analysis using image capturing tools and computer software has been attractively applied in the paper-based microfluidic devices [18]. This quantitative analysis can be easily performed using only two steps including the image capturing using a scanner or a smart phone or a digital camera and the data analysis using computer software such as Adobe Photoshop or ImageJ. The advantages of this quantitative analysis are rapidness, inexpensive instrument, ease of use and on-site measurement.

1.2 The objectives of this research

This research comprises of three aims for the development:

1. To develop a conjugation method of ractopamine (RAC) and protein carrier and apply for the fabrication of the immunoassay on the paper-based microfluidic devices using the AuNPs as a label for the RAC determination in animal feed.

2. To develop the paper-based microfluidic devices as an automated ELISA using a wax-printing method for alpha-fetoprotein (AFP) determination in human serum.

3. To develop the immunoassay on the paper-based microfluidic devices for screening thyroid diseases in human serum using a novel fluorescent label.

1.3 Scope of this research

For the achievement of the objectives, the scopes of this research are listed as below:

1. The conjugation of RAC and protein carrier was developed based on the Mannich reaction with one step, simplicity, rapidness and less chemicals requirement. The RAC-protein carrier was applied to fabricate the immunoassay on the paper-based microfluidic devices for RAC detection. The parameters, including the concentration of monoclonal antibody (mAb) conjugated to the AuNPs and the concentration of RAC-protein carrier immobilized at test line, were optimized. The immunological response of the novel RAC-protein carrier and the sensitivity of RAC detection in animal feed were analyzed using the fabricated device.

2. The paper-based microfluidic devices as the automated ELISA were fabricated using the wax-printing method. The required design of the delayed barrier was directly wax-printed on the NCM. The parameters affected to the assay were optimized such as the concentration of the immobilized antibody, the ratio of the

enzyme-labeled antibody and the ratio of the substrate. The developed device was used to detect AFP in human serum.

3. A hybrid nanocomposite of gold nanoparticles and fluorophores of europium (III) doped silica (AuNPs@SiO_2-Eu^{3+}) was synthesized as the novel fluorescent label. The obtained hybrid nanocomposite was used to fabricate the immunoassay on the paper-based microfluidic devices for the improvement of hTSH detection. The number of layers of a 3-aminopropyltriethoxysilane (*APTES*)-conjugated 4,4'-bis(1",1",1"-trifluoro-2",4"-butanedione-6"-yl)-chlorosulfo-o-terphenyl (BTBCT) europium (III) chelate (APTES-BTBCT-Eu^{3+}) were optimized to achieve an appropriate fluorescent signal. Control and the test lines on the devices were alternatively fabricated through a low-cost ballpoint pen mounted in the cutting machine. The devices were applied to determine hTSH in human serum for screening both hypo- and hyperthyroidism.

There are six chapters in this dissertation. Chapter I is the introduction. Chapter II is the theory of the immunoassay, the paper-based microfluidic devices, the labels for the immunoassay and the quantitative colorimetric assay. Chapter III presents the immunoassay on the paper-based microfluidic devices for the determination of RAC. Chapter IV reports on the development of the paper-based microfluidic devices as an automated ELISA. Chapter V presents the development of the immunoassay on the paper-based microfluidic devices using a novel fluorescent label. Finally, chapter VI is the conclusions and future perspectives.

CHAPTER II

THEORY

2.1 Immunoassay [19-21]

An immunoassay is an analytical technique for the measurement of target analytes depending on a specific binding reaction between an antibody (Ab) and a target antigen (Ag). Therefore, the Ab and the Ag are the major components in the immunoassay. The Ab, also called an immunoglobulin, is a large Y-shape protein produced by B lymphocytes of white blood cells. The Ab against a target analyte is obtained by immunizing an animal with the target analyte. The target analyte that can produce the Ab and can bind the Ab is called the Ag. The basic molecule of the immunoglobulin consists of two heavy chains and two light chains. The Ab can be divided into a monoclonal antibody (mAb) and a polyclonal antibody (pAb). The production of the pAb is done by immunizing an animal with the Ag. This induces the B lymphocytes to produce the immunoglobulins, and the pAb is purified from serum of the animal. Normally, the pAb can bind different epitopes of the Ag. In case of the mAb, after immunizing the animal with the Ag, a single clone of B lymphocytes is then selected and fused with a myeloma cell to form the hybridized cell called a hybridoma cell. The hybridoma cell can indefinitely grow in a suitable cell culture medium, and the single clone of the hybridoma cell can produce the mAb that specifically recognizes a single epitope of the Ag. Therefore, the mAb is often applied in the immunoassay because it provides higher specificity than the pAb.

The specific combination between the Ab and the target Ag is similar to the binding of an enzyme to its substrate and involves hydrophobic and electrostatic interaction. The stability of the bonding between the Ag and the Ab is based on the

complementary shape of the Ag and the binding site of the Ab. Due to the relative weakness of the forces held the Ab and the Ag together, these combinations are reversible, and the complex can dissociate depending on the strength of the binding.

$$Ag + Ab \rightleftharpoons AgAb \qquad \text{(Equation 2.1)}$$

As shown in equation 2.1, when the binding is strong, the equilibrium is located to the right. On the other hand, the equilibrium is located to the left when the binding is weak. The strength of the binding between the Ab and the Ag is referred to as its affinity and is defined by the equilibrium constant (*K*) as shown in equation 2.2.

$$K = [AgAb]/[Ag][Ab] \qquad \text{(Equation 2.2)}$$

Two general systems of the immunoassay can be basically separated including competitive and sandwich immunoassays

2.1.1 Competitive immunoassay

A competitive immunoassay is suitable for the detection of small molecules which the binding site is not enough to capture by two molecules of the Abs. The competitive immunoassay is based on the competition of two Ags to bind at the same free binding sites of the Ab. One of the two Ags consists of the Ag conjugated to a label called a labeled Ag, while the other is the similar Ag without the label called an unlabeled Ag. Therefore, the competitive immunoassay requires the labeled Ag, the unlabeled Ag and the Ab that specifically binds to its Ag (Figure 2.1).

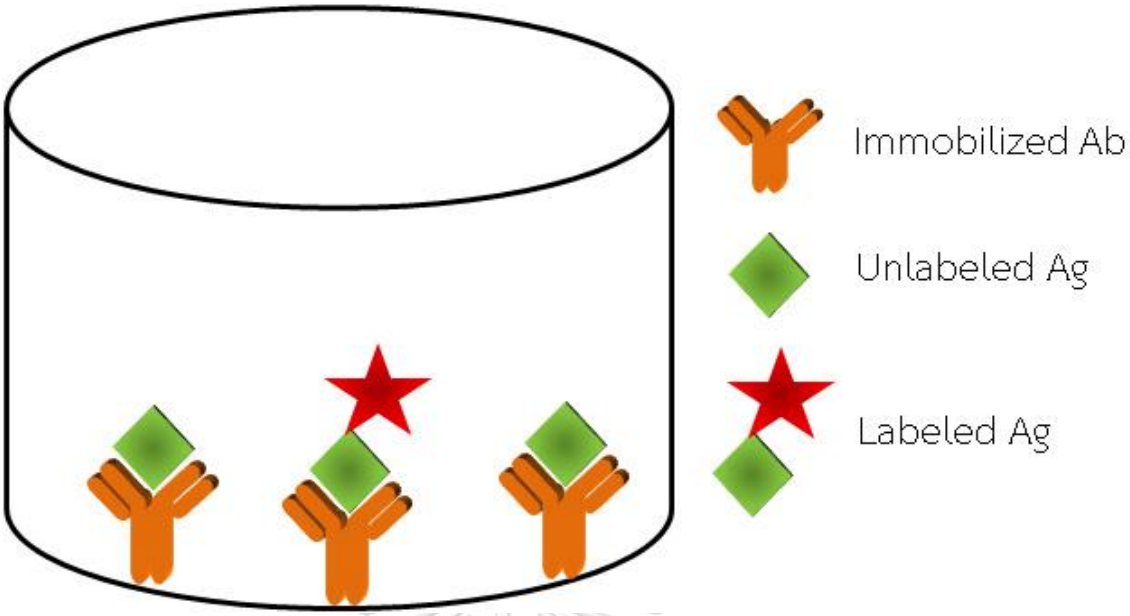

Figure 2.1 Illustration of the competitive immunoassay [21]

The quantity of the unlabeled Ag in the solution can be determined when the concentration of the Ab, the concentration of the labeled Ag and the sample volumes in all starting solutions are steady. Briefly, the Ab is immobilized onto the surface of materials such as a polystyrene plate and a nitrocellulose membrane called an immobilized Ab. Unbound substances can be removed by washing solution. The immobilized Ab is then incubated with the unlabeled Ag. After the reaction is allowed to reach equilibrium, the labeled Ag is added. The labeled Ag binds with the immobilized Ab wherever its binding sites are not already occupied by the unlabeled Ag. Therefore, a high concentration of the unlabeled Ag in the sample exhibits a weak label signal.

Figure 2.2 shows a typical standard curve of the competitive immunoassay. The concentration of the unlabeled Ag increases leading to the decrease of the label signal.

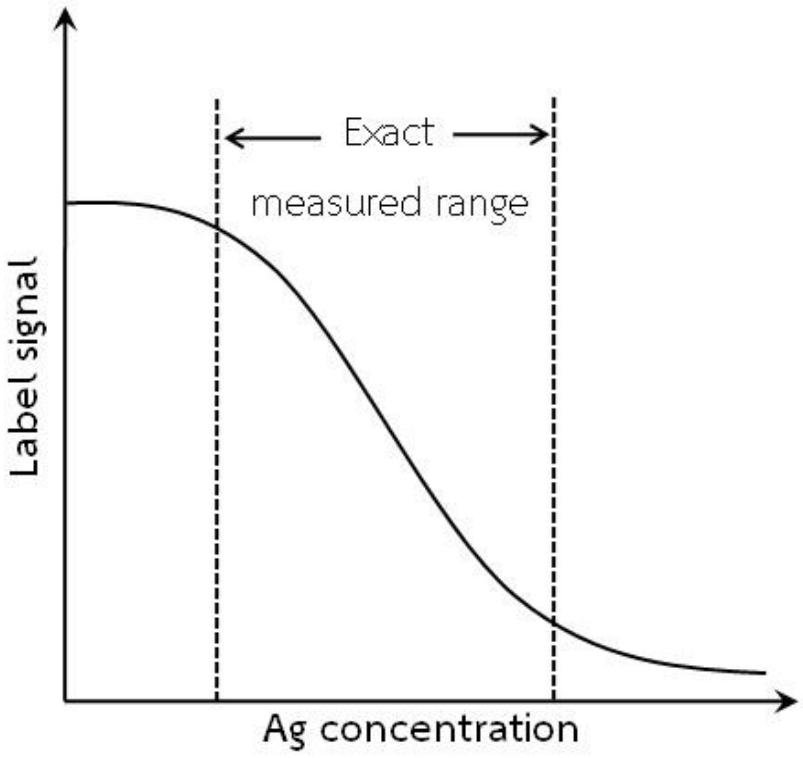

Figure 2.2 Typical standard curve of the competitive immunoassay [21]

2.1.2 Sandwich immunoassay

A sandwich immunoassay is the measurement of the amount of the Ag between two molecules of the Abs. The Ag must contain at least two antigenic sites for capable binding to the Abs in form of the sandwich (Figure 2.3). For this reason, the sandwich immunoassay suits to the quantitative of the multivalent Ags such as proteins or polysaccharides.

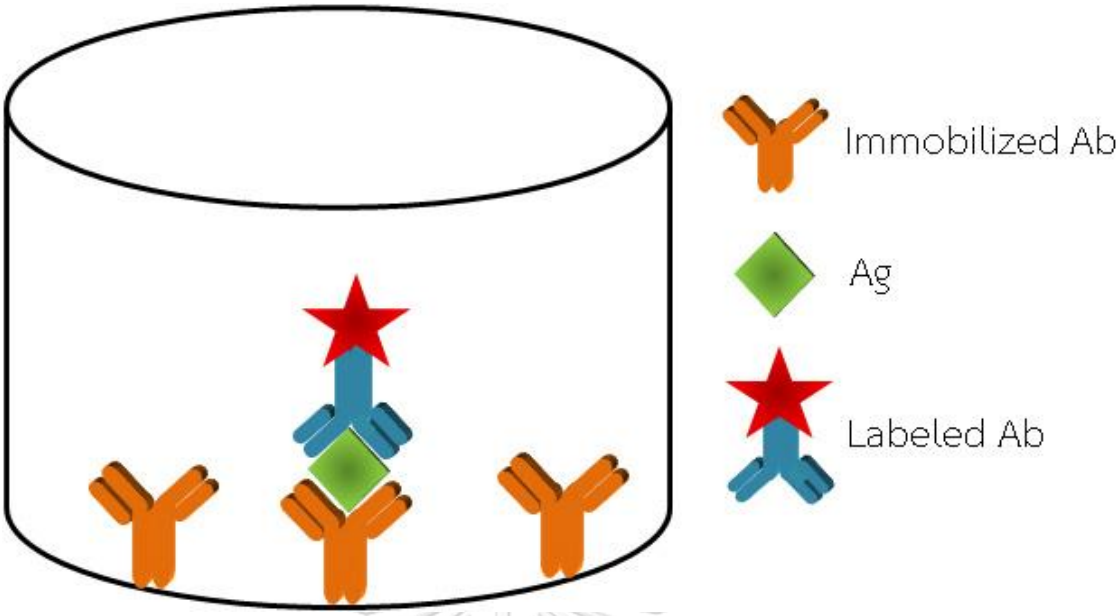

Figure 2.3 Illustration of the sandwich immunoassay [21]

In case of the sandwich immunoassay, the primary Ab (1° Ab) is immobilized on the surface. The Ag is then added and allowed to capture with the immobilized Ab. The labeled secondary Ab (2° Ab) is then added to bind with the Ag to complete the sandwich reaction. A typical standard curve of the sandwich immunoassay is shown in figure 2.4. However, in contrast to the competitive immunoassay, a weak label signal occurs with a low Ag concentration whereas a strong signal is observed with a high Ag concentration.

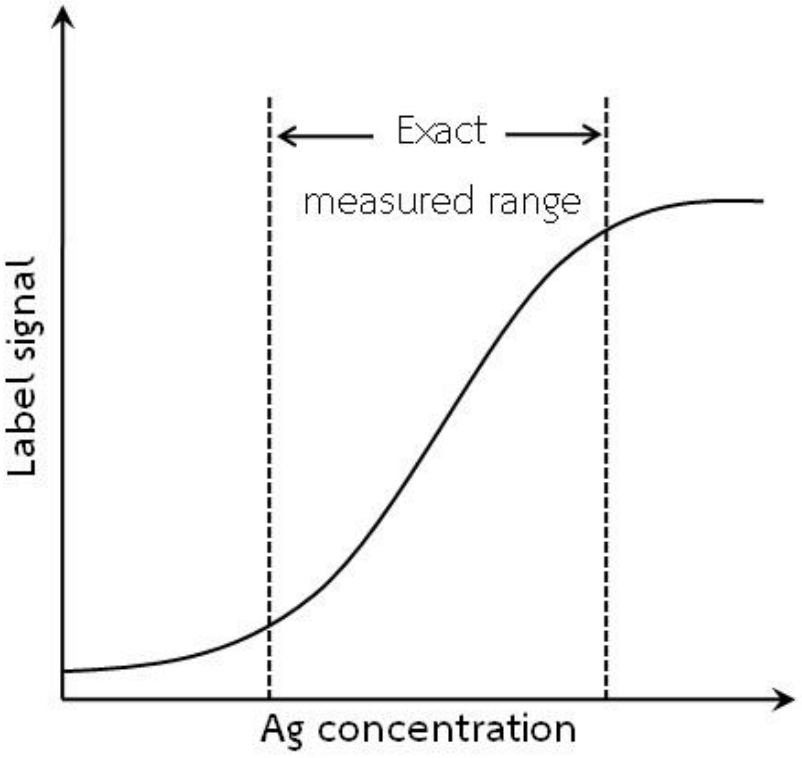

Figure 2.4 Typical standard cure of the sandwich immunoassay [21]

2.2 Paper-based microfluidic devices [7]

Paper-based microfluidic devices are an analytical tool on the paper-based materials such as a filter paper and the NCM, consisting of a hydrophobic wall and a hydrophilic area. Paper-based microfluidic devices provide various advantages such as low cost, easiness of use, portability, disposability, and off-site laboratory. Because of their advantages, a lot of research groups developed various methods for the fabrication of the hydrophobic wall of the paper-based microfluidic devices such as photolithography [7], inkjet printing [8], wax printing [9], and wax-screen printing [10].

Among the reported fabrication methods of the paper-based microfluidic devices, wax-printing method has been widely used as the fabrication method because of its benefits including easy, low-cost and rapid fabrication. Furthermore, the fabrication process could be rapidly finished without the use of organic solvent, and

the various patterns of the paper-based microfluidic devices can be easily designed using only computer software. The fabrication procedure of wax printing method is shown in Figure 2.5.

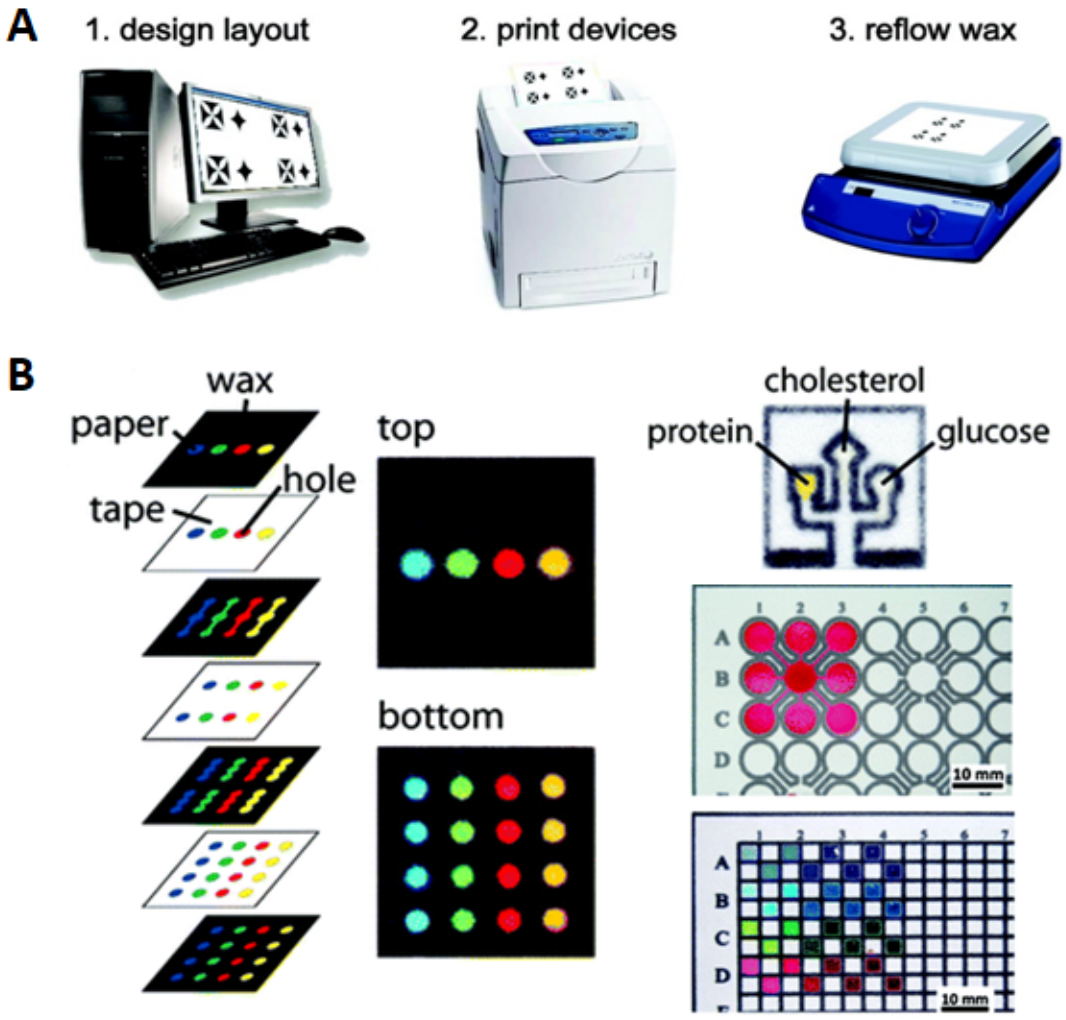

Figure 2.5 Fabrication of the paper-based microfluidic devices by wax-printing method (A) procedure of wax-printing method (1–3) (B) example of the paper-based microfluidic devices for various applications [9]

For the applications of the paper-based microfluidic devices, many researchers combine the paper-based microfluidic devices with the immunoassay to minimize a

conventional 96-microwell immunoassay called a paper-based lateral flow immunoassay.

2.2.1 Paper-based lateral flow immunoassay [22, 23]

A paper-based lateral flow immunoassay, that is also called an immunochromatography, is the combination between the immunoassay and a chromatography to offer a new analytical tool for the rapid measurement. It has been widely used as an on-site tool in various applications such as agriculture and food safety, environmental monitoring and medical diagnosis. The configuration of the device using the paper-based lateral flow immunoassay is shown in Figure 2.6. The device is made up of four pads including a sample pad, a conjugate pad, an absorbent pad and an analytical pad containing a test line and a control line.

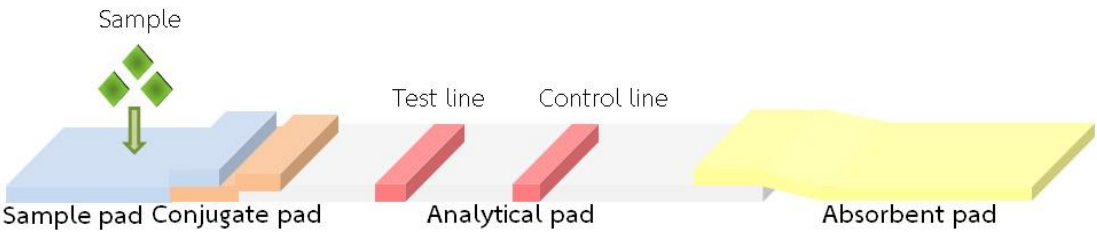

Figure 2.6 Configuration of the paper-based lateral flow immunoassay [22]

The sample pad is placed at the beginning of the device. Its major function is to absorb the sample and provide a uniform flow of the sample fluid through the conjugate pad to the analytical pad. Furthermore, the sample pad also acts as a filtration device by removing unwanted particles. Most sample pads are made from a paper filter and a glass fiber.

The conjugate pad is the most important function to deliver the labeled Ab and sample to the analytical pad. When the sample flows from the sample pad into

the conjugate pad, the labeled Ab should be released rapidly and then float with sample toward the analytical pad. Commonly, materials used to make the conjugate pad include the glass fiber, a cellulose and a propylene.

The analytical pad is the most important function of the measurement of the device. Several different membranes are available depending on capillary flow rate, thickness and surface quality. The parameters affected to capillary flow rate are pore size of membrane, pore size distribution and porosity. The NCM exhibits the most commonly used as the analytical pad due to its electrostatic protein binding. The analytical pad consists of the test and the control lines which the test line is the appearance of the results of the assay. The control line is the unspecific Ab that can capture the labeled Ab in order to confirm the operation of the device correctly.

The absorbent pad is placed at the end of the device to act as a pump or a reservoir that controls the flow of sample and encourages complete movement of the sample through the analytical pad. Most absorbent pads are made from the cellulose.

In order to description of the principle of the paper-based lateral flow immunoassay, there are two principles including a competitive paper-based lateral flow immunoassay to detect low-molecular-mass analytes such as drug residues and antibiotic, and a sandwich paper-based lateral flow immunoassay to detect high-molecular-mass components such as proteins and hormone.

2.2.1.1 Competitive paper-based lateral flow immunoassay

For the competitive paper-based lateral flow immunoassay to detect the low-molecular-mass components (Figure 2.7), the components on the device consist of the labeled Ab at the conjugate pad, the immobilized Ag-protein at the test line and the unspecific Ab at the control line as shown in Figure 2.7A. In the presence of the target Ag in sample (Figure 2.7B), it reacts with the labeled Ab at the conjugate pad, and the formed Ag-labeled Ab complexes move freely to the analytical pad. At the

test line, the complexes cannot be captured by the immobilized Ag-protein. Therefore, only one control line appears on the device. However, in case of the absence of the target Ag, no molecule can bind with the labeled Ab leading to the binding appearance between the labeled Ab and the immobilized Ag-protein, and two color lines appear on the device (Figure 2.7C).

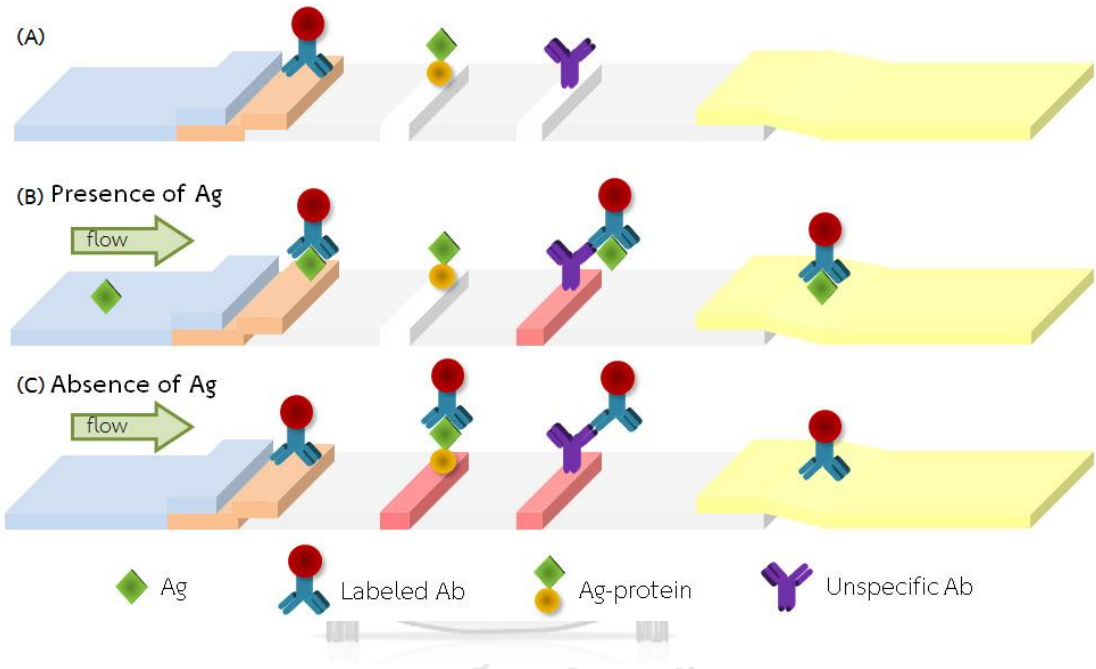

Figure 2.7 The principle of the competitive paper-based lateral flow immunoassay; (A) the components of the device, (B) the presence of target Ag and (C) the absence of target Ag [22]

2.2.1.2 Sandwich paper-based lateral flow immunoassay

In case of the sandwich paper-based lateral flow immunoassay (Figure 2.8), the components on the device consist of the labeled Ab at the conjugate pad, the immobilized Ab at the test line and the unspecific Ab at the control line as shown in Figure 2.8A. For the presence of the target Ag in sample (Figure 2.8B), it reacts with the labeled Ab at the conjugate pad, and the formed Ag-labeled Ab complexes move

freely to the analytical pad. At the test line, the complexes are captured by the immobilized Ab. Therefore, the presence of the interest target Ag in the sample results in colored test and control lines. However, in case of the absence of the target analyte, no molecule can bind with the labeled Ab exhibiting the disappearance of the color intensity of test line (Figure 2.8C).

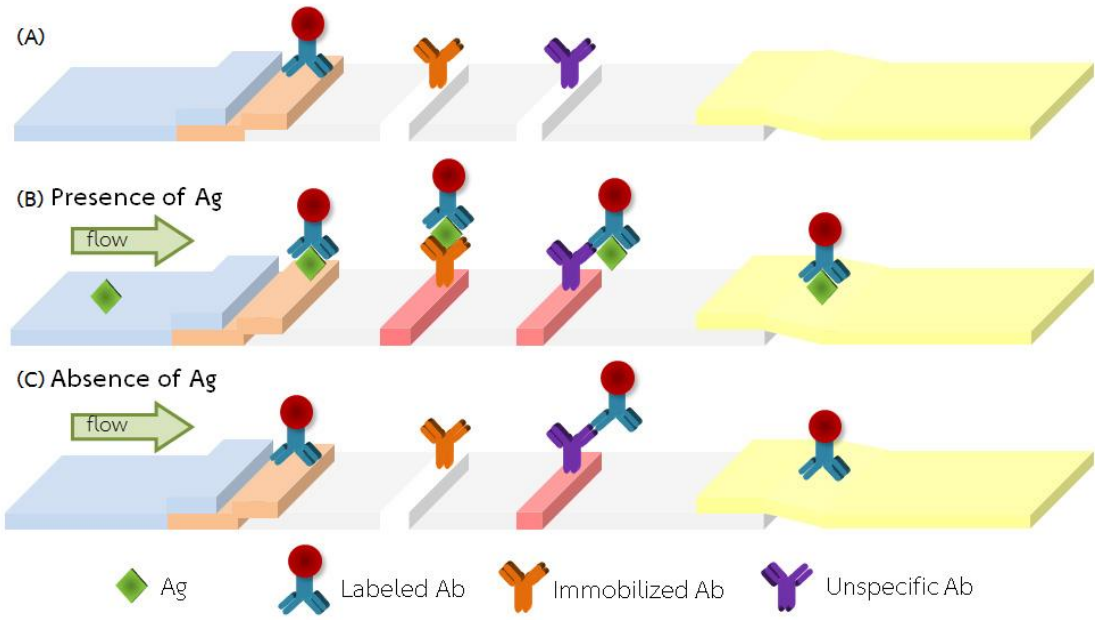

Figure 2.8 The principle of the sandwich paper-based lateral flow immunoassay; (A) the components of the device, (B) the presence of Ag and (C) the absence of Ag [22]

2.3 Labels for the immunoassay

The immunoassay technique extremely required a pure sample of either Ab or Ag for labeling with an appropriate molecule. Various types of labels are popularly used in the immunoassay technique including an enzyme, a metal and a fluorescent labels.

2.3.1 Enzyme label [24]

Enzymes are often used as labels for the detection of the Ag-Ab interactions. Detection and quantification of the binding using the enzyme label result indirectly from enzyme activity which can be determined by means of the conversion of colored or fluorescent substrates. In order to be suitable use as the label, the enzyme should possess the following characteristics. It should be high specific activity for verifiable substrates, cleaned, available in large quantities, conjugational as easily as possible and without loss of activity, and its Ab-enzyme conjugated should be able to be stored without loss of activity for as long time as possible. The enzymes frequently used in immunological procedures include an alkaline phosphatase (ALP) and a horseradish peroxidase (HRP). The use of the enzyme label requires a substrate for detecting itself such as 5-bromo-4-chloro-3'-indolylphosphate (BCIP)/nitro-blue tetrazolium (NBT) or *p*-nitrophenyl phosphate (*p*NPP) for the ALP and 3,3',5,5'-tetramethylbenzidine (TMB) for the HRP. An example of mechanism of the use of enzyme label is shown in Figure 2.9.

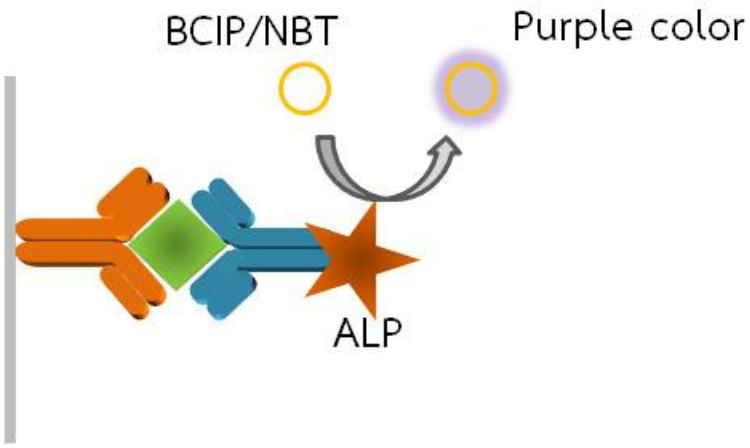

Figure 2.9 Illustration of the immunoassay mechanism using the enzyme label [24]

2.3.2 Metal label [25]

A metal label that is popularly used in the immunoassay includes gold nanoparticles (AuNPs). The AuNPs can be prepared by both chemical and physical methods. Normally, gold derivatives included chloroauric acid are reduced and controlled to grow of particles size with a nanometer scale by the chemical method. The Turkevich-Frens method [26] is mostly used as a procedure to synthesize the AuNPs with average diameter sizes between 10 and 60 nm by adjusting the ratio of a reducing agent (trisodium citrate) and gold (III) derivatives in boiling water. The advantages of the use of the AuNPs as a label are easily controllable size distribution, long-term stability and friendly biocompatibility with Ab, Ag, proteins, DNA, and RNA.

Due to the various advantages of AuNPs, they are often developed by attaching the molecular recognition motifs (functional groups) of interest to the AuNPs for the measurement of an interesting compound. In order to improve the selectivity and accuracy, various stabilizer/ligands and modified methods have been developed to enhance the stability of the AuNPs such as electrostatic interaction, covalent coupling (Au-S covalent and others.), and specific recognition (antibody-antigen, biotin-avidin, DNA hybridization and others) as shown in Figure 2.10. The applications of the AuNPs have several pathways such as heavy metal determination, small molecules detection, DNA detection, protein analysis, cellular analysis, drug delivery, analytical label and others.

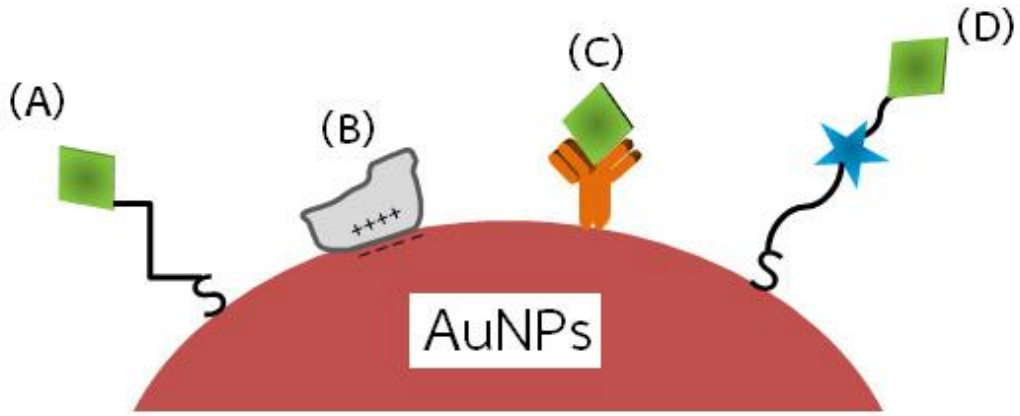

Figure 2.10 Illustration of the modification of the AuNPs; (A) thiolated or disulfide modified ligands, (B) electrostatic interaction, (C) Ab-Ag interation and (D) streptavidin-biotin binding [25]

2.3.3 Fluorescent label [27, 28]

Fluorescent dyes or fluorophores have been widely used as a probe for physical and structural parameters, indicators for molecular concentrations, and labels/tracers for visualization and localization of biomolecules in various bioassays. A fluorescent technology has been extensively applied in the immunoassay development, not only a high sensitivity of the detection, but also a variety of measurable properties of the fluorophores. Furthermore, the desirable properties of the fluorophores include gentle reactivity, high water solubility, low nonspecific adsorption, good photostability, as well as high molar extinction coefficients and quantum yields. Due to the main advantage in the high sensitivity, various fluorophores have been reported to be used as a fluorescent label such as a quantum dot, a europium and a lanthanide. For the immunoassay using the fluorescent label, the light source such as a common tungsten or halogen lamp with inexpensive filters for wavelength selection is required as excitation light for emission fluorescent signal as shown in Figure 2.11.

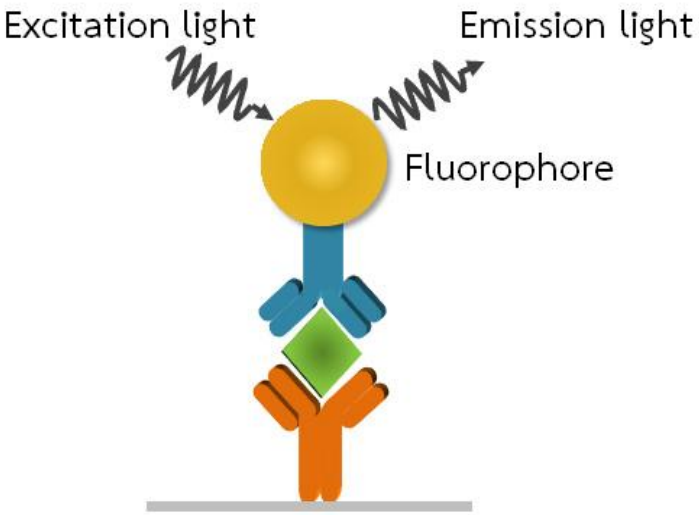

Figure 2.11 Illustration of the immunoassay mechanism using the fluorescent label [27]

2.4 Quantitative colorimetric assay [18]

A quantitative colorimetric assay is an analytical tool using a scanner or a digital camera for image capturing, and the image can be transmitted electronically and digitally to computer software for obtaining color intensity data. The data can be analyzed by a specialist, and the results of the analysis returned (ideally in real-time) to the person administering the test. For the quantitative analysis procedure as shown in Figure 2.12, the colorimetric results are firstly captured by the camera or the scanner. The photos are then exported to computer software and adjusted to the grayscale, RBG or CMYK color for increasing precision in the analysis. Finally, the test zone is selected, and the mean intensity is recorded. The advantages of this method are easiness of use, rapidity, inexpensive instrument and on-site measurement.

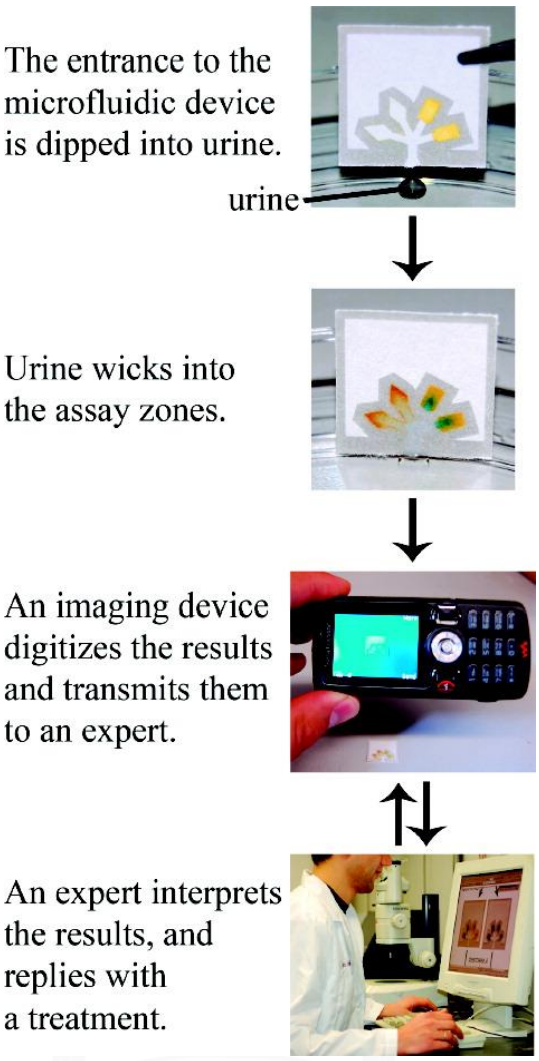

Figure 2.12 Procedure of the quantitative colorimetric assay [18]

CHAPTER III

DEVELOPMENT OF THE IMMUNOASSAY ON THE PAPER-BASED MICROFLUIDIC DEVICES FOR THE DETERMINATION OF RACTOPAMINE

This chapter is the development of the conjugation method of ractopamine (RAC) and protein carrier. The developed RAC conjugated protein carrier has been applied for the fabrication of the immunoassay on the paper-based microfluidic devices using the AuNPs as a label for the RAC determination in animal feed.

Novel ractopamine-protein carrier conjugation and its application on paper-based lateral flow strip test for ractopamine detection in animal feed

Pattarachaya Preechakasedkit[a], Nataya Ngamrojanavanich[b,c], Nanthika Khongchareonporn[c]*, Orawon Chailapakul[b,d]*

[a] Program in Biotechnology, Faculty of Science, Chulalongkorn University, Patumwan, Bangkok, 10330, Thailand

[b] Electrochemistry and Optical Spectroscopy Center of Excellence (EOSCE), Department of Chemistry, Faculty of Science, Chulalongkorn University, Patumwan, Bangkok, 10330, Thailand

[c] The Institute of Biotechnology and Genetic Engineering, Chulalongkorn University, Patumwan, Bangkok, 10330, Thailand

[d] National Center of Excellence for Petroleum, Petrochemical, Advanced Materials, Chulalongkorn University, Patumwan, Bangkok, 10330, Thailand

*Corresponding authors

Submitted manuscript

Abstract

In this work, a novel ractopamine conjugated with bovine serum albumin (RAC-BSA) has been developed via the Mannich reaction which demonstrates the mole coupling ratio of RAC-BSA of 9:1. The proposed conjugation method provided a simple and one-step method with the use of less chemicals compared with other conjugation methods for competitive immunoassays. The RAC-BSA conjugation was applied to fabricate a competitive paper-based lateral flow strip test for RAC detection in animal feed. Under optimal conditions, the limit of detection (LOD) assessed by the naked eye was found to be 1 ng g^{-1} within 5 min. A semi-quantitative analysis was also conducted with a smart phone and computer software with a linearity of 0.075-0.750 ng g^{-1}, a calculated LOD of 0.10 ng g^{-1}, a calculated limit of quantitation (LOQ) of 0.33 ng g^{-1} and a good correlation of 0.992. The recovery percentages were found in range of 96.4-103.7 with RSD of 2.5-3.6% for intra- and inter-assays. Comparison of the results obtained from the strip test to those obtained by ELISA has good agreement in terms of accuracy. Furthermore, this strip test exhibited a highly specific RAC detection without cross reactivity to related compounds. Therefore, the strip test could be acceptable for RAC detection due to its ease of use, rapid testing, affordability, portability, precision, reproducibility, high sensitivity and specificity, and long-term stability.

3.1 Introduction

Ractopamine (RAC: $C_{18}H_{23}NO_3$, Mw: 301.386 g mol^{-1}) is a synthetic organic compound in the beta-agonist group that shares a common chemical structure of the compound classified as phenethanolamine [29-31]. Beta-agonist can bind to beta-receptor on fat cells to active several enzymes in the pathway that leads to a decreased rate of lipid synthesis and storage, and increased lipid mobilization in the cells [2, 32, 33]. This group can also bind to beta-receptor on skeletal muscle cells for the activation of protein kinases leading to the enhancement of muscle protein synthesis and muscle growth [34-36]. Therefore, beta-agonist especially RAC is widely used as feed additive in cattle and swine for reducing body fats and increasing muscle tissues. Initially, the appearance of RAC residues in the edible tissue of animals has been caused by feeding animals with a feed supplement containing RAC. From previous report about the feed supplement containing RAC [37], the 5 μg g^{-1} of RAC in the feed supplement effected on the growth performance in swine and ultimate pork quality, and the maximum residue limits (MRLs) for veterinary food of RAC from the Codex Alimentarius Commission (Codex) are in the range of 10-90 ng g^{-1}, depending on types of edible tissues. Furthermore, the overall effect of RAC to human health is cardiac stimulation which causes an increased heart rate and systemic dilation of blood vessels [38-40]. This has led to an import prohibition of RAC-treated meat in many countries, notably Europe and China [41]. Therefore, the detection method for RAC in animal feed importantly exhibits and initially controls the appearance of RAC in edible tissues.

Currently, an immunoassay has been widely used as a detection method because of its major points in high specificity and sensitivity toward RAC [42-44]. The conventional immunoassay called enzyme-linked immunosorbent assay (ELISA) provides several disadvantages such as complicated steps, lengthy time, and the requirement of expensive instrument [45, 46]. A paper-based lateral flow strip test has

been proposed as a portable device to overcome the drawbacks of the conventional ELISA in terms of the use of less solutions, lower costs, rapid assay, ease of use and disposability [47, 48]. In case of the RAC detection by the immunoassay, a competitive format, which is the competition between RAC in samples and an immobilized RAC to bind with an antibody, is normally used due to the small molecules of RAC [3, 49, 50]. In addition, RAC must be conjugated to protein carriers such as bovine serum albumin (BSA) [51-53] and ovalbumin (OVA) [54-56] to form RAC-protein carrier for immobilizing on the substrate surface. Therefore, the conjugation method of RAC-protein carrier is extremely importance in the immunoassay of RAC. The previous report of RAC-protein carrier conjugation by changing the functional group of RAC to the carboxylic group [57] displays multiple steps and various types of chemicals especially pyridine to dissolve chemicals in the conjugation pathways leading to the requirement of an additional step to evaporate pyridine. Moreover, another method has also been reported by the reductive reaction of octopamine to form RAC hapten before the conjugation to the protein carrier using 1-Ethyl-3-(3-dimethylaminopropyl)-carbodiimide (EDC) and N-hydroxysuccinimide (NHS) as coupling agents indicating complicated steps and the use of several types of chemicals [58]. Due to the disadvantages of previous conjugation methods, the simple and fast method with less chemical utilization is an interesting approach as an alternative method for the conjugation of RAC and protein carrier.

Previously, there are some researchers who reported the synthesis of haptens such as aflatoxin B1-cationized BSA [59] and bisphenol A-cationized BSA [60] via the Mannich reaction. The Mannich reaction occurred when active hydrogen-containing compounds condense with aldehyde, especially formaldehyde and an amine in weak acidity [61]. The haptens synthesis via the Mannich reaction exhibits good immunological properties, simple coupling steps, stable alkylamine linkage, and the

use of fewer types of chemicals [59, 60]. Therefore, the Mannich reaction interestingly acts as a novel method of the RAC-carrier protein conjugation.

In this work, we aims to construct the RAC-protein carrier conjugation method with one step, simplicity, rapidness and smaller chemicals requirement based on the Mannich reaction. The mAb against RAC produced by our lab [57] and the RAC-protein carrier were applied to fabricate the paper-based lateral flow strip test for RAC detection. The immunological response of the novel RAC-protein carrier and the sensitivity of RAC detection in animal feed using the strip test were visually assessed by the naked-eye as a qualitative analysis within 5 min exhibiting the advantages in a simple and rapid test. A semi-quantitative analysis was also performed using a simple instrument through a smart phone coupled with computer software (ImageJ software). In addition, the strip test was also applied to quantify the amounts of RAC in animal feed to validate the performance with conventional method (ELISA).

3.2 Materials and methods

3.2.1 Chemicals and materials

Ractopamine hydrochloride (RAC), bovine serum albumin (BSA), glycine, sodium dihydrogen phosphate, disodium hydrogen phosphate, sodium choloride, pyridine, Tris(hydroxymethyl)aminomethane, succinic anhydride, N,N'-disuccinimidyl carbonate, methanol, Tween 20, sucrose and formaldehyde were purchased from Sigma Aldrich (St. Louis, MO, USA). Goat-antimouse IgG (GAM) was purchased from Jackson ImmunoResearch (West Grove, PA, USA). Gold nanoparticles (AuNPs, 20 nm) were purchased from Serve Science Co. Ltd. (Chatuchak, BKK, Thailand). Pierce™ protein assay kit was purchased from ThermoFisher Scientific (Waltham, MA, USA). All solutions were prepared using 18Ω milli-Q water. Protein G sepharose, nitrocellulose membrane

(AE99), glass fiber membrane (Standard 17 as sample pad and GF33 as conjugate pad) and absorbent pad (CF7) were purchased from Whatman-GE healthcares (Pittburgh, PA, USA).

3.2.2 Conjugation of ractopamine and protein carrier

The ractopamine-bovine serum albumin (RAC-BSA) conjugation was carried out via the Mannich reaction with slight modification [61]. BSA dissolved in 0.1 M MES buffer (pH 4.7) containing 0.15 M NaCl was initially mixed with RAC followed by adding 37% (v/v) formaldehyde. After that, the mixture solution was stirred and incubated in the dark at room temperature overnight. Finally, the mixture solution of RAC-BSA was dialyzed using 0.01 M PBS (pH 7.4) and kept at -20 ^{o}C for readiness to use.

3.2.3 Calculation of conjugate molar ratio of RAC and BSA

To confirm the conjugation of RAC-BSA, the absorbance of RAC, BSA and RAC-BSA was measured using UV-visible (UV-vis) spectrophotometer, and the conjugate molar ratio of RAC and BSA was calculated using the Beer-Lambert Law as followed [60]: The conjugate molar ratio = $[\varepsilon_{\text{conjugate 278 nm}}-\varepsilon_{\text{BSA 278 nm}}]/[\varepsilon_{\text{RAC 274 nm}}]$ where $\varepsilon_{\text{conjugate 278 nm}}$ is the molar extinction coefficient of conjugate at 278 nm (l $mol^{-1}.cm^{-1}$), $\varepsilon_{\text{BSA 278 nm}}$ is the molar extinction coefficient of BSA at 278 nm (l $mol^{-1}.cm^{-1}$) and $\varepsilon_{\text{RAC 274 nm}}$ is the molar extinction coefficient of RAC at 274 nm (l $mol^{-1}.cm^{-1}$).

3.2.4 Preparation of monoclonal antibody and gold nanoparticles conjugation

Monoclonal antibody (mAb) against RAC was obtained by immunizing a mouse with RAC-BSA as described previously [57]. The mAb was purified using protein G affinity chromatography. After that, the AuNPs as labeled was conjugated to the mAb following

the previous report method with slight modification [62]. First, the optimal concentration of the mAb conjugated to the AuNPs was selected by mixing between the AuNPs (pH 8.0) with a particle size of 20 nm and the various concentrations of the mAb between 0-200 μg mL^{-1} for 30 min. Then, 10% (w/v) NaCl was added to the mixture solution, and the optimal condition was selected by color change visualization and UV-vis characterization. After obtaining the appropriate concentration of the mAb, the mAb-AuNPs conjugated was prepared by mixing between the AuNPs and the mAb and incubating under continuous stirring at room temperature for 1 h. Then, 3% (w/v) BSA was added and incubated under continuous stirring at room temperature for 1 h to block the unbounded surface. After that, the mixture solution was centrifuged at 15,000 rpm for 30 min. Finally, the soft sediment was washed and re-suspended in 0.01 M PBS (pH 7.4) containing 3% (w/v) BSA and 2% (w/v) sucrose and kept at 4 °C. The solution of the mAb-AuNPs conjugated was characterized by a UV–vis spectrophotometer.

3.2.5 Preparation of the paper-based lateral flow strip test

The paper-based lateral flow strip test consisted of four pads (sample, conjugate, analytical, and absorbent pads). The sample and the absorbent pads were used without any pretreatment. The mAb-AuNPs conjugated was dispensed on the conjugate pad using an IsoFlo Flatbed Dispenser (Imagine Technology, USA) with a flow rate of 5 μL cm^{-1}. The analytical pad contained a test line at the bottom and a control line at the top of the NCM. RAC-BSA and GAM were respectively dispensed as the test and control lines on the NCM with a flow rate of 1 μL cm^{-1}. The concentration of RAC-BSA on the test line was studied between 0.50-1.25 mg mL^{-1} to select an appropriate amount of RAC-BSA. After dispensing, the NCM was blocked by 10% (w/v) BSA in 0.01 M PBS (pH 7.4) and dried at 37 °C for 1 h. Finally, all pads were attached on a plastic

backing card and a cassette to be ready for use. The schematic illustration of the strip test is shown in Figure 3.1A.

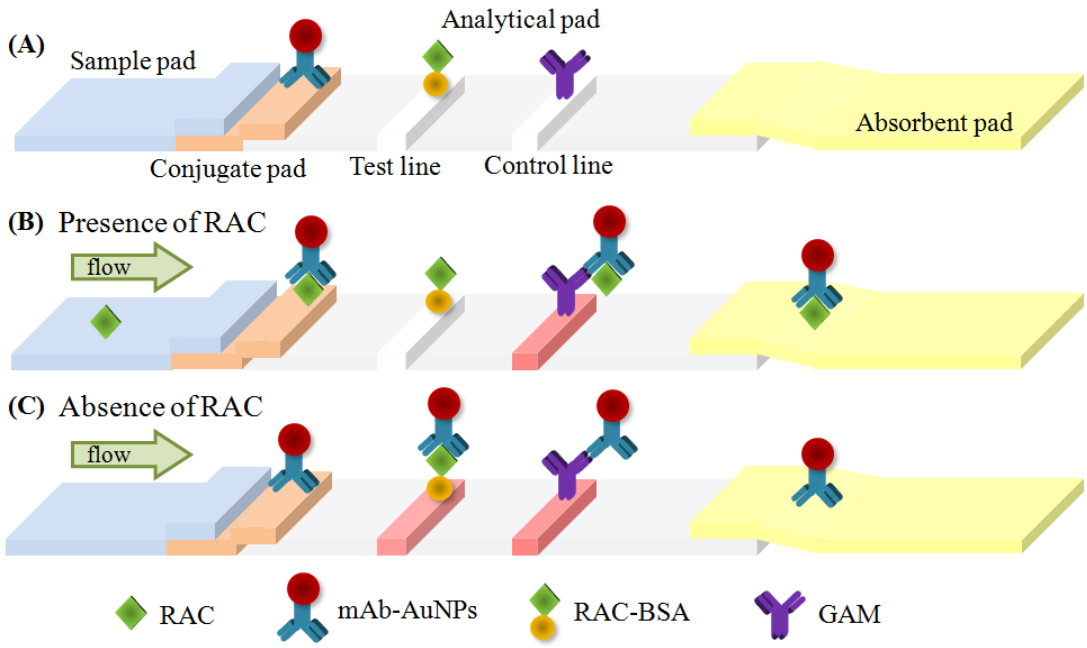

Figure 3.1 (A) Schematic illustration of the paper-based lateral flow strip test for RAC detection in (B) the presence of RAC and (C) the absence of RAC

3.2.6 Assay sensitivity and cross reactivity

The strip test was used to detect RAC by applying 100 µL of samples or various concentrations of standard RAC (0-1 ng mL^{-1}) on the sample pad. The cross reactivity of the strip test was also tested by loading the related compounds in the beta-agonist group to the sample pad. After loading the solution, each strip test was allowed to react completely, and the color intensity was evaluated by the naked eye within 5 min. In the presence of RAC in the sample as a positive result, RAC can bind to the mAb-AuNPs leading to the non-binding between the mAb-AuNPs and the immobilized RAC-BSA, so only one control line appeared on the NCM (Figure 3.1B). In the absence of RAC as a negative result, the mAb-AuNPs could bind with the immobilized RAC-BSA,

and two color lines appeared on the NCM (Figure 3.1C). For qualitative analysis assessed by the naked eye, the limit of detection (LOD) was obtained from the minimal concentration of RAC leading to the complete disappearance of color intensity at the test line. Furthermore, the color intensity was also captured using a smart phone under a light controllable box. The intensity of each result was measured by ImageJ software for semi-quantitative analysis, and the calculated limit of detection ($LOD=3SD_{blank}/slope$) and limit of quantitation ($LOQ=10SD_{blank}/slope$) were observed from a semi-quantitative calibration curve.

3.2.7 Sample preparation

Animal feed for swine without feed additive brand purchased from local markets in Thailand was used for sample analysis. All samples were prepared using the spiked method following previous report with slight modification [63]. First, 1 g of animal feed was weighted in the centrifuge tube, and various amount of RAC (0-1 ng) were spiked in animal feed. After that, 5 mL of the optimal ratio of methanol (MeOH) and a running buffer was added as extraction buffer and stirred for 15 min. The mixture was then centrifuged at 4,000 rpm for 10 min. After that, the supernatant was collected and then analyzed according to the assay procedure. Additionally, ELISA was also used to determine amount of RAC in animal feed in parallel with the result obtained from the strip test to confirm the accuracy and acceptability of method.

3.3 Results and discussion

3.3.1 Conjugation of ractopamine and protein carrier

Due to the small molecules of RAC, a competitive format, which is the competition between RAC in the sample and an immobilized RAC to bind with an

antibody, is normally used for the RAC immunoassay. The conjugation method of RAC-protein carrier to be used as the immobilized RAC is an essential requirement. Therefore, the conjugation of RAC and BSA based on the Mannich reaction was reported in this work. The mechanism of the RAC-BSA conjugation is shown in Figure 3.2.

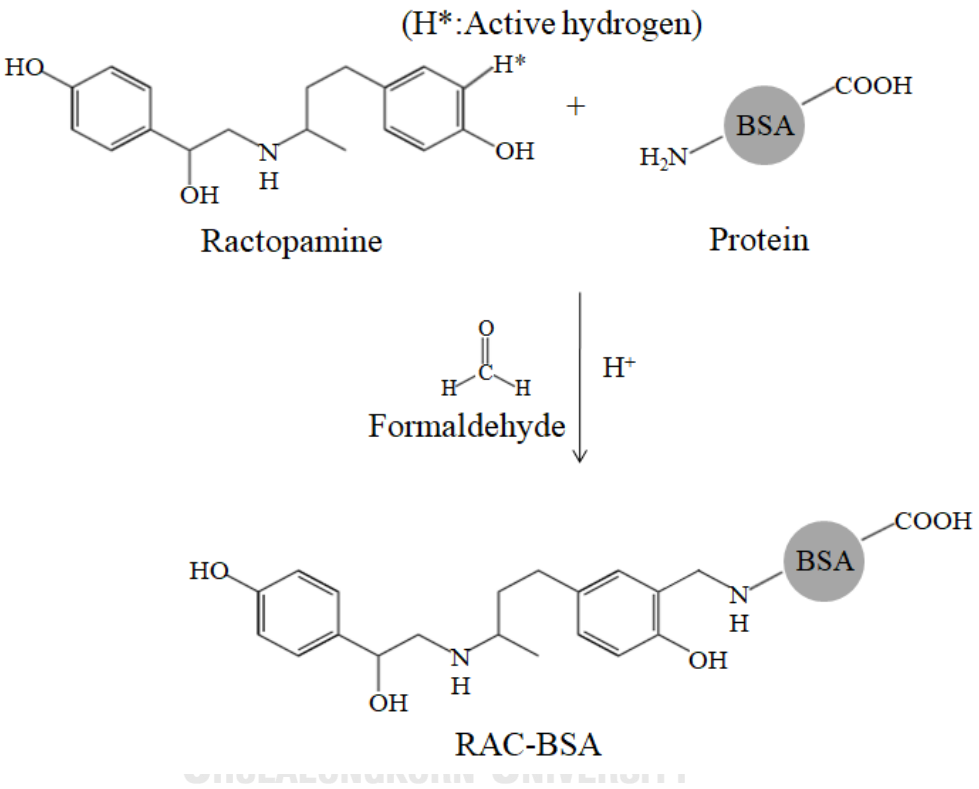

Figure 3.2 Schematic of the RAC-BSA conjugation via the Mannich reaction carried out in MES buffer (pH 7.4)

The Mannich reaction consists of the condensation of the aldehyde group which can bind to the active hydrogen of RAC at ortho position via electrophilic aromatic substation, and this reaction can be combined with amine to form the RAC-BSA conjugation. The conjugation via the Mannich reaction displays stable covalent bonds [61]. The obtained RAC-BSA also exhibited a clear solution without any pellets.

Furthermore, the UV-Vis spectra as shown in Figure 3.3A demonstrated the maximum absorbance of RAC, BSA and RAC-BSA at 274, 278 and 278 nm, respectively. The conjugate molar ratio of RAC and BSA was calculated from the Beer-Lambert Law and was found to be 9:1 (RAC:BSA) indicating successful coupling between RAC and BSA. To compare with previous conjugation methods between RAC and BSA [57, 64], the conjugate molar ratio of various methods were reported as 7:1 and 8:1. Unfortunately, the drawbacks of the previous conjugation methods required complicated steps, various types of chemicals, strong organic solvent and nitrogen gas for solvent evaporation. Therefore, the RAC-BSA conjugation following the Mannich reaction could be accepted as the conjugation method exhibiting an easy, one-step and rapid conjugation with the use of less chemicals and no need for organic solvent.

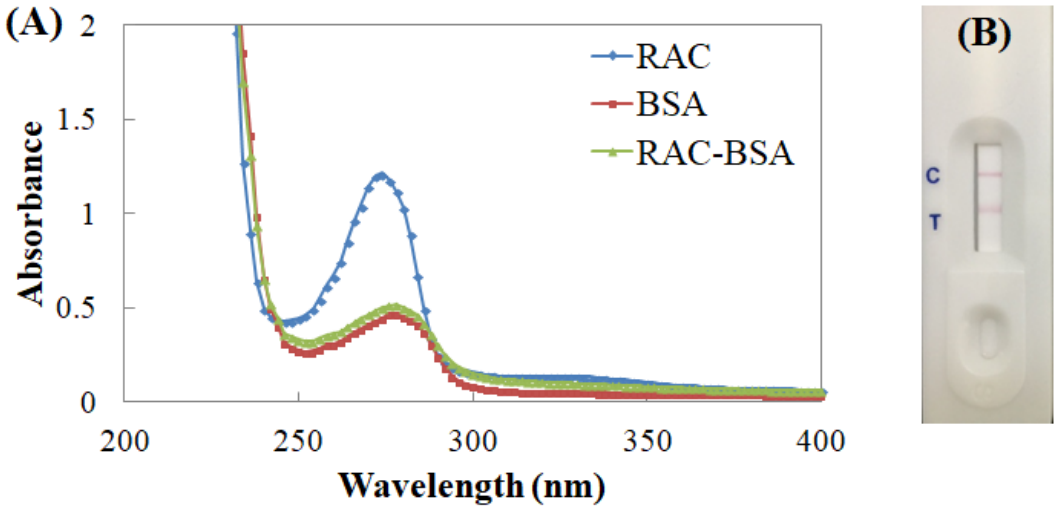

Figure 3.3 (A) the UV-Vis spectra of 0.5 mg mL^{-1} of RAC (blue line), 3.0 mg mL^{-1} of BSA (red line) and 2.0 mg mL^{-1} of RAC-BSA (green line) and (B) the paper-based lateral flow strip test for RAC detection after loading 100 µL of running buffer as negative result

After the RAC-BSA conjugation, the binding between RAC, RAC-BSA and mAb was preliminarily tested by the competitive conventional ELISA (data not shown)

indicating that the competition between the RAC-BSA conjugation and RAC to bind with the mAb could be occurred. In addition, the RAC-BSA and mAb was applied to fabricate the paper-based lateral flow strip test. After loading the running buffer as a negative result on the strip test, the color intensities appeared on both the test and control lines as well as the principle of the competitive format (Figure 3.3B). Therefore, the RAC-BSA conjugation via the Mannich reaction could be acceptably applied in the competitive paper-based lateral flow strip test.

3.3.2 Optimization of the paper-based lateral flow strip test

For the competitive paper-based lateral flow strip test, the AuNPs as labeled provide visual qualitative assay in yes/no responses depending on the concentrations of RAC. Therefore, the optimal conditions for the competitive paper-based lateral flow strip test of RAC including the effect of concentration of mAb conjugated to AuNPs and the concentration of RAC-BSA at the test line should be studied similar to the checkerboard titration in the competitive ELISA [65].

3.3.2.1 The effect of concentration of monoclonal antibody for the conjugation with AuNPs

The concentrations of the mAb between 0 and 200 μg mL^{-1} were studied for the selection of the minimal concentration of the mAb that was suitable for the conjugation with the AuNPs. The particle size of the AuNPs was approximately 20 nm and uniform in size confirmed by TEM image (Figure 3.4).

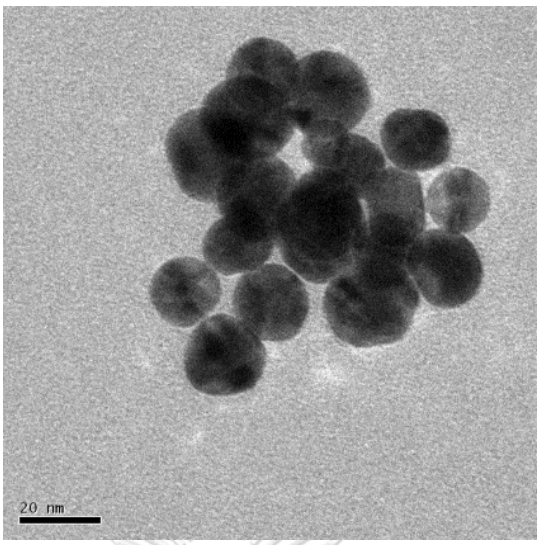

Figure 3.4 TEM image of AuNPs

The optimal concentration was selected by the color change visualization and UV-vis characterization. In case of an inappropriate amount of the mAb, the addition of NaCl after mixing between mAb and AuNPs led to the aggregation of AuNPs, and the color of the solution changed from red to purple. The result indicated that the color of the solution did not change at a concentration of 100 μg mL^{-1}, and the absorbance at 520 nm was initially stable as shown in Figure 3.5. Therefore, the concentration of 100 μg mL^{-1} was selected as an optimal value to conjugate with the AuNPs.

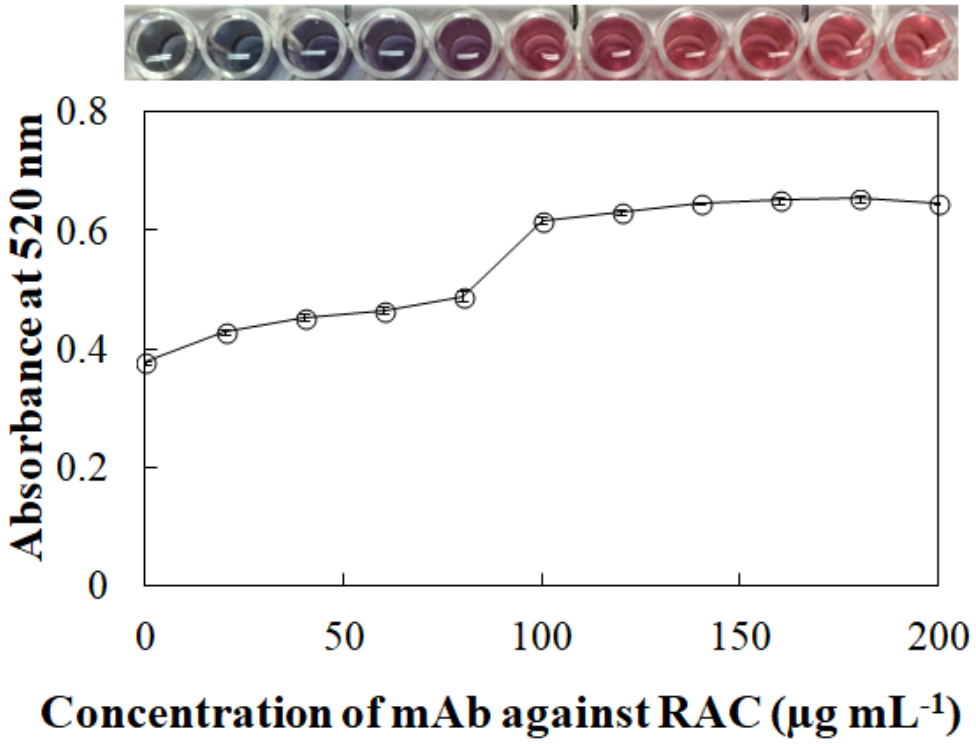

Figure 3.5 The effect of concentrations of mAb between 0-200 µg mL^{-1} on the conjugation with AuNPs characterized by color change visualization and UV-vis spectrophotometer (n=3)

Furthermore, the conjugation between the mAb and the AuNPs was also confirmed by a red-shift of the peak of the mAb-AuNPs (524 nm) compared to the AuNPs (520 nm) (Figure 3.6).

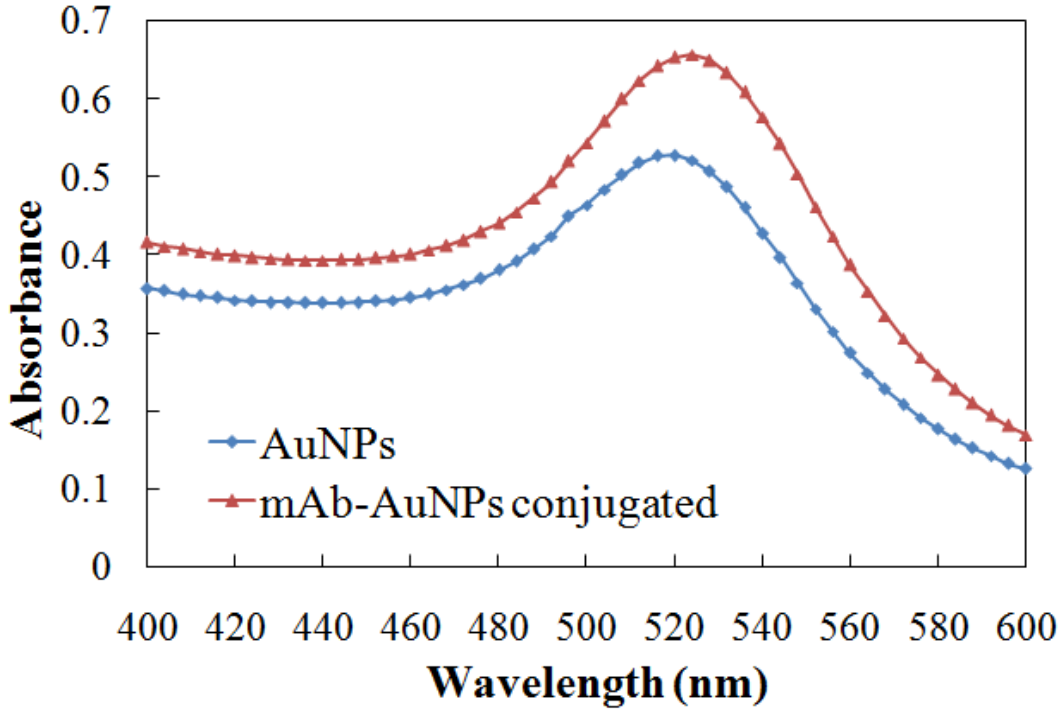

Figure 3.6 UV-vis spectra of gold nanoparticles (red line) and monoclonal antibody against RAC-gold nanoparticles conjugated (blue line)

3.3.2.2 The effect of concentration of RAC-BSA for the immobilization at test line

The detection of RAC using the competitive format is the competition between RAC in the samples and the immobilized RAC-BSA. The sensitivity of the strip test should be visually assessed from the minimal concentration of RAC leading to the complete disappearance of the color intensity at the test line. The concentration of the immobilized RAC-BSA was therefore concerned for the preparation of the strip test because the over concentration of RAC-BSA causes low sensitivity. The concentrations of RAC-BSA of 0.50, 0.75, 1.00 and 1.25 mg mL^{-1} were studied, and the running buffer as a negative result was applied for evaluating the optimal value. The results observed by the naked eye as shown in Figure 3.7 indicated that the color intensities of the test line were constant at the concentrations between 0.75-1.25 mg mL^{-1}, and then the

color intensity decreased at 0.50 mg mL^{-1} of RAC-BSA. Therefore, 0.75 mg mL^{-1} of RAC-BSA, which was the minimal concentration giving the most color intensity of negative result on the test line, was selected as an optimal concentration to be immobilized on the test line.

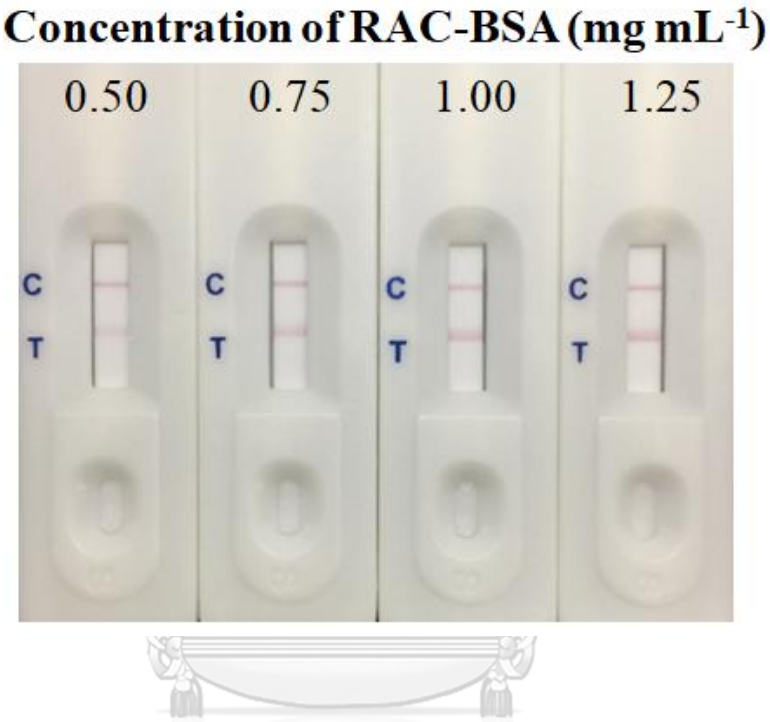

Figure 3.7 The effect of concentrations of RAC-BSA (0.50, 0.75, 1.00 and 1.25 mg mL^{-1}) on the immobilization at test line (n=3)

3.3.3 Assay sensitivity, cross reactivity and stability

Under the optimal conditions, the volume of the running buffer and standard RAC of 100 µL was loaded at the sample pad. The ability to detect standard RAC was evaluated at concentrations between 0-1 ng mL^{-1}. In case of the competitive format of qualitative analysis assessed by the naked eye, the highest color intensity appeared in the absence of RAC as negative result, and the color intensity decreased with the increasing of the concentration of RAC. The limit of detection (LOD) by the naked eye was defined as the minimal amount of standard RAC resulting in no color intensity at

the test lines. As shown in Figure 3.8, the color intensity of the test line completely disappeared at 0.75 ng mL^{-1} of RAC whereas both the test and control lines appeared at concentrations lower than 0.75 ng mL^{-1}. Therefore, the LOD of the standard RAC was found as low as 0.75 ng mL^{-1} evaluated by the naked eye within 5 min.

To compare with the previous reports of the AuNPs strip test of standard RAC detection, LODs by the naked eye were 2 and 3 ng mL^{-1} [55, 58], demonstrating that our strip test should be practically applied for the detection of RAC in real samples.

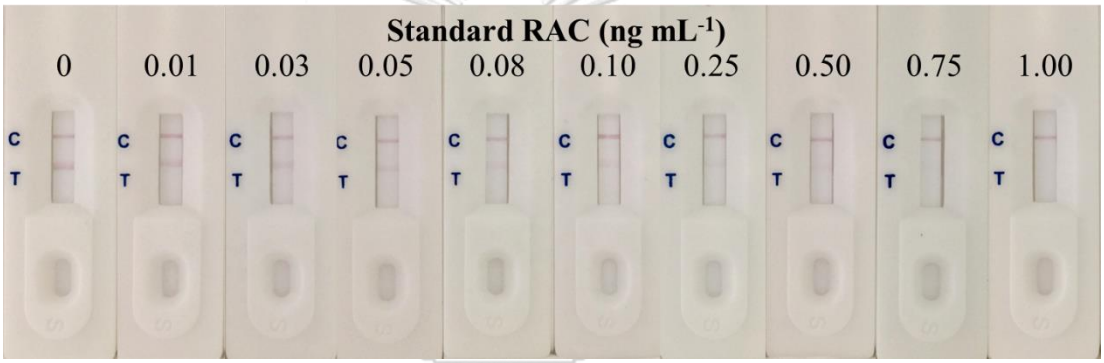

Figure 3.8 The paper-based lateral flow strip test (C: Control line, T: Test line) of standard RAC at concentrations between 0-1 ng mL^{-1}

For the cross reactivity test, a high concentration of the related compounds was applied as well as the strip test of RAC detection. The related compounds included salbutamol (SAL), clenbuterol (CLB), terbutaline (TER), norepinephrine (NE), and phenylephrine (PHE) at a concentration of 1,000 ng mL^{-1} were studied in this work compared to the negative (the absence of RAC) and positive (the presence of RAC) results. The results as shown in Figure 3.9 indicated that the test line only disappeared in case of the presence of RAC whereas the intensity of the test line appeared on the strip test loaded with SAL, CLB, TER, NE, PHE and the absence of RAC. Therefore, the developed strip test demonstrated a highly specific RAC detection.

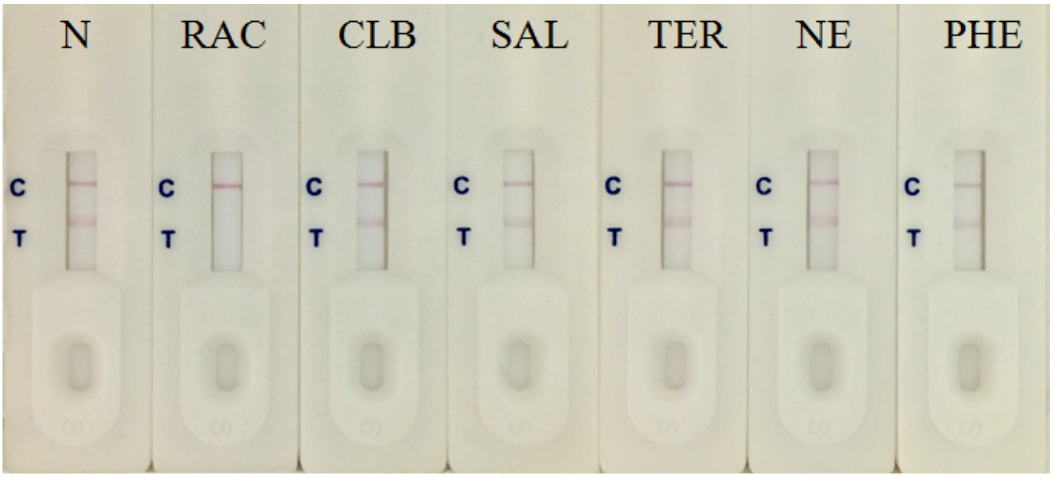

Figure 3.9 Cross reactivity test by loading running buffer (N), ractopamine (RAC), clenbuterol (CLB), salbutamol (SAL), terbutaline (TER), norepinephrine (NE), and phenylephrine (PHE)

Furthermore, the storage stability was studied after keeping the strip test at room temperature for 0 to 5 months. After loading negative control (Figure 3.10A), two color lines appeared on the all strip tests while the test line still disappeared on the all strip tests in the presence of 1 ng mL^{-1} of RAC (Figure 3.10B). These results indicated the long-term stability of the strip test (more than 5 months).

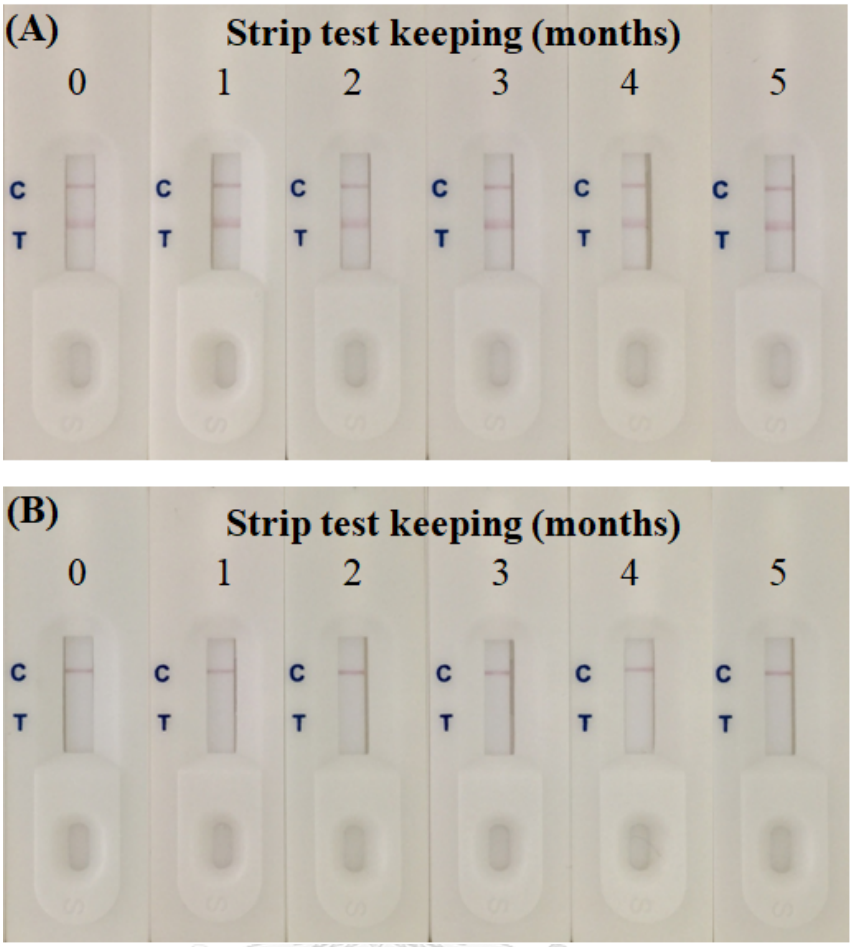

Figure 3.10 Storage stability after keeping the strip tests for 0 to 5 month after loading running buffer as negative control (A) and 1 ng mL^{-1} of RAC as positive control (B)

3.3.4 Sample application

Animal feed was selected for the application of the strip test because there was no report for the use of the strip test to directly detect RAC in animal feed. For the extraction of animal feed, organic solvent, specifically MeOH, is normally required in this process. However, there is a report indicating that an increase in MeOH concentration led to a decrease of the sensitivity to the conventional ELISA [58]. Due to the effect of MeOH, the ratios of methanol and running buffer as an extraction buffer were studied at 0:100, 5:95, 10:90, 20:80, and 40:60. The result was found that

color intensities of the test and control lines were constant until the ratio of 10:90 and then decreased (Figure 3.11). The decreasing of the intensity at high concentration of MeOH resulted from the interference of the matrix effect and the color of the animal feed. Therefore, a ratio of 10:90 was used as the extraction buffer.

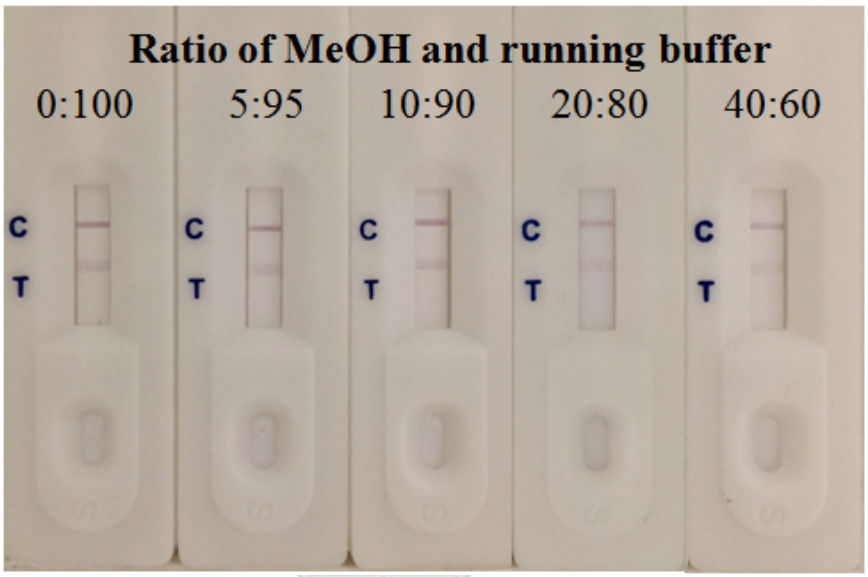

Figure 3.11 The effect of MeOH with the ratio of MeOH and running of 0:100, 5:95, 10:90, 20:80 and 40:60 toward the paper-based lateral flow strip test

After obtaining the optimal extraction buffer, RAC spiked in animal feed at final concentrations of 0.075-1.000 ng g^{-1} and non-spiked animal feed were measured using the strip test. As shown in Figure 3.12, the color intensity of test line clearly disappeared at 1 ng g^{-1} of the spiked RAC. The limit of detection (LOD) by the naked eye was thus found to be 1 ng g^{-1} of the spiked RAC in animal feed. For the application of the strip test in animal feed, the LOD of the spiked RAC (1 ng g^{-1}; 1ppb) was slightly higher than the LOD of the standard RAC (0.75 ng mL^{-1}; 0.75 ppb) because the detection system could be interfered with the matrix effect of unknown substances in animal feed. However, the LOD of the spiked RAC in this work is still lower than the

amount of RAC in the feed supplement (5 μg g^{-1}) [37], the MRLs in edible tissues (10-90 ng g^{-1}) and the previous reports of the AuNPs strip test in swine urine (>2 ng mL^{-1}) [55, 58] indicating that the proposed strip test is acceptably used for the detection of RAC sample.

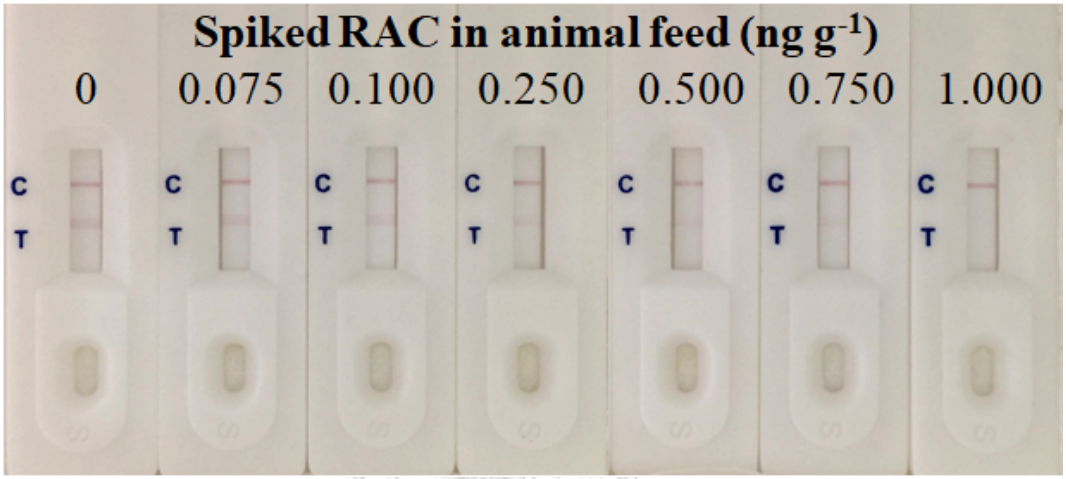

Figure 3.12 The Application of the paper-based lateral flow strip test for the non-spiked and spiked RAC detection in animal feed at 0.075-1.000 ng g^{-1}

To enhance the capability of the normal strip test evaluating only yes/no response, the semi-quantitative analysis was easily observed using ImageJ software. The relationship between the Δgray intensity and the concentrations of the non-spiked and spiked RAC in animal feed at 0.075-1.000 ng g^{-1} as shown in Figure 3.13 displayed the negative sigmoidal-shaped curve as same as the principle of the competitive format [66].

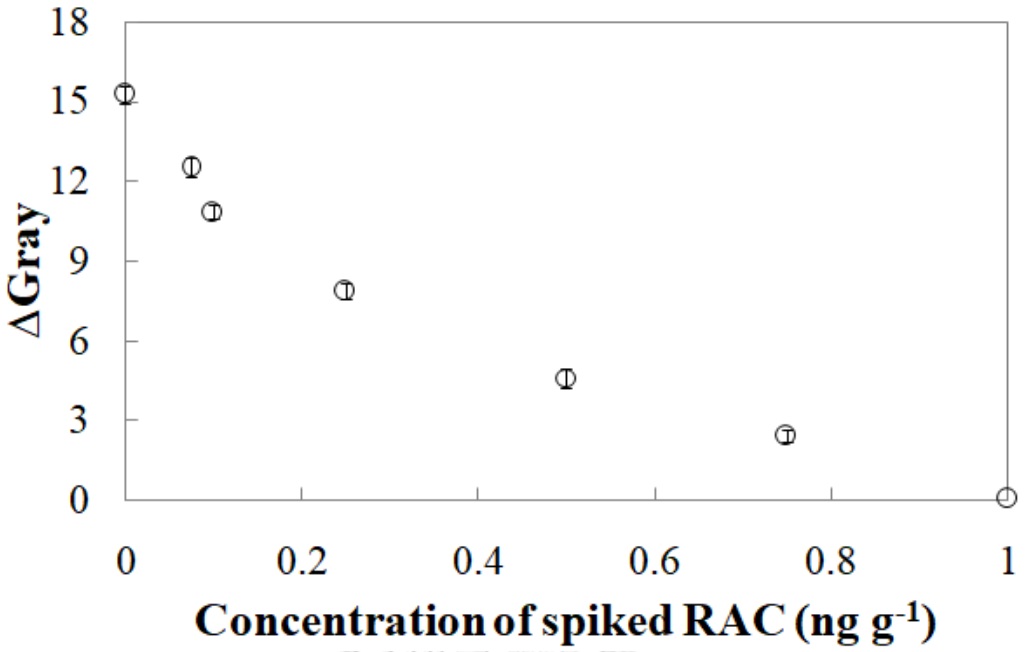

Figure 3.13 Relationship between the Δgray intensity and the concentrations of the non-spiked (0) and spiked RAC in animal feed at 0.075-1.000 ng g^{-1}

A semi-quantitative calibration curve was then constructed by plotting between the Δgray intensity and the logarithm of the concentrations of the spiked RAC as shown in Figure 3.14. The linear range was observed in the range of 0.075-0.750 ng g^{-1} with a good correlation of 0.992. The calculated LOD and LOQ were found to be 0.10 and 0.33 ng g^{-1}, respectively. The small error bars of the standard deviations observed from the independent strip test indicating high reproducibility.

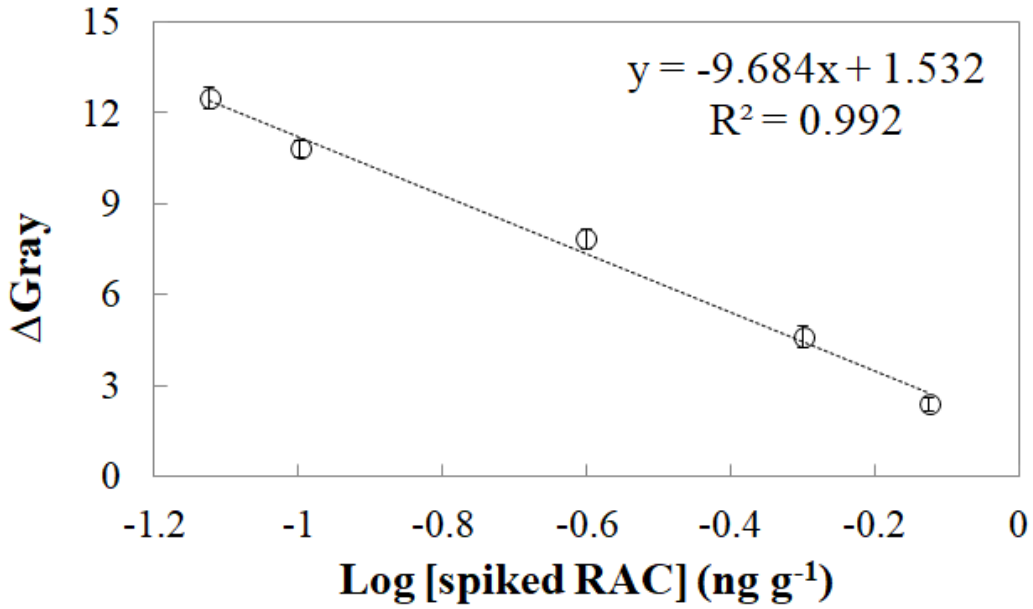

Figure 3.14 A calibration curve between the Δgray intensity and the logarithm of the concentrations of the spiked RAC at 0.075-0.750 ng g^{-1} (n = 6)

In order to test the practical applicability of the strip test, RAC spiked in animal feed at 0.10, 0.25 and 0.50 ng g^{-1} were measured to calculate recovery and relative standard derivation (RSD) percentages using the independent strip test on the same day (intra-assay) and on three different days (inter-assay) compared to conventional method (ELISA) as summarized in Table 3.1. The recovery percentages were found in a range from 96.9-100.2 with RSD of 2.5-2.8% for intra-assay (n = 6) and recovery percentages of 96.4-103.7 with RSD of 3.1-3.6% for inter-assay (n = 3). From these results, the small RSD percentages were observed for both intra- and inter-assays demonstrating the precision of the developed method. To compare the strip test with ELISA, a paired t-test at a 95% confidence interval was achieved on the results obtained from animal feed analysis. The calculated t-value obtained by the strip test is lower than the critical t-value. It could be concluded that there is no significant difference between the strip test and ELISA. Therefore, the proposed strip test could have strong

potential as an alternative device with reproducibility and precision for early screening of RAC in animal feeds.

Table 3.1 Comparison of paper-based lateral flow strip test and conventional method (ELISA) for RAC detection in animal feed

Spiked RAC ($ng\ g^{-1}$)	ELISA (n = 6) ($ng\ g^{-1}$)	Paper-based lateral flow strip test					
		Intra-assay (n = 6)			Inter-assay (n = 3)		
		RAC ($ng\ g^{-1}$)	Recovery (%)	RSD (%)	RAC ($ng\ g^{-1}$)	Recovery (%)	RSD (%)
0.10	0.09 ± 0.01	0.09 ± 0.01	96. 9	2.7	0.11 ± 0.01	103.7	3.6
0.25	0.24 ± 0.02	0.24 ± 0.02	98.3	2.8	0.22 ± 0.03	96.4	3.1
0.50	0.52 ± 0.04	0.51 ± 0.02	100.2	2.5	0.53 ± 0.02	100.8	3.3

3.4 Conclusion

A novel conjugation method of RAC-BSA based on the Mannich reaction was successfully developed providing advantages over the previous conjugation methods in term of simplicity, rapidity, single step and the requirement of less chemicals. This conjugation method gave RAC-BSA with a reasonable mole coupling ratio of 9:1. The RAC-BSA conjugation was applied to prepare the paper-based lateral flow strip test for RAC detection in animal feed. The limit of detections (LODs) could be observed using two methods including the qualitative analysis through naked-eye visualization and semi-quantitative analysis through the calculation from the semi-quantitative

calibration curve. The LOD of RAC detection in animal feed by the naked-eye was found to be 1 ng g^{-1} within 5 min without cross reactivity from the related compounds. The semi-quantitative analysis of RAC in animal feed using the strip test displayed linearity in the range of 0.075-0.750 ng g^{-1} with a good correlation of 0.992. The calculated LOD and LOQ were respectively found as low RAC as 0.1 and 0.33 ng g^{-1}. For the practical applicability test, the recoveries could be observed in a range of 96.4-103.7% with RSD of 2.5-3.6% for intra- and inter-assays, and the obtained results from the strip test agreed well with those obtained from ELISA. Therefore, the construction of a one-step, low cost and portable strip test was successfully applied for highly sensitive and specific detection of RAC with reproducibility and precision. Furthermore, the conjugation method based on the Mannich reaction could be further recommended to conjugate various compounds containing active hydrogen with carrier protein, and the proposed strip test could be applied for the detection of RAC in other samples such as swine urine and meats.

CHAPTER IV

DEVELOPMENT OF THE PAPER-BASED MICROFLUIDIC DEVICES AS AN AUTOMATED ENZYME-LINKED IMMUNOSORBENT ASSAY

This chapter reports the development of the paper-based microfluidic devices as an automated and one-step ELISA using a wax-printing method for the alpha-fetoprotein (AFP) determination in human serum.

Development of an automated wax-printed paper-based lateral flow device for alpha-fetoprotein enzyme-linked immunosorbent assay

Pattarachaya Preechakasedkit[a], Weena Siangproh[b], Nanthika Khongchareonporn[c], Nataya Ngamrojanavanich[c,d]*, Orawon Chailapakul[d,e]*

[a] Program in Biotechnology, Faculty of Science, Chulalongkorn University, Patumwan, Bangkok, 10330, Thailand

[b] Department of Chemistry, Faculty of Science, Srinakharinwirot University, Wattana, Bangkok, 10110, Thailand

[c] The Institute of Biotechnology and Genetic Engineering, Chulalongkorn University, Patumwan, Bangkok, 10330, Thailand

[d] Electrochemistry and Optical Spectroscopy Center of Excellence (EOSCE), Department of Chemistry, Faculty of Science, Chulalongkorn University, Patumwan, Bangkok, 10330, Thailand

[e] Center for Petroleum, Petrochemicals and Advanced Materials, Chulalongkorn University, Patumwan, Bangkok, 10330, Thailand

* Corresponding authors

Biosensors & Bioelectronics 102 (2018): 27-32

Abstract

In this study, a novel wax-printed paper-based lateral flow device has been developed as an alternative approach for an automated and one-step enzyme-linked immunosorbent assay (ELISA). The design pattern consisted of a non-delayed channel, a wax-delayed channel, a test zone and a control zone. This system was easily fabricated on a nitrocellulose membrane using a wax-printing method and then baked in an oven at 100 °C for 1 min. The four barriers of the wax-delayed channel could delay the flow time for 11 s compared to the flow time of the non-delayed channel. To use the device under optimal conditions, alpha-fetoprotein (AFP) was detected at a limit of detection (LOD) of 1 ng mL^{-1} and assessed with the naked eye within 10 min. A colorimetric intensity was also measured using a smart phone and computer software at a linear range of 0.1-100 ng mL^{-1} with a good correlation. Furthermore, the proposed device was successfully applied to detect AFP in human serum. Therefore, the wax-printing demonstrates a user-friendly, easy and quick method for the fabrication of the device, which could be used as a one-step, portable, disposable, low-cost, simple, instrument-free and point-of-care device for the automated ELISA.

4.1 Introduction

The enzyme-linked immunosorbent assay (ELISA) has been widely used as an analytical technique in many applications, especially in medical diagnosis, because of its key advantages, namely high specificity and sensitivity [67-70]. Initially, the conventional ELISA is performed in a 96-microwell plate and requires complicated steps, long analysis time and high volume of chemicals [71-74]. To reduce analysis time and volume of chemicals, in 2010, Cheng and co-workers firstly reported a paper-based ELISA by fabricating hydrophobic and hydrophilic areas on a filter paper using photolithography [6]. The layout of paper-based ELISA was similar to the plastic 96-microwell plates. Nevertheless, this paper-based ELISA still required complicated steps (at least 4 steps). To overcome these drawbacks, many researchers have developed a lateral flow immunoassay combined with ELISA (LFIA-ELISA) [75], using a nitrocellulose membrane (NCM) as a paper-based material to simplify the conventional ELISA and shorten the analysis time [32, 76, 77]. The LFIA-ELISA has attracted over the traditional gold nanoparticles-based LFIA in higher sensitivity leading to early-stage diagnosis and treatment of diseases [78, 79]. Unfortunately, colorimetric signals resulting from ELISA cannot be directly detected when using only an enzyme-labeled antibody [13, 80]. An additional step of the addition of a substrate solution is also required to produce the colorimetric signal [81-83]. Consequently, the conventional LFIA-ELISA requires at least 2 steps by loading a sample solution on the device until reaction completion and then immersing the device in the substrate solution for colorimetric evaluation [84, 85]. Additionally, washing steps are usually required before immersing the device in the substrate solution to remove the residue enzyme, which may cause the high background color on the device [86]. Therefore, the development of an automated LFIA-ELISA is a potential and interesting approach for overcoming the above drawbacks.

The automated sandwich LFIA-ELISA has been firstly developed by direct fabrication of a delayed channel on the NCM using inkjet printing [12]. The organic

solvent, including dipropylene glycol methyl ether acetate containing acrylic polymer, was used as solvent ink for patterning the delayed channel on the NCM. Although the automated device was successfully developed, this method still required solvent ink, which is a hazardous chemical for human health and an environmental contaminant. Another delayed-release sandwich LFIA-ELISA using a substrate pad attached to an asymmetric polysulfone membrane has also been reported for the automated assay [87]. The substrate pad should be prepared with complicated steps before being attached to the asymmetric polysulfone membrane. Then, the substrate pad attached to the asymmetric polysulfone membrane was stacked on the NCM. However, the limitations of this delayed-release technique are the use of complicated steps and the need for several types of materials to fabricate the delayed-release device.

Interestingly, a wax-printing method has been widely used to fabricate the paper-based devices because of several benefits, including low cost, ease of fabrication and no need of organic solvents [88, 89]. In 2010, Lu and co-workers firstly reported the wax printing on the NCM as the paper-based device [90]. The device, consisting of 3 mm diameter round as detection zones, was applied for a dot immunoassay. The dot immunoassay on the device still needed complicated steps (4 steps). The first time for using wax-printed pillars as delay barriers on the LFIA was reported by Riva and co-workers [91]. The existent wax-printed pillars could increase binding reaction times between human IgG as a model analyte and a gold nanoparticles-labeled antibody leading to the sensitivity improvement. Another improvement of LFIA has also been reported by fabricating three-dimensional paper-based devices using wax printing [92]. The devices were designed with multiple layers (5 layers) which each layer contained different reagents for immunoassay procedures and signal enhancement to improve sensitivity of gold nanoparticles label. Although the wax-delayed barriers were used for improving sensitivity of LFIA, there is no report about the use of the wax-delayed barriers for developing as the automated LFIA-ELISA.

In this study, a wax-printed paper-based lateral flow device has been developed as a novel, alternative, automated, one-step and instrument-free LFIA-ELISA. The advantages of the device over the conventional LFIA-ELISA and paper-based ELISA are short analysis time and single-loading sample leading to suitable use for point-of-care testing. The required design of the delayed barrier was directly fabricated on the NCM using the wax-printing method. The assay parameters were optimized, including the concentration of the immobilized antibody, the ratio of the enzyme-labeled antibody and the ratio of the substrate to obtain an optimal device. To demonstrate the usefulness of the proposed device, alpha-fetoprotein (AFP) was selected as an appropriate analyte. AFP is well-known as a key tumor marker for the early diagnosis of patients with liver cancer [93, 94]. Normally, the maximum level of AFP in healthy human is lower than 25 ng mL^{-1}, and the abnormally increased levels of AFP can cause various cancerous diseases such as hepatocellular cancer, yolk sac cancer, liver metastasis from gastric cancer, testicular cancer, and nasopharyngeal cancer [95, 96]. Therefore, the proposed device for rapid screening of AFP levels acts as a great significance for early cancer diagnosis and treatment. Furthermore, the data analysis using this device could be easily obtained from qualitative measurement by the naked eye and quantitative measurement through a smart phone and computer software.

4.2 Materials and Methods

4.2.1 Chemicals and materials

Bovine serum albumin (BSA), glycine, sodium dihydrogen phosphate, disodium hydrogen phosphate, sodium choloride, Tris(hydroxymethyl)aminomethane, casein, magnesium chloride and Tween 20 were purchased from Sigma Aldrich (St. Louis, MO,

USA). Alpha-fetoprotein (AFP), AFP monoclonal antibodies (10-1390 as a secondary antibody and 10-1391 as a primary antibody) were purchased from Fitzgerald (North Acton, MA, USA). Alkaline phosphatase (ALP) conjugation kit was purchased from Abcam (Cambridge, UK), BCIP/NBT (5-bromo-4-chloro-3'-indolyphosphate *p*-toluidine salt, nitro-blue tetrazolium chloride) substrate and substrate buffer solutions were purchased from Nacalai Tesque (Tokyo, Japan). Goat-antimouse IgG (GAM) was purchased from Jackson ImmunoResearch (West Grove, PA, USA). Standard pooled human serum was purchased from Kohjin Bio (Saitama, Japan). All solutions were prepared using 18Ω milli-Q water. Nitrocellulose membrane (AE100), glass fiber membrane (Standard 17) and absorbent pad (CF7) were purchased from Whatman-GE healthcares (Pittburgh, PA, USA).

4.2.2 Reagents preparation

Firstly, GAM was prepared to the concentration of 0.5 mg mL^{-1} using 0.01 M PBS buffer (pH 7.4), and the concentration of the AFP primary antibody (AFP 1° Ab) was varied using the same buffer. The AFP secondary antibody (AFP 2° Ab) was conjugated to ALP using ALP conjugation kits to be used as the enzyme-labeled antibody (AFP 2° Ab-ALP), and the optimal amount of the enzyme-labeled antibody were optimized. The BCIP/NBT substrate was diluted using the substrate buffer at various ratios to select an optimal value. The blocking buffer was 100 mM Tris buffer (pH 9.2) with 1% (w/v) casein, and the washing buffer was 0.01 M PBS (pH 7.4) containing 0.05% Tween 20. 100 mM Tris buffer (pH 9.2) was used as running buffer and diluted buffer of AFP.

4.2.3 Design of the wax-printed paper-based lateral flow device for sandwich ELISA

The design of the device for the sandwich ELISA is shown in Figure 4.1A. The components of the device consisted of three pads including sample, wax-printed and absorbent pads. The key concept of the wax-printed pad was the control of the reagent flow to complete the sandwich ELISA using single-loading sample. The wax-printed pad comprised of a non-delayed channel and a wax-delayed channel before merging into one main channel of a detection region containing test and control zones. The wax-delayed channel was specially designed with four barriers to delay the solution flow before passing a substrate region while the solution directly flowed through the non-delayed channel into an enzyme-labeled antibody region. At the detection region, the positions of the test and control zones were respectively labeled with T and C alphabets.

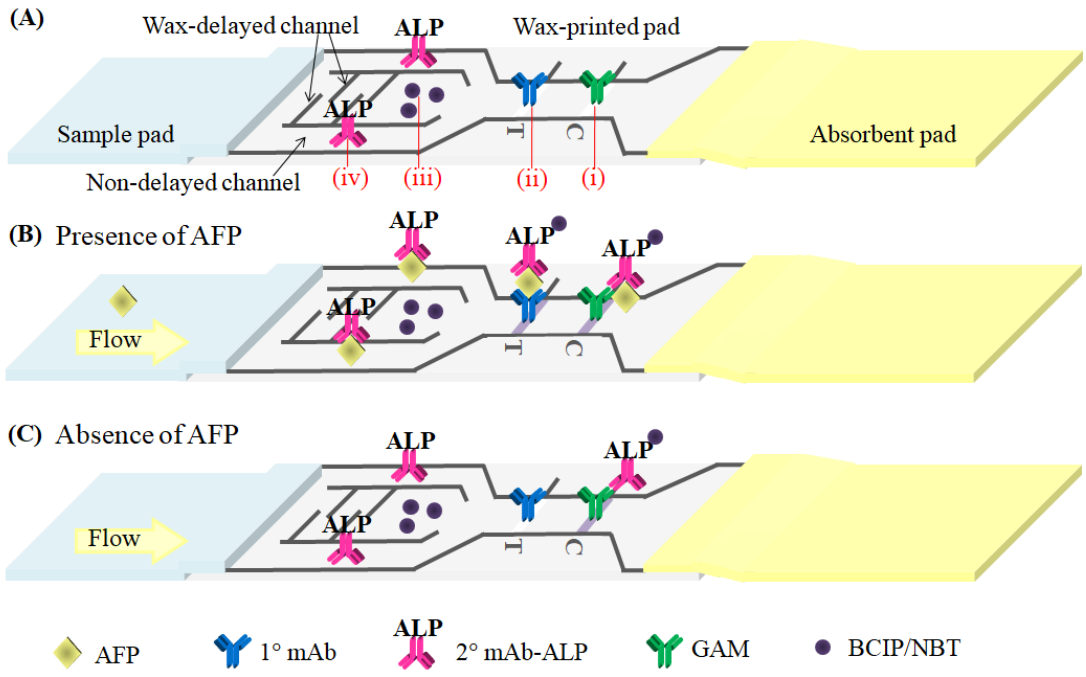

Figure 4.1 (A) Schematic illustration of the device which the wax-printed pad consisted of (i) GAM at the control zone, (ii) the AFP 1° Ab at the test zone, (iii) the BCIP/NBT at the substrate region and (iv) the AFP 2° Ab at the enzyme-labeled antibody region for (B) the presence of AFP and (C) the absence of AFP

4.2.4 Fabrication of the wax-printed paper-based lateral flow device

The pattern of the wax-printed pad was designed using the Adobe Illustrator program. The designed pattern was printed on the NCM using a wax printer (Xerox ColorQube 8570, Japan). After printing, the NCM was placed in an oven at 100 °C for 1 min to penetrate the wax into the NCM to create the barriers. Subsequently, 0.2 µL of GAM and the AFP 1° Ab were immobilized at the detection region on the control (i) and test (ii) zones of the wax-printed pad by pipetting, respectively. After drying for 30 min, the wax-printed pad was blocked using the blocking buffer for 30 min and compared to the unblocking pad, followed by three washings using the washing buffer. The wax-printed pad was then baked for 1 h at 37 °C. Afterwards, 0.5 µL of the

enzyme-labeled antibody and the substrate solution were spotted onto the wax-printed pad at the enzyme-labeled antibody region (iv) and the substrate region (iii), respectively, and allowed to dry. Finally, the wax-printed pad was placed on the backing card, subsequently attaching the sample and the absorbent pads. At this point, the device was ready for use.

4.2.5 Data analysis

After loading 100 µL of the AFP standard or samples on the device, the sandwich reaction was allowed completely, and the result data were visually assessed with the naked eye. In the presence of AFP (Figure 4.1B), the solution firstly flowed through the non-delayed channel, and the AFP was able bind to the AFP 2° Ab-ALP to form the AFP and AFP 2° Ab-ALP complex. Then, the complex moved to be captured by the AFP 1° Ab at the T zone in the sandwich form. At that time, the solution also flowed through the wax-delayed channel to delay the flow time, and the BCIP/NBT gradually moved to bind to the complex and export the purple color signal on the T and C zones. Conversely, in the absence of AFP (Figure 4.1C), the flow procedure also occurred as well as the presence of AFP. However, no molecule could bind to the AFP 2° Ab-ALP, and the color signal only appeared on the C zone. Furthermore, the data analysis of the developed method was quantitatively evaluated through a smart phone and computer software (Image J).

4.3 Results and Discussion

4.3.1 Automated solution flow on the wax-printed paper-based lateral flow device

As previous work [97], the sample pad of gold nanoparticles-based LFIA was cut in a trapezoid shape to be bigger size than the NCM. The trapezoid shape of sample pad could facilitate the solution flow speed and improve sensitivity. This concept has interestingly attracted for the modification in our device design. The proposed device was designed to be the size of 6 mm in a width and 55 mm in a length as shown in Figure 4.2. The NCM was wax-printed to be used as a wax-printed pad consisting of the non-delayed channel, the wax-delayed channel with four barriers, the test zone and the control zone. The absorbent and the sample pads were placed on the top and the bottom of the wax-printed pad, respectively. For wax-printed design of this device, the top and the bottom of the detection region were designed to be the trapezoid shape, and the detection region was smaller than the normal size. The trapezoid shape at the bottom of the detection region could help the solution merged from two non-delayed channels, and the trapezoid shape at the top could facilitate the absorbed of the solution by the absorbent pad. The small size of the detection region could decrease the volume of reagents (0.2 µL per each) immobilized on the T and C zones.

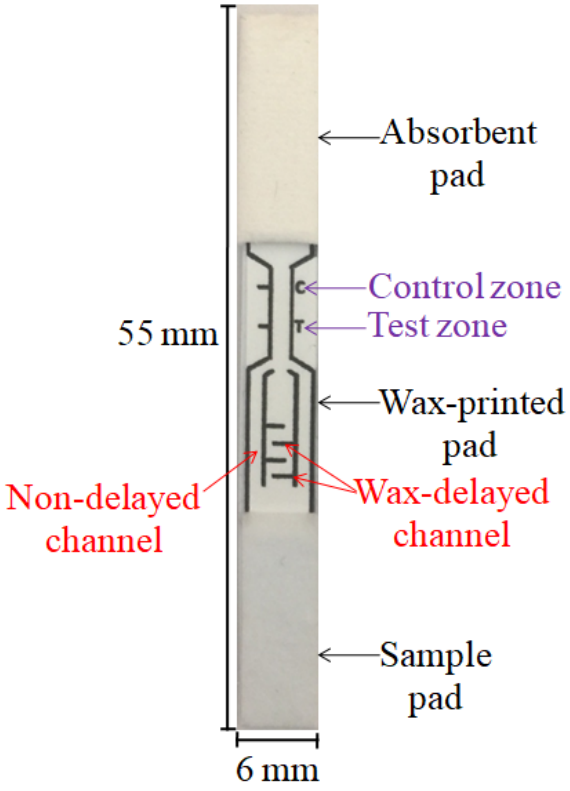

Figure 4.2 The device with the size of 6 mm in a width and 55 mm in a length consisting of the sample pad at the bottom of the wax-printed pad, the wax-printed pad, and the absorbent pad at the top of the wax-printed pad which the wax-printed pad contained the non-delayed channel, the wax-delayed channel with four barriers, the test zone and the control zone

To clearly evaluate the automated solution flow, two different colors of food-colored dyes were dropped on the enzyme-labeled antibody region and the substrate region (Figure 4.3A). After loading 100 µL of running buffer, the solution flowed by capillary force from the sample pad to the wax-printed pad (Figure 4.3B). The solution moved through the non-delayed channel to the enzyme-labeled antibody region, and the food-colored dyes could gradually migrate at approximately 32 s (Figure 4.3C), whereas the solution that flowed through the wax-delayed channel reached the substrate region at 43 s (Figure 4.3D). These results indicated that the four barriers of

the wax-delayed channel could successfully delay the flow time for 11 s approximately compared to the flow time of the non-delayed channel. After that, the solution from two non-delayed channels was merged before migrating to the detection region (Figure 4.3E) and was then flowed to the test zone (Figure 4.3F). The solution also migrated from the substrate region to the detection region (Figure 4.3G). Then, the residue solution from the enzyme-labeled antibody region was absorbed by the absorbent pad (Figure 4.3H) followed by the absorbed of the residue solution from the substrate region (Figure 4.3I). Finally, all residue solution was completely absorbed by the absorbent pad (Figure 4.2J), and the reaction of the running buffer flow using the food-colored dyes spotted on the enzyme-labeled antibody and the substrate regions was completed within 360 s.

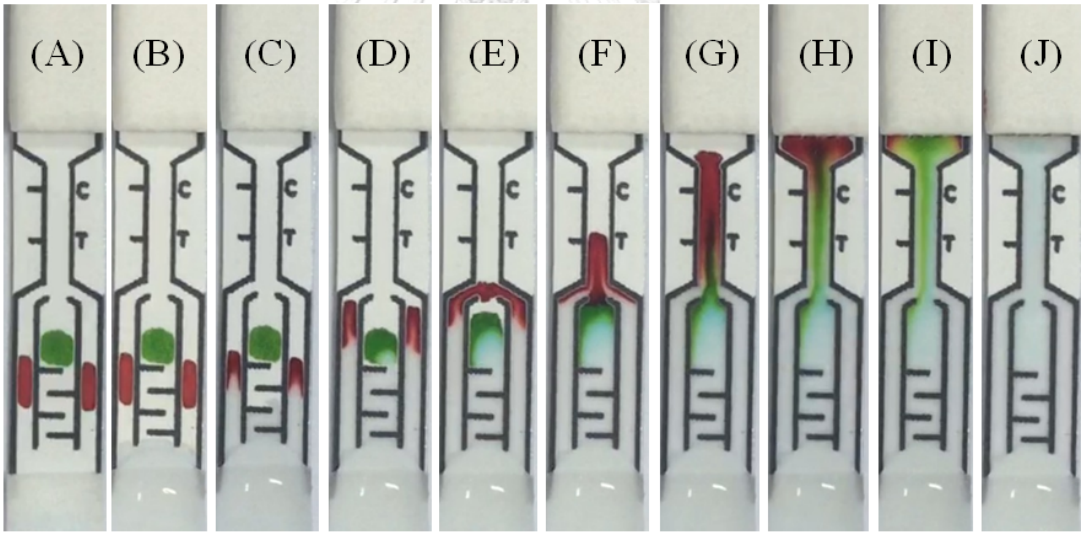

Figure 4.3 Automated solution flow on the device using the different food-colored dyes on the enzyme-labeled antibody and substrate regions which the images were captured at (A) 0 s, (B) 10 s, (C) 32 s, (D) 43 s, (E) 58 s, (F) 75 s, (G) 105 s, (H) 215 s, (I) 250 s and (J) 360 s

4.3.2 Optimization of the wax-printed paper-based lateral flow device

To prepare the device, the blocking step of the wax-printed pad before dropping the enzyme-labeled antibody and the substrate, was compared to the unblocking pad. In this comparison, the concentration of the AFP 1°Ab was 1 mg mL^{-1} with 1:10 AFP 2°Ab-ALP and BCIP/NBT ratios (solution:buffer), and 100 µL of 100 ng mL^{-1} AFP. After loading the AFP (Figure 4.4), the results from the use of the unblocking pad indicated that the movement of the solutions was not good enough to produce the color signals on the T and C zones. Conversely, all solutions of the ELISA completely moved using the blocking pad, demonstrating the color signals on the T and C zones. Consequently, the blocking step enabled to optimize the automated migration on the device.

Additionally, conventional paper-based ELISA normally gives a qualitative visual signal by adding the substrate to the enzyme-labeled antibody in yes/no responses according to analyte concentrations. Therefore, the optimal parameters, including the effect of the concentration of the immobilized antibody (AFP 1°Ab), the ratio of the enzyme-labeled antibody (AFP 2°Ab-ALP) and the ratio of the substrate (BCIP/NBT) should be studied herein similar to the checkerboard titration in the conventional ELISA [98].

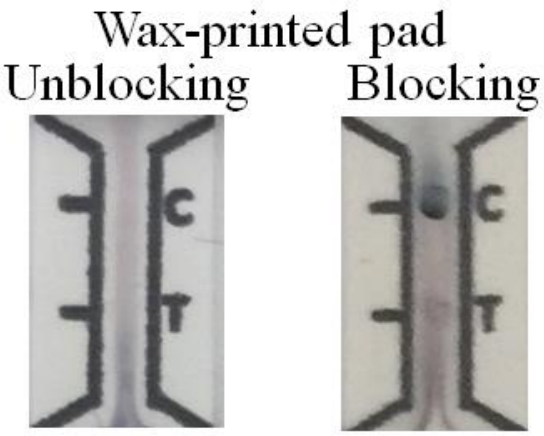

Figure 4.4 The effect of the unblocking and blocking wax-printed pads using 1 mg mL^{-1} of the immobilized antibody, the enzyme-labeled antibody and substrate ratios of 1:10

4.3.2.1 The effect of the concentration of the immobilized antibody

The use of a suitable concentration of the immobilized antibody affects the highest efficiency and the lowest cost of the device. The effect of the concentration of the AFP 1°Ab as the immobilized antibody was studied herein using concentration of 0.50, 0.75, 1.00 and 1.25 mg mL^{-1}. The device was prepared by fixing the AFP 2°Ab-ALP and the BCIP/NBT ratios of 1:10 (solution:buffer), and 100 µL of 100 ng mL^{-1} AFP was loaded. As shown in Figure 4.5, the results indicated that the color intensity on the T zone increased when the concentration of the AFP 1°Ab increased. However, at a concentration of the AFP 1°Ab of 1.25 mg mL^{-1}, the color intensity of the C zone was too weak because the AFP and AFP 2°Ab-ALP complex was well captured at a higher concentration of the AFP 1°Ab, and no enough complex was able bind to GAM at the C zone. Therefore, the concentration of AFP 1°Ab of 1.00 mg mL^{-1}, which gave a clear signal with equal color intensity on both T and C zones, was selected as the optimal value to prepare the device.

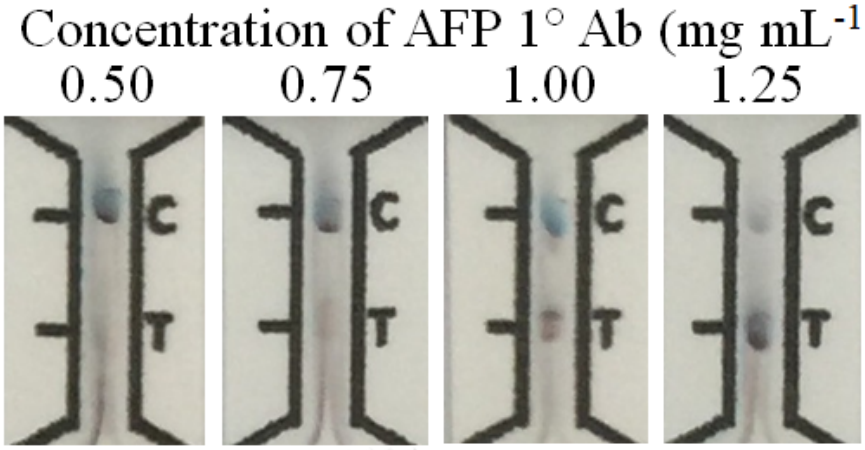

Figure 4.5 The effect of the concentration of the immobilized antibody between 0.50-1.25 mg mL^{-1} using the enzyme-labeled antibody and substrate ratios of 1:10

4.3.2.2 The effect of the ratio of the enzyme-labeled antibody

After obtaining the optimal concentration of the AFP 1°Ab of 1.00 mg mL^{-1}, the effect of the ratio of the AFP 2°Ab-ALP as the enzyme-labeled antibody was then studied using different AFP 2°Ab-ALP ratios of 1:1, 1:5, 1:10 and 1:15 (solution:buffer). The BCIP/NBT ratio used was 1:10 loading 100 µL of the 100 ng mL^{-1} AFP. The results showed that the high concentration of the AFP 2°Ab-ALP decreased the migration of both the loading buffer and the AFP 2°Ab-ALP molecule, leading to the weak color intensities of the T and C zones at the ratios of 1:1 and 1:5, respectively (Figure 4.6). For the 1:10 and 1:15 ratios, the solution could move well on the device. However, the color intensity of the ratio 1:15 was also weak because the amount of the AFP 2°Ab-ALP was insufficient. Therefore, the AFP 2°Ab-ALP ratio of 1:10 demonstrating the good color intensity for both T and C zones was chosen in this study.

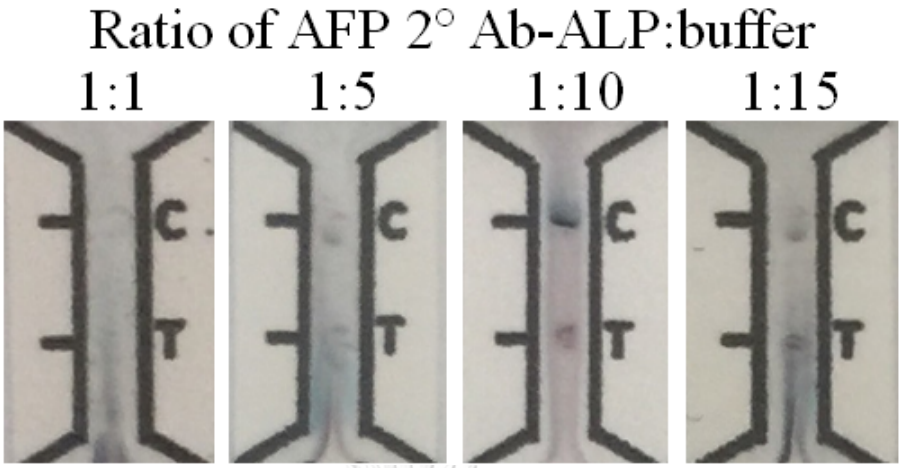

Figure 4.6 The effect of the ratio of the enzyme-labeled antibody at 1:1, 1:5, 1:10 and 1:15 using 1 mg mL^{-1} of the immobilized antibody and the substrate ratio of 1:10

4.3.2.3 The effect of the ratio of the substrate

After selecting the concentration of the AFP 1°Ab of 1.00 mg mL^{-1} and the AFP 2°Ab-ALP ratio of 1:10, the effect of the ratio of the BCIP/NBT as the substrate was finally studied using the BCIP/NBT ratios of 1:1, 1:5, 1:10 and 1:15 (solution:buffer). After loading 100 µL of the 100 ng mL^{-1} AFP, the results were presented in Figure 4.7. According to the binding interaction between the ALP and the BCIP/NBT [99], the BCIP firstly binds to the ALP, resulting in the blue color, and then the BCIP is oxidized by the NBT, resulting in the purple color. The use of the BCIP/NBT ratio of 1:1 indicated that the blue color of the BCIP only appeared because some wax barriers were destroyed. After destroying the wax, the direct binding between the enzyme-labeled antibody and the substrate occurred generating the purple color at the enzyme-labeled antibody and substrate regions. However, a few enzyme-labeled antibodies and BCIP molecules could still migrate on the wax-printed pad, resulting in the blue color of BCIP on the C line. After using 1:5, 1:10, 1:15 ratios, the color intensities

decreased with the increase in the diluted substrate buffer. Therefore, the BCIP/NBT ratio of 1:5 was selected as the optimal condition to fabricate the device for AFP.

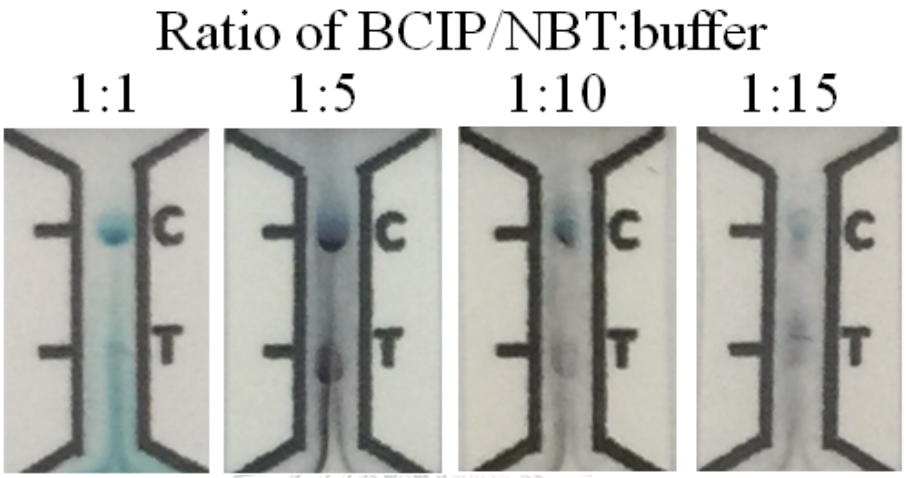

Figure 4.7 The effect of the ratio of the substrate at 1:1, 1:5, 1:10 and 1:15 using 1 mg mL^{-1} of the immobilized antibody and the enzyme-labeled antibody ratio of 1:10

4.3.3 Determination of alpha-fetoprotein using the wax-printed paper-based lateral flow device

After obtaining the optimal conditions, as mentioned above, the device was conducted by loading the standard AFP in the concentration range of 0-100 ng mL^{-1}. For a qualitative assay visualized with the naked eye, the color intensity on the T zone appeared in the presence of AFP whereas the absence of AFP gave the disappearance of the intensity on the T zone. The increase in the concentration of AFP also increased the color intensity on the T zone. A limit of detection (LOD) of the qualitative assay was selected from the minimal amount of the standard AFP that still allowed detecting the color intensity of the T zone after loading the solution for 10 min. The color intensity of the T zone was visually detected up to a concentration of 1 ng mL^{-1} AFP (Figure 4.8). Therefore, the normal range of AFP levels (lower than 25 ng mL^{-1}) was

inside the LOD of 1 ng mL^{-1} AFP, indicating that the device could be used for screening cancerous diseases caused by high AFP levels. In addition, the proposed device has a higher sensitivity than the gold nanoparticles test strip and shows a sensitivity of 1 ng mL^{-1}, which is similar to that of the quantum dot test strip [15]. However, the use of the quantum dot test strip still needs a special instrument to obtain a fluorescent signal.

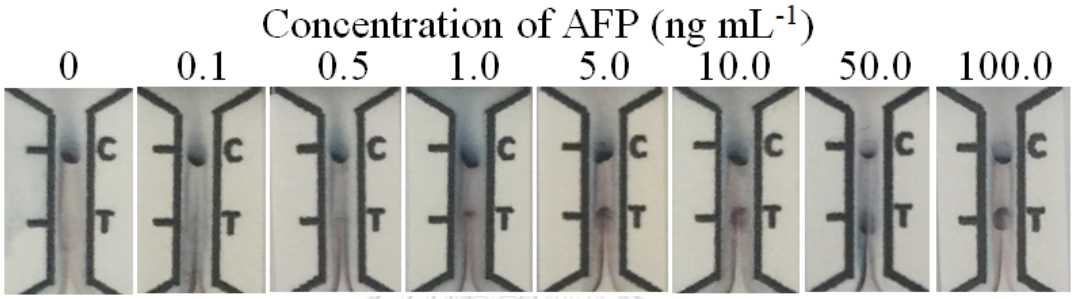

Figure 4.8 Photographic images of the device after loading the AFP concentration between 0 and 100 ng mL^{-1}

Normally, a qualitative analysis demonstrates only yes/no response through the naked eye which is not enough for identifying the amount of analyte in sample. A quantitative analysis using camera phones and computer software has been reported to enhance capability of colorimetric assay [18]. After the normal qualitative analysis, this device was quantitatively examined in triplicate by plotting the Δgray intensity as a function of the AFP concentration (Figure 4.9).

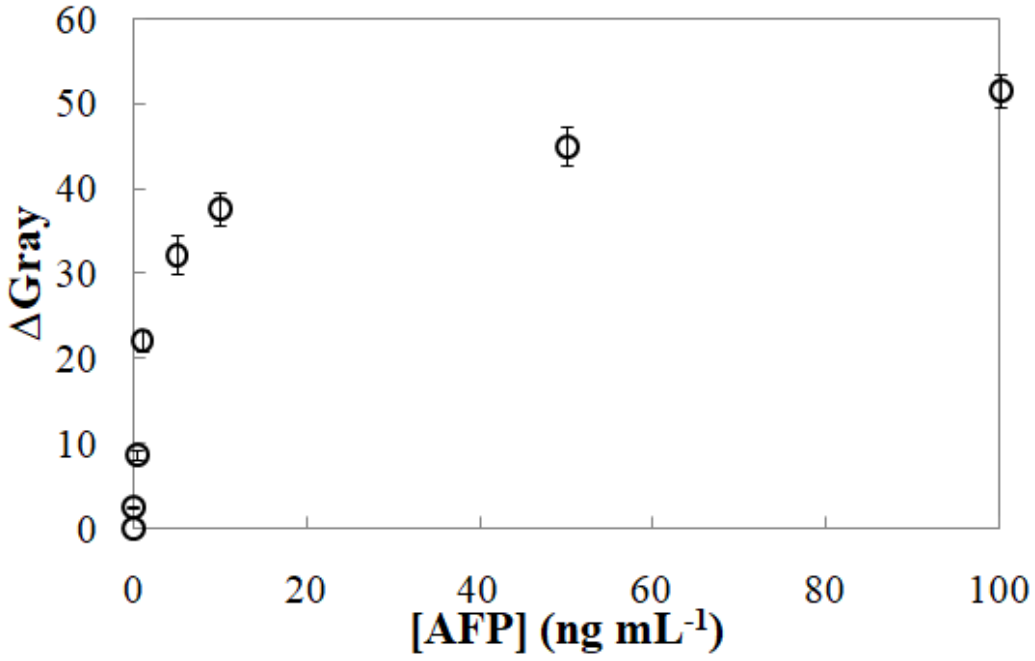

Figure 4.9 The relationship between Δgray and various concentrations of the AFP between 0 and 100 ng mL^{-1}

A quantitative calibration curve plot of the Δgray as a function of the logarithm of the AFP concentration provided a linear range between 0.1-100 ng mL^{-1} with a good correlation of 0.988 (Figure 4.10). The small error bars of the standard deviations using three independent devices indicated high reproducibility. The calculated LOD from equation of the calibration curve was also found to be 0.1 ng mL^{-1} (LOD = Blank + SD_{Blank}).

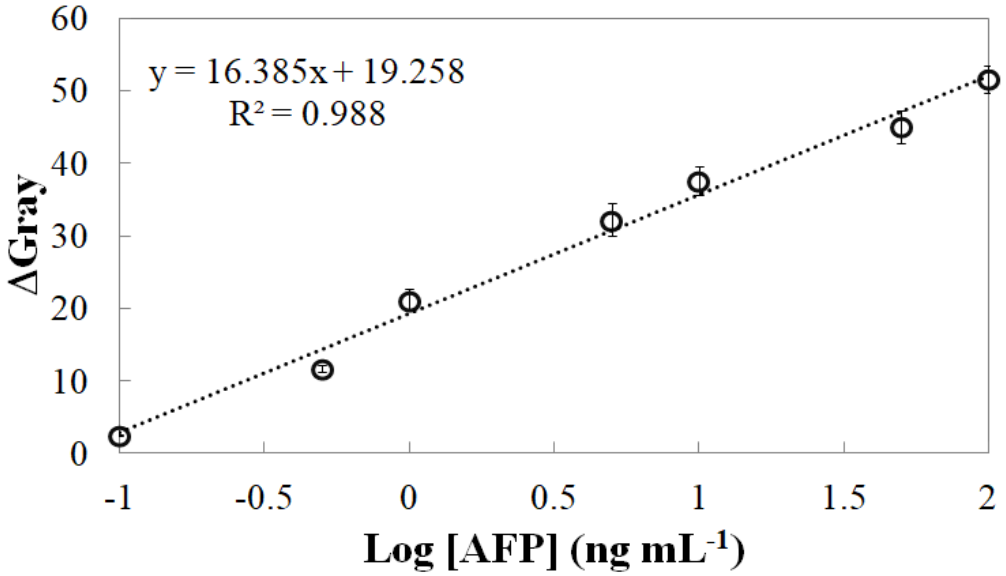

Figure 4.10 A quantitative calibration curve plot of Δgray as a function of the logarithm of the AFP concentration (n = 3)

4.3.4 Sample application

The practical applicability of the device was tested by detecting the spiked AFP in human serum samples at a final concentration of 1, 5, 25, 50, 75 ng mL^{-1} and non-spiked human serum (Figure 4.11A). The results indicated that no T zone was detected in the non-spiked human serum, while the color signal on the T zone could be observed after loading the spiked AFP in human serum ($\geq$1 ng mL^{-1}). The Δgray as a function of the spiked AFP concentration in triplicate was also plotted demonstrating the small error bars (Figure 4.11B).

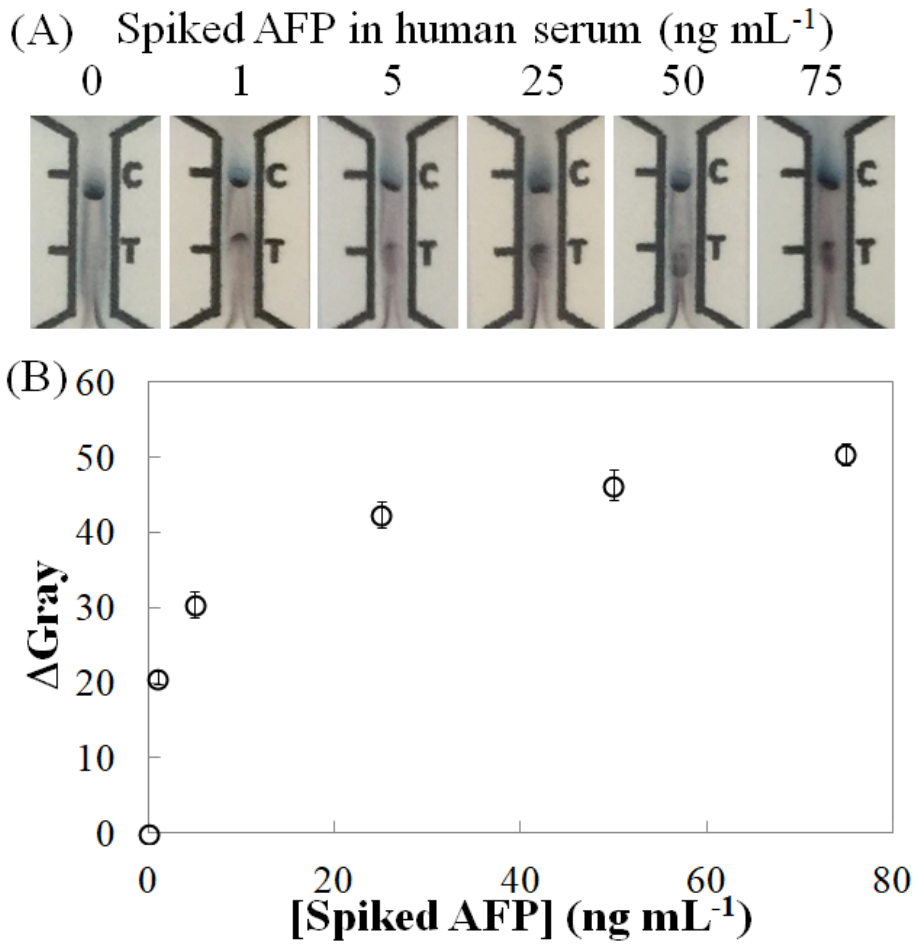

Figure 4.11 (A) Photographic images of the device application in the AFP spiked human serum at a final concentration of 0, 1, 5, 25, 50 and 75 ng mL^{-1} and (B) a relationship between Δgray and the AFP spiked human serum (n = 3)

Furthermore, the recoveries also ranged from 96.0% to 106.0% with the relative standard deviation (RSD) ranging from 3.0 to 4.2% as outlined in Table 4.1. Therefore, this proposed device could be accepted as an alternative device to screen and determine the AFP levels in biological fluids.

Table 4.1 Recoveries of the spiked AFP in human serum detected by the wax-printed device (n = 3)

Spiked AFP concentration (ng mL^{-1})	Measured concentration (ng mL^{-1})	Recovery (%)	RSD (%)
0	ND	ND	ND
1.0	1.0 ± 0.1	100.0 ± 4.4	4.2
5.0	4.8 ± 0.2	96.0 ± 3.3	3.5
25.0	24.6 ± 0.9	98.4 ± 3.6	3.6
50.0	51.6 ± 1.8	103.2 ± 3.5	3.5
75.0	79.5 ± 2.4	106.0 ± 3.2	3.0

*ND=Not Detectable

4.4 Conclusion

An automated and one-step enzyme-linked immunosorbent assay (ELISA) was developed using a novel wax-printed paper-based lateral flow device. The simple and user-friendly wax-printing method enabled to fabricate a large amount of the designed pattern on the NCM within 2 min (1 min for printing and 1 min for wax-melting). The flow time on the device was effectively delayed using the barriers of the wax-delayed channel. The proposed device, under optimal conditions, enabled to determine the AFP levels within 10 min in both qualitative and quantitative analysis with a LOD of 1 ng mL^{-1}, a calculated LOD of 0.1 ng mL^{-1}, a linear range of 0.1-100 ng mL^{-1} and a good correlation of 0.988. The spiked AFP levels were successfully detected in human serum demonstrating the recovery percentages ranging from 96.0 to 106.0 and RSD ranging from 3.0-4.2%. Consequently, the proposed device exhibits as an alternative approach

for the AFP detection comprising of a fast analysis, on-site and equipment-free measurements, portability and disposability. Furthermore, the proposed device could be further improved reproducibility by printing T and C lines using high precision equipment and developed to the detection of several other biomarkers.

CHAPTER V

DEVELOPMENT THE IMMUNOASSAY ON THE PAPER-BASED MICROFLUIDIC DEVICES USING A NOVEL FLUORESCENT LABEL

This chapter presents the development of the immunoassay on the paper-based microfluidic devices for screening both hypothyroidism and hyperthyroidism using a hybrid nanocomposite of gold nanoparticles and fluorophores of europium (III) doped silica (AuNPs@SiO_2-Eu^{3+}) as a novel fluorescent label.

Gold nanoparticle core - europium (III) chelate fluorophore-doped silica shell hybrid nanocomposite for lateral flow immunoassay of human thyroid stimulating hormone with dual signal readout

Pattarachaya Preechakasedkit[a] , Kota Osada[b], Yuta Katayama[b], Nipapan Ruecha[b], Koji Suzuki[b], Orawon Chailapakul[c]*, Daniel Citterio[b]*

[a] Program in Biotechnology, Faculty of Science, Chulalongkorn University, Patumwan, Bangkok, 10330, Thailand.

[b] Department of Applied Chemistry, Faculty of Science and Technology, Keio University, Yokohama, Kanagawa, 223-8522, Japan

[c] Electrochemistry and Optical Spectroscopy Center of Excellence (EOSCE), Department of Chemistry, Faculty of Science, Chulalongkorn University, Patumwan, Bangkok, 10330, Thailand

*Corresponding authors

Analyst 143 (2018): 564-570

Abstract

Hybrid nanocomposite particles composed of a gold core coated with a europium (III)-chelate fluorophore-doped silica shell (AuNPs@SiO_2-Eu^{3+}) have been synthesized and applied as antibody labels in lateral flow immunoassay (LFIA) devices for the determination of human thyroid stimulating hormone (hTSH). Labeling of monoclonal anti-hTSH antibodies with AuNPs@SiO_2-Eu^{3+} nanocomposites allows for both colorimetric and fluorometric observation of assay results on LFIA devices, relying on visible light absorption due to the localized surface plasmon resonance of the Au-core and the fluorescence emission of the Eu(III)-chelate-modified shell under UV handlamp irradiation (365 nm), respectively. The possibility for dual signal readout provides an attractive alternative for LFIAs: instantaneous naked eye observation of the AuNP colorimetric signal as in conventional LFIAs for hypothyroidism detection, and more sensitive fluorescence detection to assess hyperthyroidism.The limits of detection (LOD) for naked eye observation of LFIA devices are 5 μIU mL^{-1} and 0.1 μIU mL^{-1} for the colorimetric and fluorimetric detection, respectively. Using the fluorescence detection scheme in combination with a smartphone and digital color analysis, a quantitative linear relationship between the red intensity and the logarithmic concentration of hTSH was observed (R^2=0.988) with a calculated LOD of 0.02 μIU mL^{-1}. Finally, LFIA devices were effectively applied for detecting hTSH in spiked diluted human serum with recovery values between 100 – 116%.

5.1 Introduction

The human thyroid stimulating hormone (hTSH), a 28 kDa glycoprotein hormone secreted by thyrotroph cells in the pituitary gland, is a key protein in the control of thyroid function, which is an important factor affecting human health [100, 101]. Commonly, the normal level of hTSH has been reported to be in the range of 0.5—5 μIU mL^{-1}. Deviating levels of hTSH cause hyperthyroidism at lower levels and hypothyroidism at higher levels [102]. Therefore, a simple screening and monitoring method covering the normal range of hTSH is essential for the identification of patients having abnormal hTSH levels. Immunoassays, making use of the specific binding interaction between an antigen and an antibody, are the most widely used analytical methods for hTSH detection, because of their high specificity and sensitivity [103, 104]. Lateral flow immunoassays (LFIAs) are a particularly attractive immunoassay format for hTSH detection with many advantageous features, such as low cost, short analysis time, simplicity, disposability, portability and on-site measurements, while requiring only small amounts of reagents [105, 106]. In this context, gold nanoparticles (AuNPs) are commonly used as antibody labels for colorimetric visual detection. Unfortunately, immunoassays relying on AuNP labels alone suffer from relatively low analytical sensitivity [107]. Typically, commercial LFIA devices using AuNPs as labels can be only applied for hTSH detection in the hypothyroidism range [108], due to their low sensitivity. In order to increase the detection sensitivity for immunoassays in general, different labels and detection methods have been reported, such as enzyme labels [109, 110], electrochemiluminescent labels [111, 112], redox active labels [113, 114] and organic fluorophores [115, 116]. Although these approaches provide higher detection sensitivity compared to AuNP labels, many of them lack the operational simplicity of the latter by suffering from drawbacks such as requiring longer analysis

time, expensive instruments and multiple operation steps. In particular, most of these alternative labels are not readily applicable to LFIAs.

Recently, a hybrid nanocomposite of AuNP-conjugated malachite green isothiocyanate for a highly sensitive surface-enhanced Raman scattering (SERS)-based LFIA has been reported for screening hTSH levels [108]. However, a Raman microscope and qualified personnel for instrument operation and data analysis are required. Direct naked eye readout, the most advantageous feature of LFIAs, is not possible.

Among several types of alternative antibody labels, hybrid nanocomposite materials [108, 117, 118] combining multiple functionalities into a single unit are most promising in terms of analytical sensitivity, while maintaining operational simplicity. In this work, a hybrid nanocomposite composed of a AuNP core and a europium (III) chelate fluorophore-doped silica shell (AuNPs@SiO_2-Eu^{3+}) is proposed and its application as antibody label for a lateral flow immunoassay of hTSH is demonstrated. The AuNPs display a strong visual light absorption, due to the localized surface plasmon resonance (LSPR) phenomenon [119]. Fluorophore-doped silica nanoparticles provide higher stability than free fluorophores, because they isolate and protect the light emitter from direct environmental influence, such as photo decomposition by free radicals caused by light exposure [120]. Finally, europium (III) chelate fluorophores show a large Stokes shift, which prevents signal self-quenching and allows for high dye loading into nanoparticles [121].

A LFIA based on antibody labeling with a hybrid nanocomposite of AuNPs@SiO_2-Eu^{3+} has been developed for simple and instantaneous hTSH detection. An optimized AuNPs@SiO_2-Eu^{3+} core/shell nanocomposite was synthesized and characterized. The high colloidal stability of the AuNPs allowed the immobilization of a silica shell doped with relatively large amounts of fluorophores without particle aggregation. The hybrid nanocomposite utilized as antibody label in this work enables dual signal detection, providing an attractive alternative for LFIAs: the instantaneous

naked eye observation of the AuNP colorimetric signal as in conventional LFIAs for hypothyroidism detection, and the more sensitive detection of the europium (III) chelate fluorescence under UV-hand lamp irradiation to assess hyperthyroidism.

5.2 Experimental section

5.2.1 Reagents and materials

(3-Aminopropyl)triethoxysilane (APTES) and tetraethyl orthosilicate (TEOS) were purchased from Tokyo Chemical Industry Co., Ltd (Tokyo, Japan). 28% ammonia solution, bovine serum albumin (BSA), sodium bicarbonate, sodium carbonate, sucrose and Tween 20 were purchased from Wako Pure Chemical Industries Ltd (Osaka, Japan). 3-(Trihydroxysilyl)propylmethyl phosphonate, monosodium salt solution (THPMP), O-[2-(3-mercaptopropionyl-amino)ethyl]-O'-methylpolyethylene glycol (m-PEG-SH, Mw=5000), tetrachloroauric[III]acid trihydrate, gold nanoparticles (20 nm diameter, OD 1, stabilized suspension in 0.1 mM PBS, reactant free) and goat anti-mouse IgG were purchased from Sigma Aldrich (St. Louis, MO, USA). Human thyroid stimulating hormone 98% pure (hTSH) was purchased from RayBiotech (Norcross, GA, USA). Monoclonal mouse antibodies (mAbs) recognizing hTSH (Clone: 5403, 5404) were purchased from MedixBiochemica (Espoo, Finland). All solutions were prepared using 18 mΩ Milli-Q water. Nitrocellulose membranes (NCMs) attached to a backing card (HF180MC100) were purchased from Millipore Corporation (Billerica, MA, USA), and the absorbent pad (CF7) was purchased from Whatman-GE Healthcare Life Sciences (Pittsburgh, PA, USA). Standard pooled human serum was purchased from Kohjin Bio (Saitama, Japan).

5.2.2 Preparation of AuNPs@SiO_2-Eu^{3+}core/shell nanocomposites

The preparation of fluorescent AuNPs@SiO_2-Eu^{3+} core/shell nanocomposites was undertaken in three steps: (1) AuNPs were prepared by the reduction of tetrachloroauric[III]acid trihydrate using sodium citrate. Briefly, 100 mL of 0.01% (w/v) $HAuCl_4$ solution was heated at 100 °C and 1 mL of 0.01% (w/v) trisodium citrate was quickly added under stirring. After 30 min of refluxing and cooling to room temperature, the surface of the AuNPs was modified with thiol-terminated polyethylene glycol (m-PEG-SH) by adding 1.59 mL of 5 mg mL^{-1} ethanolic m-PEG-SH into 60 mL of the as-prepared AuNP colloid solution to improve the colloidal stability of the AuNPs in solution [122]. After stirring for 30 min under dark condition, the modified AuNPs were spinned down by centrifugation at 20,000 g for 30 min and washed three times with ethanol to remove excess reagents. Finally, the PEGylated AuNPs were re-dispersed into a mixture consisting of 48 mL ethanol, 11.25 mL water and 0.75 mL of 28% aqueous ammonia solution. (2) A silica shell was grown on the AuNPs by adding TEOS (60 µL) to the PEGylated AuNP solution prepared under (1) above and stirring at room temperature for 2 h under dark condition, followed by washing according to the washing step described just above. The washed AuNPs were re-dispersed in 57.5 mL of ethanol. (3) A 3-aminopropyltriethoxysilane (*APTES*)-conjugated 4,4'-bis(1",1",1"-trifluoro-2",4"-butanedione-6"-yl)-chlorosulfo-o-terphenyl (BTBCT) europium (III) chelate (APTES-BTBCT-Eu^{3+}) was obtained by adding 14.4 µL of 100 mg/mL ethanolic solution of $EuCl_3 \cdot 6H_2O$ (3.9 µmol) into a mixed solution of 4.65 mg of BTBCT (7.7 µmol) (synthesized according to a previously published method [123]) and 3.6 µL of APTES (15.4 µmol) in 1 mL of absolute ethanol. 1 mL of the resulting APTES-BTBCT-Eu^{3+} solution was used for the formation of the Eu^{3+} complex doped silica shell without any purification. After mixing 57.5 mL of the bare silica shell coated AuNP dispersion described under (2) above with 2.5 mL of 28% aqueous ammonia solution and 30 µL

of TEOS (10% (v/v) in ethanol) and stirring for 15 min under dark condition, 1 mL of the as-synthesized ethanolic APTES-BTBCT-Eu^{3+} solution was added, and the resulting mixture was stirred for 24 h under dark condition at room temperature. Finally, the obtained AuNPs@SiO_2-Eu^{3+} core/shell nanocomposites were centrifuged and re-dispersed in 57.5 mL of ethanol and stored at 4 °C until use. This Eu^{3+} complex doped silica shell coating process was repeated multiple times until reaching the desired number of coatings.

To reduce aggregation of AuNPs@SiO_2-Eu^{3+} nanocomposites and increase their dispersion stability, the nanocomposites were further surface-modified with APTES and THPMP [124]. For this purpose, 150 µL of 10% (v/v) ethanolic TEOS solution and 2.5 mL of 28% aqueous ammonia solution were added to the AuNPs@SiO_2-Eu^{3+} dispersion described above (57.5 mL), followed by stirring at room temperature for 1 h. Then, 60 µL of a 10% (v/v) aqueous THPMP solution was added, and after stirring for 15 min, another 60 µL of 10% (v/v) ethanolic TEOS solution was added. The resulting mixture was stirred at room temperature for 24 h. The obtained amine/phosphonate-modified AuNPs@SiO_2-Eu^{3+} were centrifuged at 20,000 g, washed once with ethanol and twice with water, re-suspended in 60 mL of water, and finally stored at 4 °C for further use. The functionalized AuNPs@SiO_2-Eu^{3+} nanocomposites were characterized using transmission electron microscopy (TEM), dynamic light scattering (DLS), UV-VIS and fluorescence spectrophotometry.

5.2.3 Conjugation of monoclonal antibody to AuNPs@SiO_2-Eu^{3+}

For conjugation of the anti-hTSH antibody 5404 to the AuNPs@SiO_2-Eu^{3+} label, the nanocomposites were briefly centrifuged to exchange the water for 0.025 M carbonate buffer (pH 9.5). 1 mL of the buffer-suspended nanocomposite was then mixed with 80 µg/mL of anti-hTSH antibody. After standing for 12 h at 4 °C, nonspecific

sites of the conjugate were blocked by directly adding 100 µL of 0.01 M PBS (pH 7.4) containing 2% (w/v) BSA and 4% (w/v) sucrose for 6 h at 4 °C. Finally, the conjugate was concentrated by centrifugation at 8000 g for 10 min, followed by removal of the supernatant and resuspension in 100 µL of 0.01 M PBS (pH 7.4) with 2% (w/v) BSA, 4% (w/v) sucrose and 0.05% (v/v) Tween 20. The ready to use labeled antibodies were stored at 4 °C.

5.2.4 Fabrication of lateral flow immunoassay (LFIA) devices

Test (T) and control (C) lines were fabricated on a NCM (2.5 × 15 cm) with a plastic backing card using an 0.8 mm Souffle ballpoint pen (Sakura Seiki Co., Ltd., Tokyo, Japan) mounted in a computer-controlled Silhouette Cameo craft cutting device (Silhouette America, Inc., Lindon, UT, USA). First, the inks of the ballpoint pens were removed, and the ink holding tubes were sonicated in water to remove residual ink and dried at 37 °C for 30 min. After that, 50 µL of 2 mg mL^{-1} of anti-hTSH 5403 for the T line and 0.5 mg mL^{-1} of goat anti-mouse IgG for the C line were filled into independent ink holding tubes and the pens were re-assembled. Line drawing was performed after setting the cutting mode of the craft cutter to copy paper (medium) with a speed of 3 cm s^{-1} and a thickness setting of 1, and the position of C and T lines was adjusted at 0.7 and 1.2 cm distance from the top of the NCM, respectively (Figure 5.1). The NCM was dried at 37 °C for 30 min. The residual volume of antibody solution inside pens can be stored at 4 °C for further use. The absorbent pad (2.2 × 15 cm) was attached to the end of the NCM with 2 mm of overlap and then cut into 4.0 mm-width devices.

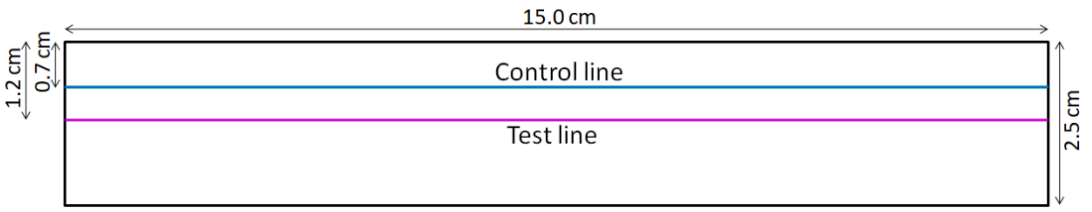

Figure 5.1 Nitrocellulose membrane with drawing position of T and C lines

5.2.5 Assay procedure using the LFIA devices and data analysis

For the detection of hTSH, 200 µL of various concentrations of aqueous hTSH standards (0-50 µIU mL^{-1}) prepared in 0.01 M PBS (pH 7.4) was mixed with 4 µL of AuNPs@SiO_2-Eu^{3+} labeled anti-hTSH in a 96-well plate for 5 min. LFIA devices were then immersed into the mixed solutions from the NCM side for 25 min. To evaluate the fluorescence signal, UV hand lamps (Funakoshi, Tokyo, Japan) were used as exciting light source inside a Mini UV viewing cabinet (UVP, Upland, CA, USA), and the emission signal was captured with an iPhone 6 plus (Apple, Cupertino, CA, USA) through a 520 nm longpass filter (Sigma Koki Co., Ltd, Tokyo, Japan). For quantitative data analysis, the color intensity (gray scale value for colorimetric assay or red (R) value for fluorescence assay) of test lines was extracted from recorded photographs using the ImageJ software (NIH, Bethesda, MD, USA).

5.2.6 Application in human serum

Human serum was prepared by 10-fold dilution in 0.01 M PBS (pH 7.4) as non-spiked sample. Spiked serum samples were prepared by adding the standard hTSH at concentrations of 0.5, 5 and 10 µIU mL^{-1}, which covers the normal and hypothyroidism ranges. Samples were analyzed following the assay procedure described above.

5.3 Results and discussion

5.3.1 Design and characterization of AuNPs@SiO_2-Eu^{3+} nanocomposites

AuNPs@SiO_2-Eu^{3+} core/shell nanocomposites were prepared and applied to LFIA devices in this work. The preparation of the AuNPs@SiO_2-Eu^{3+} core/shell nanocomposites is schematically shown in Figure 5.2.

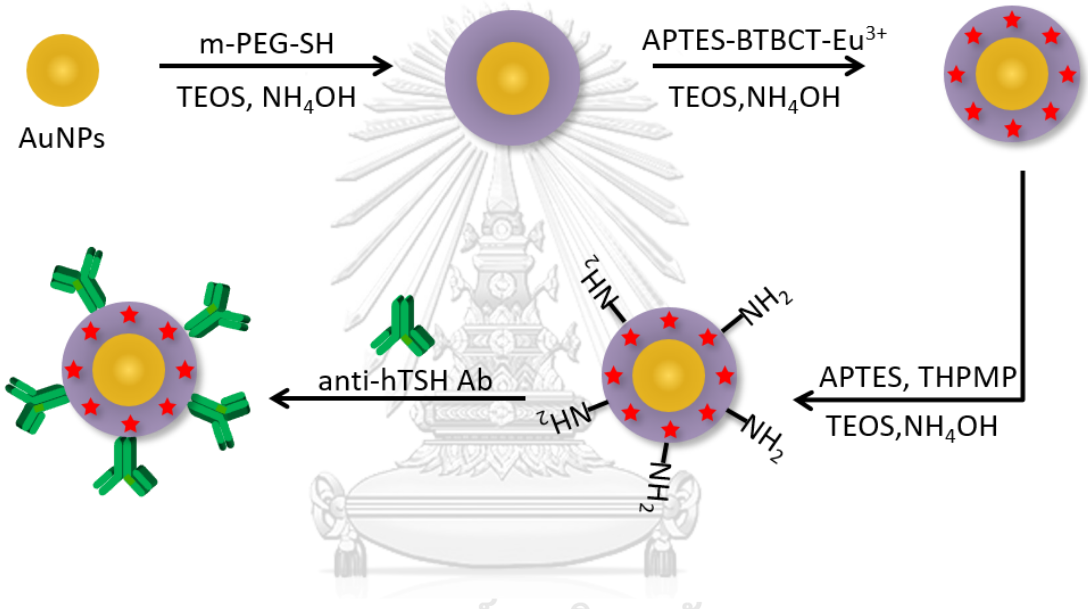

Figure 5.2 Schematic of AuNPs@SiO_2-Eu^{3+} nanocomposite preparation

First, the AuNP cores were synthesized using classical sodium citrate reduction (Figure 5.3), followed by surface modification with m-PEG-SH. These AuNPs served as conventional colorimetric antibody labels and simultaneously as core for silica shell functionalization. The average particle size measured by DLS was approximately 45.1 $\pm$ 5.3 nm.

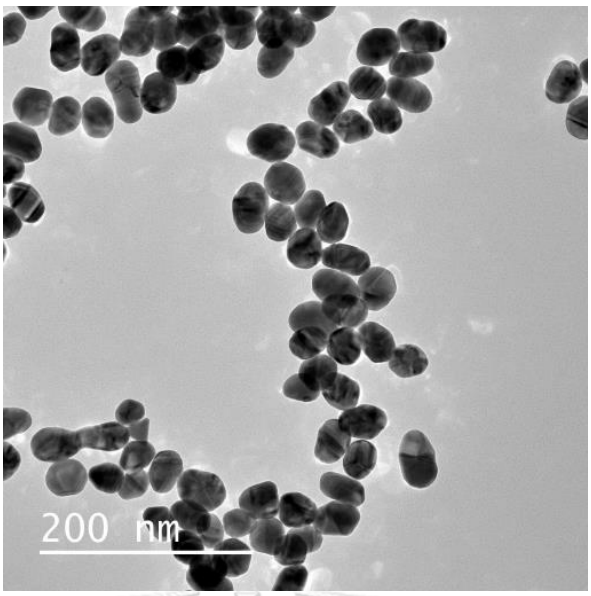

Figure 5.3 TEM image of AuNPs used as core

A bare silica layer was coated onto the AuNPs to act as a spacer between the Au surface and the fluorescent Eu^{3+} complex to prevent fluorescence quenching known to occur in close proximity to a gold surface [125]. Next, a BTBCT-Eu^{3+} complex fluorophore-doped silica layer was built up by covalently linking the APTES-conjugated fluorophore into a TEOS-built silica layer. This fluorophore doping process was repeated multiple times to achieve the highest possible fluorescence signal without sacrificing the colloidal stability of the labeling NPs. The increasing absorbance at 335 nm originating from the BTBCT ligand indicated increasing amounts of BTBCT-Eu^{3+} fluorophore surrounding the AuNPs@SiO_2 nanoparticle surface upon repeated doping cycles, while the AuNP LSPR absorbance peak at around 540 nm remained unchanged (Figure 5.4).

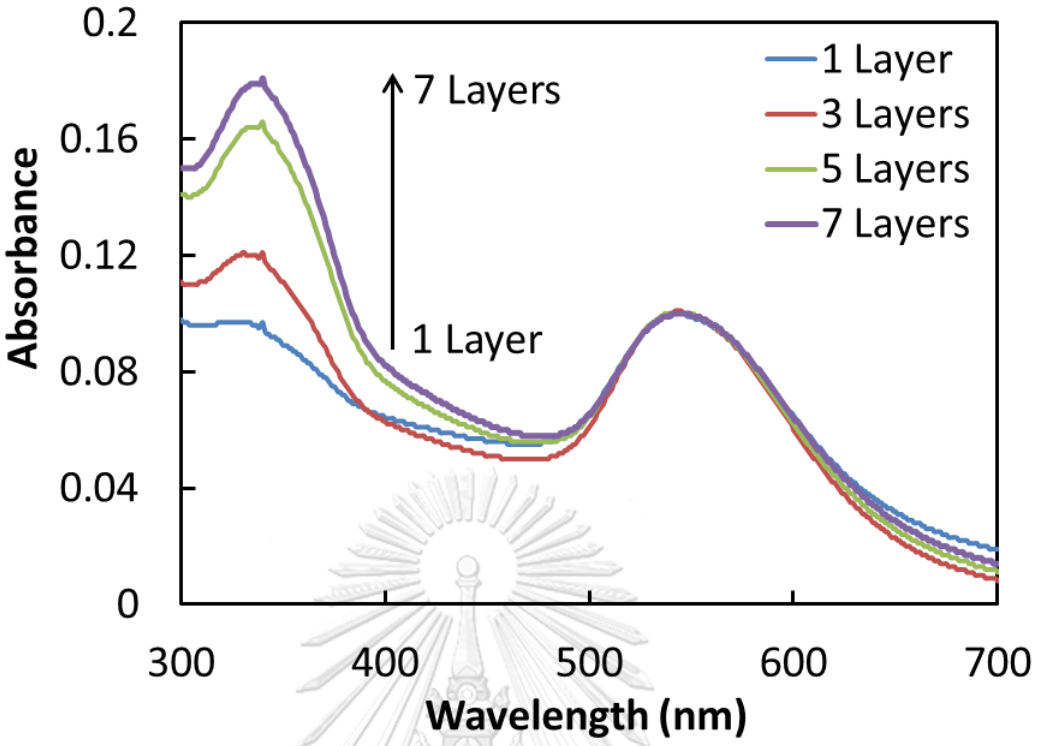

Figure 5.4 UV-vis absorption spectra of AuNPs@SiO_2-Eu^{3+} upon increasing numbers of fluorophore doping cycles

At the same time, the fluorescence emission intensity of Eu^{3+} at 620 nm significantly increased with increasing numbers of fluorophore doping cycles (Figure 5.5).

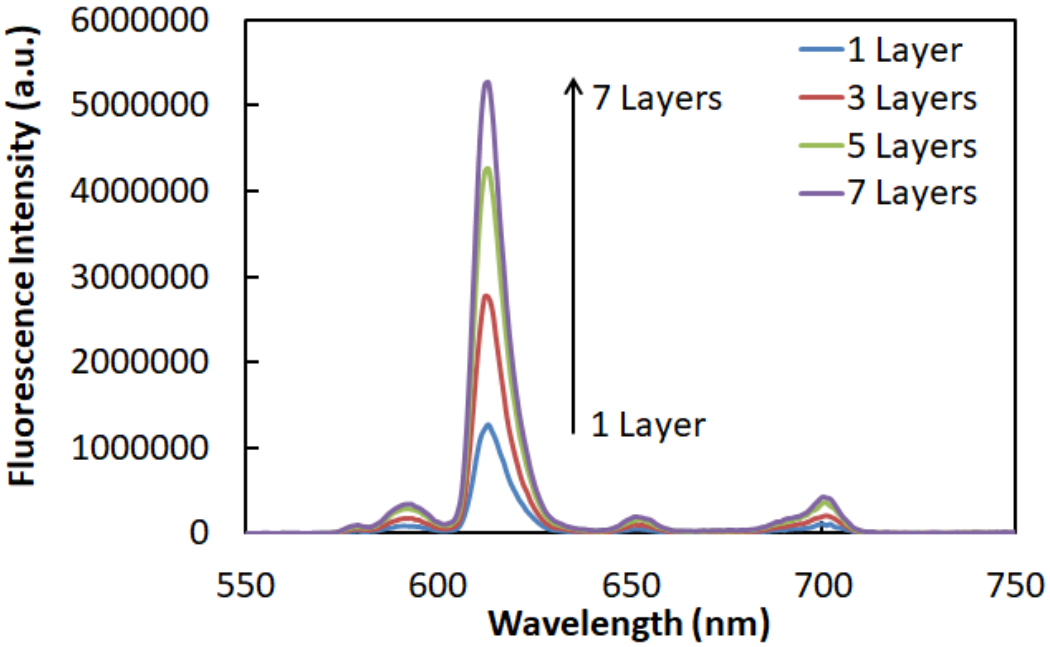

Figure 5.5 Fluorescence emission spectra of AuNPs@SiO_2-Eu^{3+} upon increasing numbers of fluorophore doping cycles

Under TEM images (Scale: 1 μM) in Figure 5.6, Stable dispersion of nanocomposites was observed up to 5 cycles of fluorophore doping, whereas strong NP aggregation occurred at larger numbers of doping cycles (Figure 5.6D). Therefore, 5 fluorophore shell doping cycles were selected as optimum condition for further experiments. Finally, the surface of the optimized AuNPs@SiO_2-Eu^{3+} nanocomposites was modified with phosphonate and amino groups to improve the long-term colloidal stability of the nanoparticles [124, 126] and to increase their dispersion stability [125], respectively.

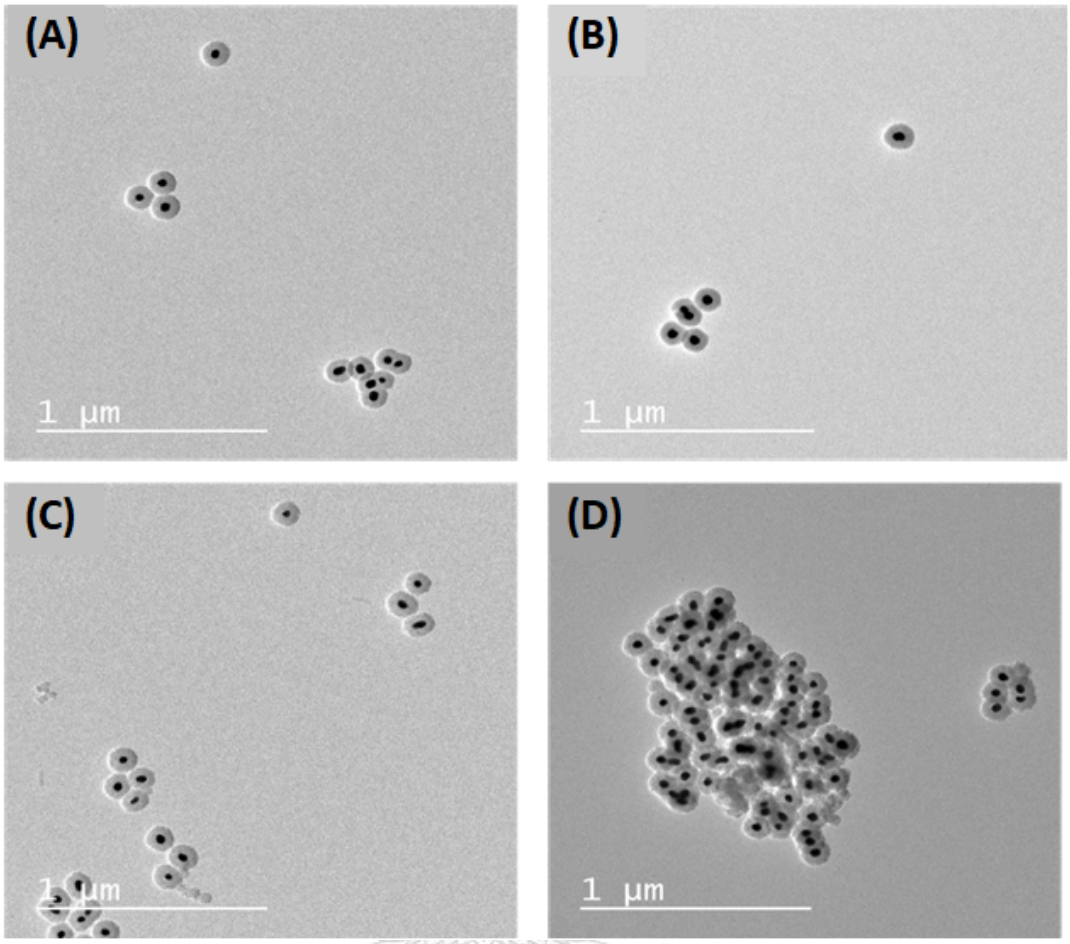

Figure 5.6 TEM images of AuNPs@SiO_2-Eu^{3+} nanocomposites after different numbers of APTES-BTBCT-Eu^{3+} fluorophore doping cycles from (A-D) 1, 3, 5 and 7 layers

A TEM image (Scale: 200 nM) of the final AuNPs@SiO_2-Eu^{3+} nanocomposite labeling nanoparticles is shown in Figure 5.7, with an average size of 167.2 ± 2.4 nm measured by DLS.

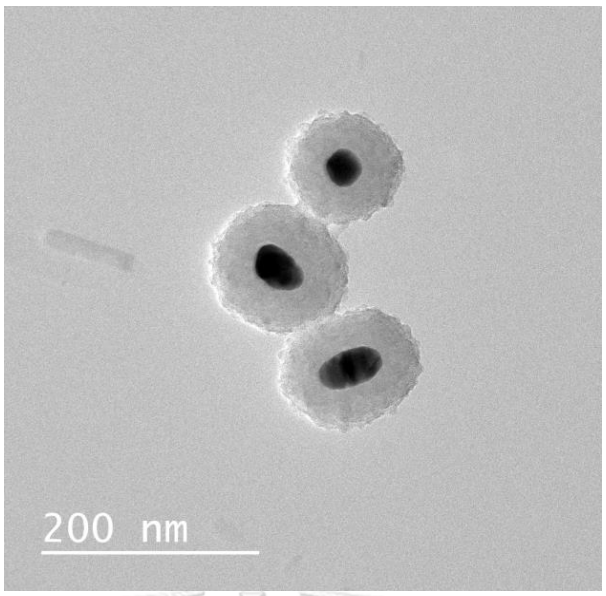

Figure 5.7 TEM image of the final AuNPs@SiO_2-Eu^{3+} after 5 cycles of fluorophore doping and surface modification with phosphonate and amino groups

5.3.2 Fabrication of control and test lines using a ballpoint pen mounted in a cutting device

Most previously reported methods of capture antibody deposition for the formation of control lines (C) and test lines (T) lines on nitrocellulose membranes for LFIAs rely on dispensing systems [30]. Although this method provides good deposition reproducibility, it requires an expensive instrument and a relatively high volume of reagent solution for initial filling (300 µL). A known low-cost approach is the use of micropipettes [62]. However, applying a reagent solution from a micropipette has some limitations, including significantly lower deposition reproducibility and inhomogeneous capture antibody distribution along the drawn line, leading to inconstant color intensities and hence, difficulties for quantitative analysis. In this work, a conventional ballpoint pen mounted in a computer-controlled cutting device was evaluated as an alternative method for the deposition of reagents for C and T lines onto NCMs. For this purpose, the knife blade originally mounted in the cutting device was replaced by a

pen holder for the ballpoint pen (Figure 5.8A). With the pen applied in this study, widths of C and T lines were found to be 1.5 mm.

The deposition reproducibility was confirmed by analyzing the gray scale intensity of ballpoint pen drawn control lines after loading 0.01 M PBS (pH 7.4) as running buffer solution (Figure 5.8B). The results indicated nearly constant intensities of 7 independently fabricated LFIA devices. Therefore, the computer-controlled cutting device in combination with the selected ballpoint pen is a suitable alternative simple and low cost approach for reproducible T and C line fabrication, requiring only small volumes of antibody solution.

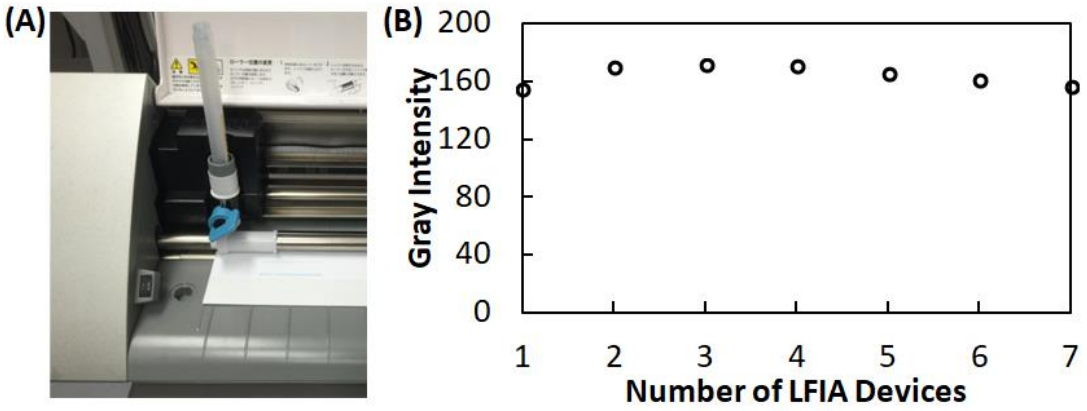

Figure 5.8 (A) Image of a ballpoint pen mounted in a craft cutting devices, and (B) Gray scale intensity of the control line of 7 independently ballpoint pen fabricated LFIA devices

5.3.3 Dual signal detection LFIA for hTSH

In most cases, signaling from LFIAs relies on direct visual observation of the reddish AuNP LSPR absorbance for qualitative assays, or the measurement of the colorimetric signal intensity for quantitative assays, for example by a densitometer. Alternatively, fluorescently labeled antibodies in combination with UV light excitation

can be used. The latter generally enable dual colorimetric / fluorometric signal detection [127, 128]. However, the molar extinction coefficients of commonly used fluorescent compounds are significantly lower compared to AuNPs. In this work, the AuNPs@SiO_2-Eu^{3+} hybrid nanocomposites serve as multifunctional labels for the optional colorimetric or fluorescence-based signal readout. The resulting LFIAs cannot only be used for the naked eye-based colorimetric hTSH detection relying on conventional AuNPs, but also for the more sensitive fluorescence-based detection of lower hTSH levels. The operating principle of the AuNPs@SiO_2-Eu^{3+}-based LFIA is illustrated in Figure 5.9. Conventional LFIA strips are composed of four constituents: a sample loading pad, a conjugated pad with pre-deposited labeled signaling antibody, a NCM and an absorbent pad. The LFIA strips applied in this work consist only of a NCM and an absorbent pad. The sample to be analyzed is pre-mixed with a solution containing AuNPs@SiO_2-Eu^{3+}-conjugated antibodies. The solution-phase results in increased reaction rates between the antigen and the labeled antibodies compared to the solid phase approach using sample loading and conjugate pads. The LFIA device is then directly immersed into the solution containing the complex formed between the antigen and the AuNPs@SiO_2-Eu^{3+}-conjugated antibody. In this way, most hTSH bound to AuNPs@SiO_2-Eu^{3+}-conjugated antibodies reach the test line, contributing to the signal. In the case of the solid phase approach, the interaction time between hTSH and AuNPs@SiO_2-Eu^{3+}-conjugated antibodies is limited by the flow time required to reach the test line, which might result in the capture of hTSH not bound to AuNPs@SiO_2-Eu^{3+}-conjugated antibodies and therefore, not contributing to a signal.

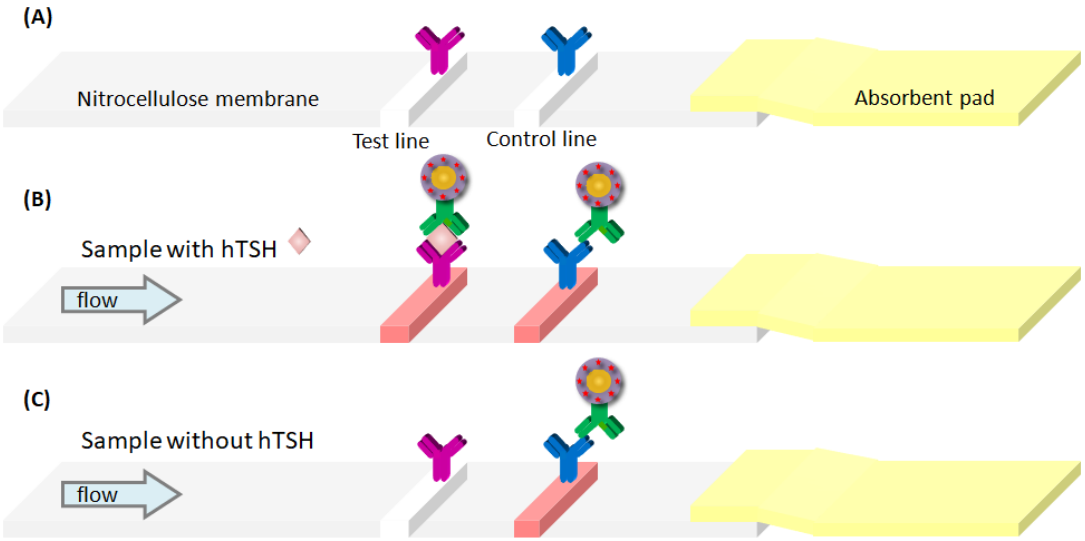

Figure 5.9 Schematic illustration of the AuNPs@SiO_2-Eu^{3+}-based LFIA for hTSH detection: before (A) and after applying a sample solution in the presence (B) or absence (C) of hTSH.

Figure 5.10A shows the visually perceived colorimetric signal originating from the AuNP core of the labeling nanocomposites for standard solutions containing various concentrations of hTSH. Figure 5.10B on the other hand, shows a photograph taken of the identical LFIA strips under 365 nm UV irradiation from a handheld lamp, allowing to observe the fluorescence emission from the SiO_2-Eu^{3+} shell. The lowest detectable hTSH concentrations based on simple naked eye observation of test lines on LFIA devices were found to be 5 μIU mL^{-1} in colorimetric detection mode (Figure 5.10A) and 0.1 μIU mL^{-1} in fluorometric mode (Figure 5.10B), indicating a 50-fold lower limit of detection (LOD) when using the fluorescence signal. It should be noted that the darkened areas visually observed at test line positions in Figure 5.10A are shadows caused by minor indent grooves formed in the NCM during ballpoint pen application of capture antibodies. These grooves are clearly distinguishable from the red colorimetric signal induced by the presence of the AuNPs@SiO_2-Eu^{3+}-conjugated

signaling antibody. For more quantitative data analysis, the red color intensity on the RGB scale observed for the fluorescence signal (Figure 5.10B) was extracted by digital colorimetry.

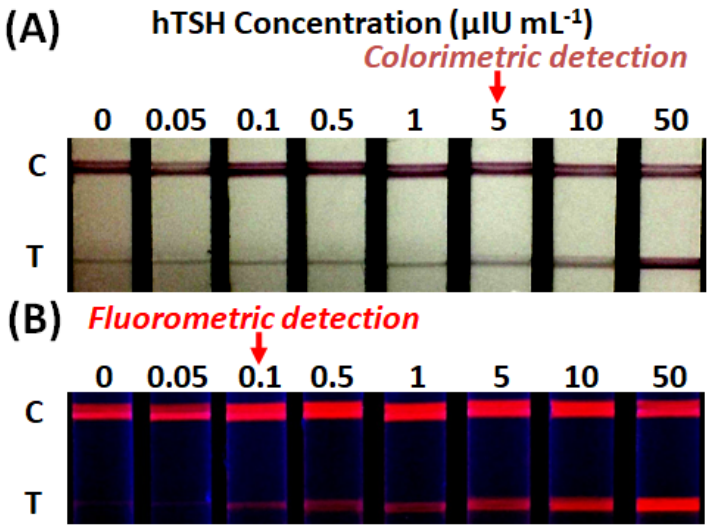

Figure 5.10 Photographs of LFIA devices after application of different concentrations of hTSH between 0 and 50 μIU mL^{-1} in (A) colorimetric (under ambient light) and (B) fluorometric (under 365 nm UV light) readout

The corresponding calibration curve is shown in Figure 5.11. A logarithmically linear response was observed in the range of 0.05-50 μIU mL^{-1}. The small error bars obtained for assays performed with three independent devices indicate a high reproducibility. The calculated LOD from equation (LOD = $Mean_{blank}$ + $3SD_{blank}$) was found to be 0.02 μIU mL^{-1}.

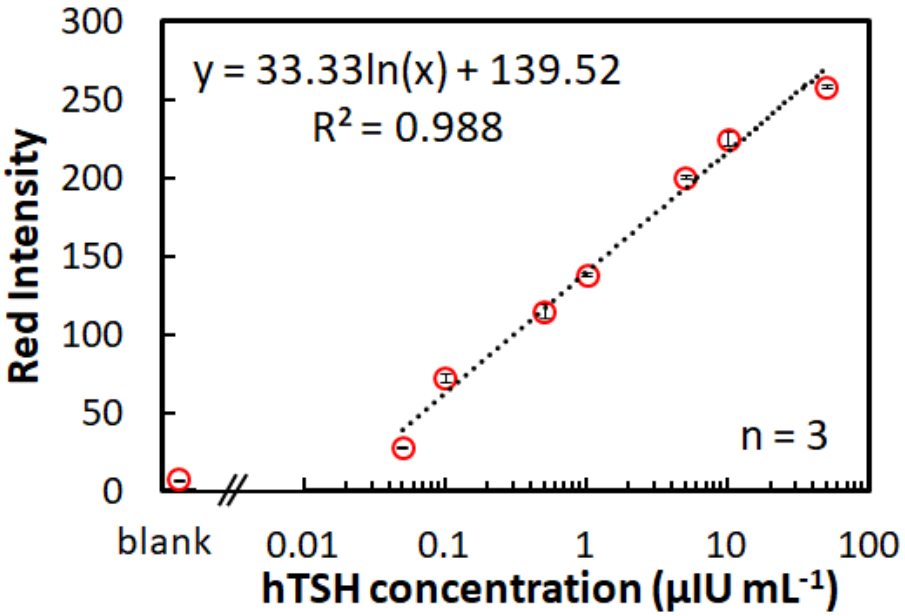

Figure 5.11 A quantitative calibration curve for hTSH in fluorometric readout based on the red intensity (RGB scale), error bars indicate the standard deviations for measurements performed in triplicate

The LFIA devices developed in this study can provide medically relevant information by simple visual inspection under circumstances where digital colorimetry is not available. With a visual LOD of approximately 5 μIU mL^{-1}, the colorimetric observation allows to instantaneously identify cases of hypothyroidism, whereas fluorometric observation under UV irradiation can indicate normal hTSH levels or hyperthyroidism, as schematically summarized in Figure 5.12.

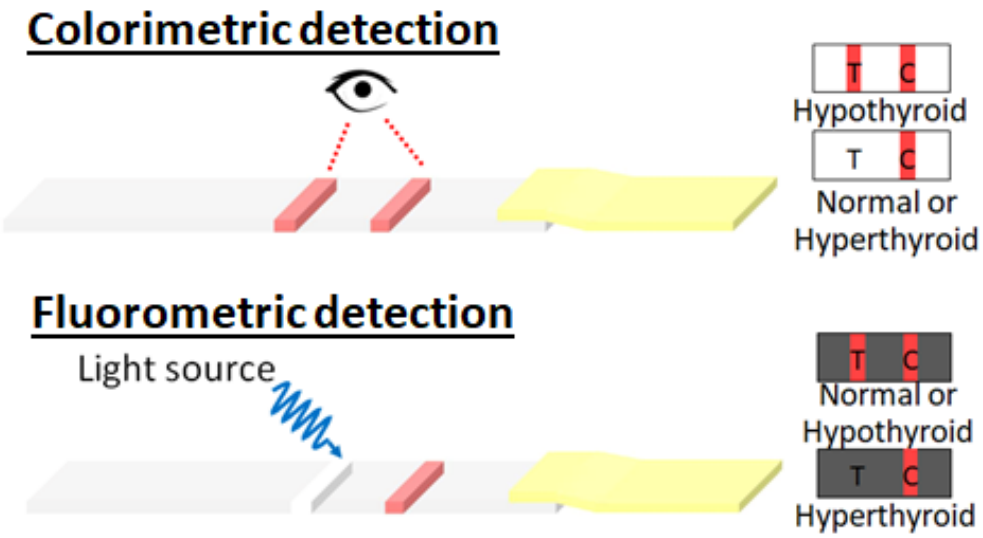

Figure 5.12 Schematic illustration of naked eye identification of hypothyroid and normal / hyperthyroid samples.

Conventional naked eye-based LFIAs for hTSH detection rely on AuNPs alone as labels. To compare their sensitivity with the AuNPs@SiO_2-Eu^{3+}-based system developed in this study, identical LFIAs based on simple AuNP labels were prepared. Commercially available AuNPs with an average size of 20 nm conjugated to anti-hTSH antibodies by physical adsorption were used as labels and hTSH detection performed under identical conditions. The visual LOD was found to be 1 μIU mL^{-1} (Figure 5.13), which is 5-times lower than the one observed for colorimetric detection with the LFIA devices developed in this work. The different sizes and the different surface chemistries of the unmodified commercially available AuNPs and the AuNPs@SiO_2-Eu^{3+} can result in a different number of antibodies conjugated to a single labeling particle [108]. In addition, steric crowding of the significantly larger AuNPs@SiO_2-Eu^{3+} compared to the smaller commercial AuNP label could also influence the capture of the complex formed between hTSH and the labeled antibody at the test line. However, the

fluorescence-based LFIA achieves 10-fold lower visual detection limits and therefore, is applicable for hyperthyroidism screening in human serum samples.

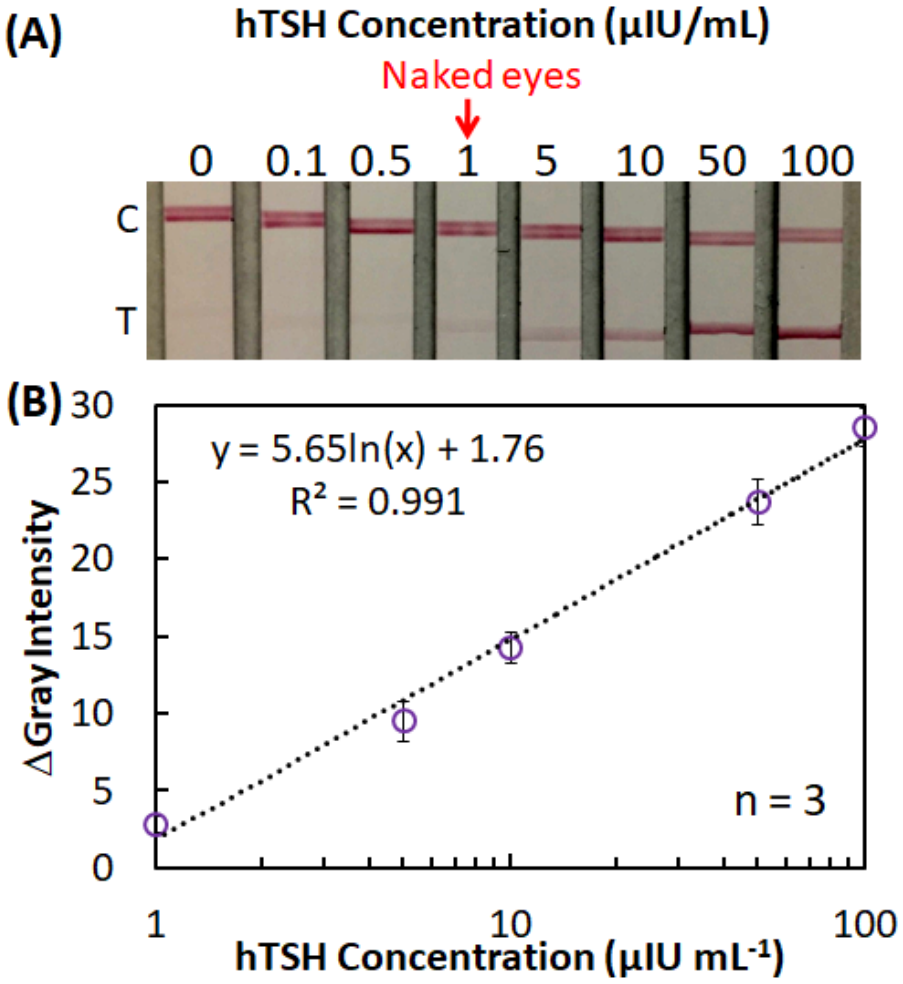

Figure 5.13 (A) Photograph of AuNPs-based LFIA applied to the detection of various concentrations of hTSH from 0-100 µIU mL^{-1}; and (B) corresponding calibration curve obtained by gray scale analysis of test lines, error bars indicate the standard deviations for measurements performed in triplicate.

The storage stability of the developed LFIA was studied over a period of two months. Prepared devices were kept at 4 °C for two months, and then used to measure the gray scale intensity of the control line after applying hTSH-free running

buffer solution (Figure 5.14). The colorimetric intensities were found to be identical to freshly prepared device, indicating reasonable storage stability of the devices.

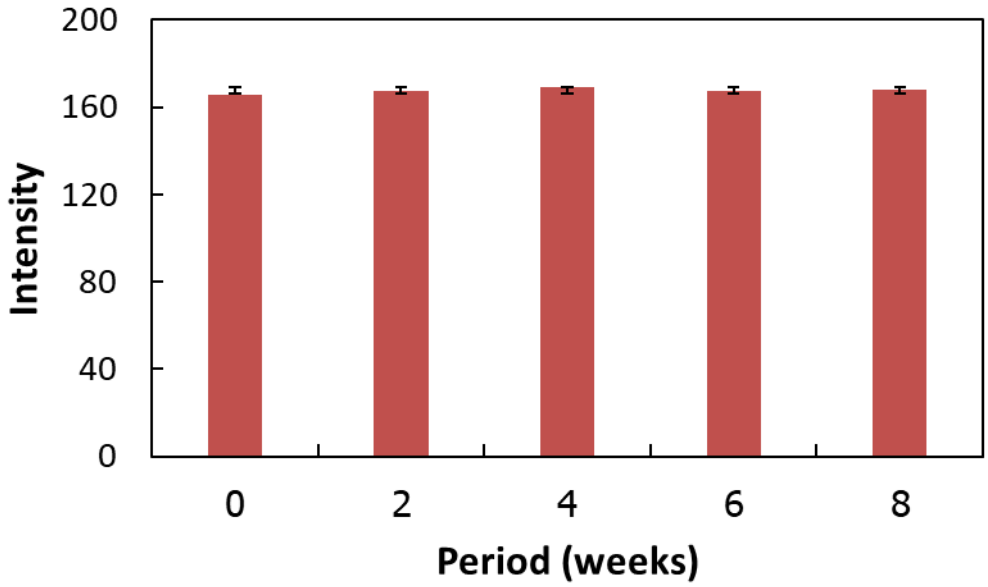

Figure 5.14 Gray scale intensity of the control line after keeping device for 0-8 weeks

5.3.4 hTSH detection in spiked human serum

In order to test the practical applicability of the developed AuNPs@SiO_2-Eu^{3+}-based LFIA devices, diluted human serum samples spiked with hTSH at final concentrations of 0.5, 5 and 10 μIU mL^{-1}, as well as non-spiked human serum were subjected to LFIAs. Diluted serum was required to reduce the viscosity and to guarantee the reproducible flow of sample liquid. The results are shown in Figure 5.15 and Table 5.1. The recovery values obtained from triplicate analysis of hTSH spiked samples were found to be in the range from 110% to 116%. For non-spiked human serum, no clear test line was observable by visual inspection for colorimetric (Figure 5.15A) and fluorometric detection (Figure 5.15B). However, digital colorimetry applied to the fluorescence detection gave a red intensity value clearly distinguishable from

the background, resulting in a hTSH concentration of 0.05 ± 0.01 μIU mL^{-1}, corresponding to 0.5 μIU mL^{-1} of the undiluted serum. These results indicate that the developed device could be used as an alternative method for screening and determining hTSH levels in biological fluids.

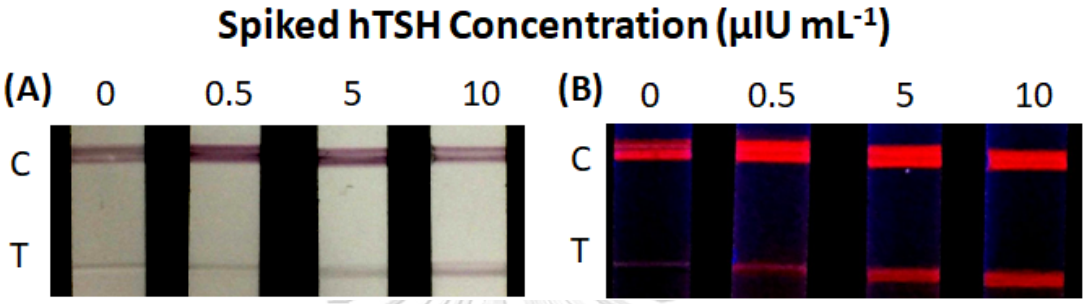

Figure 5.15 Photographs of AuNPs@SiO_2-Eu^{3+}-based LFIA devices applied to hTSH spiked human serum samples at concentrations of 0, 0.5, 5 and 10 μIU mL^{-1} observed under (A) ambient light or (B) 365 nm UV light irradiation.

Table 5.1 Recoveries of the spiked hTSH in human serum using AuNPs@SiO_2-Eu^{3+}-based LFIA devices with fluorometric detection (n = 3).

Spiked hTSH concentration (μIU mL^{-1})	Measured concentration* (μIU mL^{-1})	Recovery (%)
0	0.05 ± 0.01	---
0.5	0.50 ± 0.01	100.0 ± 2.4
5.0	5.53 ± 0.19	110.6 ± 3.8
10.0	11.62 ± 0.36	116.2 ± 3.6

*Values corrected for blank hTSH concentration

5.4 Conclusion

In this work, a hybrid nanocomposite composed of a AuNP core and a europium (III) chelate fluorophore-doped silica shell (AuNPs@SiO_2-Eu^{3+}) for application as labeling reagent for hTSH detection with LFIAs has been developed. The nanocomposites can be used to simultaneously obtain colorimetric and fluorescent signals for screening hypothyroidism and hyperthyroidism. A low-cost and simple fabrication method of control and test lines on nitrocellulose membranes for LFIA devices has been achieved by a ballpoint pen mounted in a craft cutting devices, providing good color intensity reproducibility. The LODs for hTSH measurements based on visual inspection were found to be 5 μIU mL^{-1} for colorimetric assays and 0.1 μIU mL^{-1} for fluorescent assays with an analysis time within 30 min. The quantitative analysis of the fluorescence signal results in a logarithmically linear response range between 0.05-50 μIU mL^{-1} with a squared regression coefficient of 0.988. Furthermore, the application of the developed devices to the determination of hTSH in spiked human serum showed good accuracy and precision of the method. Therefore, the AuNPs@SiO_2-Eu^{3+}-based LFIA devices with dual signaling could provide an alternative method for the early screening of both hypothyroidism and hyperthyroidism.

CHAPTER VI

CONCLUSIONS AND FUTURE PERSPECTIVES

6.1 Conclusions

The conclusions were divided into three parts as follow:

Part I: Novel ractopamine-protein carrier conjugation and its application on paper-based lateral flow strip test for ractopamine detection in animal feed

The conjugation of RAC-BSA has been successfully prepared via the Mannich reaction which is simple, rapid and one-step method. The mole coupling ratio of the obtained RAC-BSA was 9:1. For the use of the RAC-BSA, the paper-based lateral flow strip test was fabricated using the obtained RAC-BSA for immobilizing on the test line. The strip test was applied to detect RAC in animal feed within 5 min with the LOD of 1 ng g^{-1} under the naked eye, the calculated LOD of 0.1 ng g^{-1} from the semi-quantitative calibration curve and the linear range of 0.075-0.750 ng g^{-1} with a good correlation. The developed strip test was highly specific to RAC detection without cross-reactivity from the related compounds. The recovery percentages were also observed to be less than 103.7 with less RSD. Therefore, the obtained RAC-BSA is effective to be applied for the preparation of the strip test, and the proposed strip test could be agreement as an alternative device for RAC detection with portable, instrument-free, low-cost, rapid and easy to use.

Part II: Development of an automated wax-printed paper-based lateral flow device for alpha-fetoprotein enzyme-linked immunosorbent assay

The development of an automated and one-step ELISA has been proposed using a novel wax-printed paper-based lateral flow device. A wax-printed pad as an analytical device was easily and user-friendly fabricated using a wax-printing method consisting of a non-delayed channel, a wax-delayed channel, a test zone and a control zone. The four barriers on the wax-delayed enabled to delay the flow time compared to the non-delayed channel. Under optimal conditions, the proposed device could be determined AFP within 10 min with a linear range of 1-100 ng mL^{-1} and a good correlation. Furthermore, the LOD of 1 ng mL^{-1} covered the normal levels of AFP in human body (less than 25 ng mL^{-1}). The device was also applied to detect AFP in human serum successfully with the recovery less than 106.0% and RSD less than 4.2%. Therefore, the device is suitable for screening AFP level with short time analysis, on-site and equipment-free measurements, portability and ease of use.

Part III: Gold nanoparticle core - europium (III) chelate fluorophore-doped silica shell hybrid nanocomposite for lateral flow immunoassay of human thyroid stimulating hormone with dual signal readout

A hybrid nanocomposite of gold nanoparticles as core and fluorophores of europium (III) doped silica as shell (AuNPs@SiO_2-Eu^{3+}) has been developed as a novel and alternative label for paper-based LFIA of hTSH. The test and control lines on the paper-based LFIA device for hTSH detection could be easily fabricated using a low-cost ballpoint pen mounted in the printer cutter machine. The developed nanocomposites exhibited a great potential for screening both thyroid diseases included hypothyroidism through colorimetric signal (LOD: 5 μIU mL^{-1}) and hyperthyroidism through fluorescence signal (LOD: 0.1 μIU mL^{-1}). The quantitative analysis of fluorescence signal provides linear range between 0.05-50 μIU mL^{-1} with a

good correlation. The developed devices were effectively applied for the hTSH detection in the spiked human serum with recovery less than 116%. Therefore, the AuNPs@SiO_2-Eu^{3+} paper-based LFIA with dual signal demonstrates an alternative and interesting device for early screening both hypothyroidism and hyperthyroidism.

6.2 Future perspectives

The immunoassay on the paper-based microfluidic devices is a potential device for agriculture and food safety, medical diagnosis and environmental monitoring due to its high sensitivity and selectivity, portability, rapid and instrument-free measurements and the use of less amount of solution. Therefore, the immunoassay on the paper-based microfluidic devices developed in this dissertation has been tendency as an analytical device in many applications. For example, the conjugation method via the Mannich reaction could be used to conjugate the other compounds containing active hydrogen with carrier protein which the conjugation molecule could be possibly applied in the immunoassay on the paper-based microfluidic devices or various immunoassay techniques. Furthermore, the developed wax-printed devices for the automated and one-step ELISA will be applied in other biomarkers detection, and the new pattern could be appropriately designed on the device for a new approach in the detection enhancement. Finally, the hybrid nanocomposite of AuNPs@SiO_2-Eu^{3+} will be used to prepare the immunoassay on the paper-based microfluidic devices for the detection of other biological molecules.

REFERENCES

[1] Du, W., Zhao, G., Fu, Q., Sun, M., Zhou, H. and Chang, C. Combined microextraction by packed sorbent and high-performance liquid chromatography-ultraviolet detection for rapid analysis of ractopamine in porcine muscle and urine samples. Food Chemistry 145 (2014): 789-95.

[2] He, L., Su, Y., Zeng, Z., Liu, Y. and Huang, X. Determination of ractopamine and clenbuterol in feeds by gas chromatography–mass spectrometry. Animal Feed Science and Technology 132(3–4) (2007): 316-323.

[3] Shelver, W.L. and Smith, D.J. Development of an immunoassay for the beta-adrenergic agonist ractopamine. Journal of Immunoassay 21(1) (2000): 1-23.

[4] Wu, Y., Xu, F., Jiang, H., Tao, X., Zhu, K., Liu, W., Cui, Y., Huang, X. and Ding, S. Determination of Salbutamol, Clenbuterol, and Brombuterol in Urine by a Highly Sensitive Chemiluminescence Enzyme Immunoassay. Analytical Letters 47(16) (2014): 2761-2773.

[5] Zhou, Y., Li, Y.S., Pan, F.G., Liu, Z.S. and Wang, Z. The development and optimization of ELISA for the determination of tetrodotoxin. Journal of Medical Colleges of PLA 22(6) (2007): 347-351.

[6] Cheng, C.M., Martinez, A.W., Gong, J., Mace, C.R., Phillips, S.T., Carrilho, E., Mirica, K.A. and Whitesides, G.M. Paper-Based ELISA. Angewandte Chemie International Edition 49(28) (2010): 4771-4774.

[7] Martinez, A.W., Phillips, S.T., Butte, M.J. and Whitesides, G.M. Patterned paper as a platform for inexpensive, low-volume, portable bioassays. Angewandte Chemie International Edition 46(8) (2007): 1318-20.

[8] Abe, K., Suzuki, K. and Citterio, D. Inkjet-printed microfluidic multianalyte chemical sensing paper. Analytical Chemistry 80(18) (2008): 6928-34.

[9] Carrilho, E., Martinez, A.W. and Whitesides, G.M. Understanding wax printing: a simple micropatterning process for paper-based microfluidics. Analytical Chemistry 81(16) (2009): 7091-5.

[10] Dungchai, W., Chailapakul, O. and Henry, C.S. A low-cost, simple, and rapid fabrication method for paper-based microfluidics using wax screen-printing. Analyst 136(1) (2011): 77-82.

[11] Rojanathanes, R., Sereemaspun, A., Pimpha, N., Buasorn, V., Ekawong, P. and Wiwanitkit, V. Gold nanoparticle as an alternative tool for a urine pregnancy test. Taiwanese Journal of Obstetrics and Gynecology 47(3) (2008): 296-299.

[12] Apilux, A., Ukita, Y., Chikae, M., Chailapakul, O. and Takamura, Y. Development of automated paper-based devices for sequential multistep sandwich enzyme-linked immunosorbent assays using inkjet printing. Lab on a Chip 13(1) (2013): 126-135.

[13] Shih, C.M., Chang, C.L., Hsu, M.Y., Lin, J.Y., Kuan, C.M., Wang, H.K., Huang, C.T., Chung, M.C., Huang, K.C., Hsu, C.E., Wang, C.Y., Shen, Y.C. and Cheng, C.M. Paper-based ELISA to rapidly detect *Escherichia coli*. Talanta 145 (2015): 2-5.

[14] Zhu, L., He, J., Cao, X., Huang, K., Luo, Y. and Xu, W. Development of a double-antibody sandwich ELISA for rapid detection of Bacillus Cereus in food. Scientific Reports 6 (2016): 16092.

[15] Yang, Q., Gong, X., Song, T., Yang, J., Zhu, S., Li, Y., Cui, Y., Li, Y., Zhang, B. and Chang, J. Quantum dot-based immunochromatography test strip for rapid, quantitative and sensitive detection of alpha fetoprotein. Biosensors and Bioelectronics 30(1) (2011): 145-150.

[16] Liang, R.L., Xu, X.P., Liu, T.C., Zhou, J.W., Wang, X.G., Ren, Z.Q., Hao, F. and Wu, Y.S. Rapid and sensitive lateral flow immunoassay method for determining alpha fetoprotein in serum using europium (III) chelate microparticles-based lateral flow test strips. Analytica Chimica Acta 891 (2015): 277-83.

[17] Zhang, F., Zou, M., Chen, Y., Li, J., Wang, Y., Qi, X. and Xue, Q. Lanthanide-labeled immunochromatographic strips for the rapid detection of *Pantoea stewartii* subsp. stewartii. Biosensors and Bioelectronics 51 (2014): 29-35.

[18] Martinez, A.W., Phillips, S.T., Carrilho, E., Thomas, S.W., Sindi, H. and Whitesides, G.M. Simple Telemedicine for Developing Regions: Camera Phones and Paper-Based Microfluidic Devices for Real-Time, Off-Site Diagnosis. Analytical Chemistry 80(10) (2008): 3699-3707.

[19] Lentz, A.K. and Feezor, R.J. Principles of immunology. Nutrition in Clinical Practice 18(6) (2003): 451-460.

[20] Brown, I.R.F. Analytical biochemistry: By David J Holme and Hazel Peck. Biochemical Education 12(4) (1984): 189-189.

[21] Luttmann, W., Bratke, K., Kupper, M. and Myrtek, D. Immunology, United states of America: Academic Press Publications, 2006.

[22] Verheijen, R. Immunological strip tests, pp. 134-166. Birkhäuser Basel: Basel, 2002.

[23] Paek, S.H., Lee, S.H., Cho, J.H. and Kim, Y.S. Development of rapid one-step immunochromatographic assay. Methods 22(1) (2000): 53-60.

[24] Li, X.M., Yang, X.Y. and Zhang, S.S. Electrochemical enzyme immunoassay using model labels. TrAC Trends in Analytical Chemistry 27(6) (2008): 543-553.

[25] Wang, Z. and Ma, L. Gold nanoparticle probes. Coordination Chemistry Reviews 253(11) (2009): 1607-1618.

[26] Ma, L.N., Liu, D.J. and Wang, Z.X. Synthesis and applications of gold nanoparticle probes. Chinese Journal of Analytical Chemistry 38(1) (2010): 1-7.

[27] Ozinskas, A.J. Principles of fluorescence immunoassay, pp. 449-496. Springer US: Boston, MA, 1994.

[28] Nishi, K., Isobe, S.-I., Zhu, Y. and Kiyama, R. Fluorescence-based bioassays for the detection and evaluation of food materials. Sensors 15(10) (2015): 25831.

[29] Shishani, E., Chai, S.C., Jamokha, S., Aznar, G. and Hoffman, M.K. Determination of ractopamine in animal tissues by liquid chromatography-fluorescence and liquid chromatography/tandem mass spectrometry. Analytica Chimica Acta 483(1–2) (2003): 137-145.

[30] Zhang, M.Z., Wang, M.Z., Chen, Z.L., Fang, J.H., Fang, M.M., Liu, J. and Yu, X.P. Development of a colloidal gold-based lateral-flow immunoassay for the rapid simultaneous detection of clenbuterol and ractopamine in swine urine. Analytical and Bioanalytical Chemistry 395(8) (2009): 2591.

[31] Wang, W., Zhang, Y., Wang, J., Shi, X. and Ye, J. Determination of β-agonists in pig feed, pig urine and pig liver using capillary electrophoresis with electrochemical detection. Meat Science 85(2) (2010): 302-305.

[32] Gao, H., Han, J., Yang, S., Wang, Z., Wang, L. and Fu, Z. Highly sensitive multianalyte immunochromatographic test strip for rapid chemiluminescent detection of ractopamine and salbutamol. Analytica Chimica Acta 839 (2014): 91-96.

[33] Shen, L. and He, P. An electrochemical immunosensor based on agarose hydrogel films for rapid determination of ractopamine. Electrochemistry Communications 9(4) (2007): 657-662.

[34] Li, C., Li, J., Jiang, W., Zhang, S., Shen, J., Wen, K. and Wang, Z. Development and application of a gel-based immunoassay for the rapid screening of salbutamol and ractopamine residues in pork. Journal of Agricultural and Food Chemistry 63(48) (2015): 10556-10561.

[35] Liang, X., Zhang, K., Zhang, J., Li, F., Zhao, Q., Tang, C. and Meng, Q. Ractopamine residues in beef cattle hair during and after treatment. Journal of Analytical Toxicology 40(2) (2016): 153-8.

[36] Liu, X., He, X., Moore, C., Wang, G. and Coulter, C. Highly sensitive and specific liquid chromatography- tandem mass spectrometry method for testing

ractopamine in cow and sheep urine. Journal of Analytical Toxicology 33(6) (2009): 289-93.

[37] Patience, J.F., Shand, P., Pietrasik, Z., Merrill, J., Vessie, G., Ross, K.A. and Beaulieu, A.D. The effect of ractopamine supplementation at 5 ppm of swine finishing diets on growth performance, carcass composition and ultimate pork quality. Canadian Journal of Animal Science 89(1) (2009): 53-66.

[38] Du, W., Zhao, G., Fu, Q., Sun, M., Zhou, H. and Chang, C. Combined microextraction by packed sorbent and high-performance liquid chromatography–ultraviolet detection for rapid analysis of ractopamine in porcine muscle and urine samples. Food Chemistry 145 (2014): 789-795.

[39] Shelver, W.L. and Smith, D.J. Application of a monoclonal antibody-based enzyme-linked immunosorbent assay for the determination of ractopamine in incurred samples from food animals. Journal of Agricultural and Food Chemistry 50(10) (2002): 2742-2747.

[40] Smith, D.J. and Shelver, W.L. Tissue residues of ractopamine and urinary excretion of ractopamine and metabolites in animals treated for 7 days with dietary ractopamine. Journal of Animal Science 80(5) (2002): 1240-9.

[41] Niño, A., Granja, R., Wanschel, A. and Salerno, A.G. The challenges of ractopamine use in meat production for export to European Union and Russia. Food Control 72 (2017): 289-292.

[42] Han, J., Gao, H., Wang, W., Wang, Z. and Fu, Z. Time-resolved chemiluminescence strategy for multiplexed immunoassay of clenbuterol and ractopamine. Biosensors and Bioelectronics 48 (2013): 39-42.

[43] Lei, Y.C., Tai, Y.T., Hsieh, K.H., Lin, C.P., Chang, T.H., Li, W.R., Sheu, S.Y., Yao, C.H. and Kuo, T.F. A polyclonal antibody-based immunoassay for determination of growth stimulant ractopamine: Comparative study with recent advances in immunoassay methods. Taiwan Veterinary Journal 39(4) (2013): 212-224.

[44] Shelver, W.L. and Smith, D.J. Determination of ractopamine in cattle and sheep urine samples using an optical biosensor analysis: Comparative study with HPLC and ELISA. Journal of Agricultural and Food Chemistry 51(13) (2003): 3715-3721.

[45] Holme, D.J. and Peck, H. Analytical biochemistry, Malaysia: Designs and Patents Act, 1998.

[46] Berlina, A.N., Zherdev, A.V., Xu, C., Eremin, S.A. and Dzantiev, B.B. Development of lateral flow immunoassay for rapid control and quantification of the presence of the colorant Sudan I in spices and seafood. Food Control 73 (2017): 247-253.

[47] Teerinen, T., Lappalainen, T. and Erho, T. A paper-based lateral flow assay for morphine. Analytical and Bioanalytical Chemistry 406(24) (2014): 5955-65.

[48] Tang, R., Yang, H., Choi, J.R., Gong, Y., Hu, J., Feng, S., Pingguan-Murphy, B., Mei, Q. and Xu, F. Improved sensitivity of lateral flow assay using paper-based sample concentration technique. Talanta 152 (2016): 269-276.

[49] Liu, L., Kuang, H., Peng, C., Wang, L. and Xu, C. Fragment-based hapten design and screening of a highly sensitive and specific monoclonal antibody for ractopamine. Analytical Methods 6(1) (2014): 229-234.

[50] Haasnoot, W., Stouten, P., Lommen, A., Cazemier, G., Hooijerink, D. and Schilt, R. Determination of fenoterol and ractopamine in urine by enzyme immunoassay. Analyst 119(12) (1994): 2675-80.

[51] Hu, L.M., Luo, K., Xia, J., Xu, G.M., Wu, C.H., Han, J.J., Zhang, G.G., Liu, M. and Lai, W.H. Advantages of time-resolved fluorescent nanobeads compared with fluorescent submicrospheres, quantum dots, and colloidal gold as label in lateral flow assays for detection of ractopamine. Biosensors and Bioelectronics 91 (2017): 95-103.

[52] Ren, M.L., Chen, X.L., Li, C.H., Xu, B., Liu, W.J., Xu, H.Y. and Xiong, Y.H. Lateral flow immunoassay for quantitative detection of ractopamine in swine urine. Biomedical and Environmental Sciences 27(2) (2014): 134-7.

[53] Shi, C.Y., Deng, N., Liang, J.J., Zhou, K.N., Fu, Q.Q. and Tang, Y. A fluorescent polymer dots positive readout fluorescent quenching lateral flow sensor for ractopamine rapid detection. Analytica Chimica Acta 854 (2015): 202-208.

[54] Zhang, Y., Wang, F., Fang, L., Wang, S. and Fang, G. Rapid determination of ractopamine residues in edible animal products by enzyme-linked immunosorbent assay: Development and investigation of matrix effects. Journal of Biomedicine and Biotechnology 2009 (2009): 579175.

[55] Li, X., Zhang, G., Deng, R., Yang, Y., Liu, Q., Xiao, Z., Yang, J., Xing, G., Zhao, D. and Cai, S. Development of rapid immunoassays for the detection of ractopamine in swine urine. Food Additives & Contaminants: Part A 27(8) (2010): 1096-103.

[56] Dong, J.X., Li, Z.F., Lei, H.T., Sun, Y.M., Ducancel, F., Xu, Z.L., Boulain, J.C., Yang, J.Y., Shen, Y.D. and Wang, H. Development of a single-chain variable fragment-alkaline phosphatase fusion protein and a sensitive direct competitive chemiluminescent enzyme immunoassay for detection of ractopamine in pork. Analytica Chimica Acta 736 (2012): 85-91.

[57] Buakeaw, A., Puthong, S., Kongkavitoon, P., Khongarsa, K., Komolpis, K. and Khongchareonporn, N. Production of monoclonal antibodies for ractopamine residue detection in pork. Maejo International Journal of Science and Technology 10(2) (2016): 175-186.

[58] Gu, H.Y., Liu, L.Q., Song, S.S., Kuang, H. and Xu, C.L. Development of an immunochromatographic strip assay for ractopamine detection using an ultrasensitive monoclonal antibody. Food and Agricultural Immunology 27(4) (2016): 471-483.

[59] Zhou, Y., Wu, J., Yu, W., Xu, Y., Wang, P., Xie, B. and Chen, F. Preparation for aflatoxin B(1)-cationized bovine serum albumin based on Mannich-type reaction. Journal of Immunological Methods 328(1-2) (2007): 79-88.

[60] Feng, Y., Zhou, Y., Zou, Q., Wang, J., Chen, F. and Gao, Z. Preparation and characterization of bisphenol A-cationized bovine serum albumin. Journal of Immunological Methods 340(2) (2009): 138-143.

[61] Hermanson, G.T. Chapter 19 - Preparation of hapten–carrier immunogen conjugates, pp. 743-782. Academic Press: New York, 2008.

[62] Preechakasedkit, P., Pinwattana, K., Dungchai, W., Siangproh, W., Chaicumpa, W., Tongtawe, P. and Chailapakul, O. Development of a one-step immunochromatographic strip test using gold nanoparticles for the rapid detection of *Salmonella typhi* in human serum. Biosensors and Bioelectronics 31(1) (2012): 562-566.

[63] Lin, X., Ni, Y., Li, S. and Kokot, S. A novel method for simultaneous analysis of three beta2-agonists in foods with the use of a gold-nanoparticle modified glassy carbon electrode and chemometrics. Analyst 137(9) (2012): 2086-2094.

[64] Wang, Z., Liu, M., Shi, W., Li, C., Zhang, S. and Shen, J. New haptens and antibodies for ractopamine. Food Chemistry 183 (2015): 111-114.

[65] Dai, M., Gong, Y., Liu, A., Zhang, L., Lin, J., Zhang, M. and Yu, X. Development of a colloidal gold-based lateral-flow immunoassay for the rapid detection of phenylethanolamine A in swine urine. Analytical Methods 7(10) (2015): 4130-4137.

[66] Hage, D.S., Thomas, D.H. and Beck, M.S. Theory of a sequential addition competitive binding immunoassay based on high-performance immunoaffinity chromatography. Analytical Chemistry 65(11) (1993): 1622-30.

[67] Liu, Y., Cai, M., Wu, W., Fang, Y., She, P., Xu, S., Li, J., Zhao, K., Xu, J., Bao, N. and Deng, A. Multichannel electroanalytical devices for competitive ELISA of phenylethanolamine A. Biosensors and Bioelectronics 99(15) (2018): 21-27.

[68] Yu, Y., Zhang, X., Zhao, B., Sun, Y., Zhang, X., Bai, T., Lu, J., Li, Z., Liu, L., Wang, D., Shu, Y., Zhou, J. and Qin, K. A sandwich ELISA for the detection of neuraminidase of avian influenza A(H7N9) virus. Journal of Virological Methods 247 (2017): 58-60.

[69] Liu, D., Li, X., Zhou, J., Liu, S., Tian, T., Song, Y., Zhu, Z., Zhou, L., Ji, T. and Yang, C. A fully integrated distance readout ELISA-Chip for point-of-care testing with sample-in-answer-out capability. Biosensors and Bioelectronics 96 (2017): 332-338.

[70] Felin, E., Näreaho, A. and Fredriksson-Ahomaa, M. Comparison of commercial ELISA tests for the detection of Toxoplasma antibodies in the meat juice of naturally infected pigs. Veterinary Parasitology 238 (2017): 30-34.

[71] Li, L., Peng, A.H., Lin, Z.Z., Zhong, H.P., Chen, X.M. and Huang, Z.Y. Biomimetic ELISA detection of malachite green based on molecularly imprinted polymer film. Food Chemistry 229 (2017): 403-408.

[72] Damle, R.G., Patil, A.A., Bhide, V.S., Pawar, S.D., Sapkal, G.N. and Bondre, V.P. Development of a novel rapid micro-neutralization ELISA for the detection of neutralizing antibodies against Chandipura virus. Journal of Virological Methods 240 (2017): 1-6.

[73] Lei, J., Shi, T., Sun, D., Mo, K., Yan, Y., Jin, Y., Liao, M. and Zhou, J. Development and application of nsp5-ELISA for the detection of antibody to infectious bronchitis virus. Journal of Virological Methods 243 (2017): 182-189.

[74] Liu, Y., Lin, M., Zhang, X., Hu, X., Lin, J., Hao, J., He, D., Zhang, X., Xu, C., Zhong, J., Xie, Y., Zhang, C. and Liu, X. Development of competitive ELISA for the

detection of bovine serum albumin using single-chain variable fragments. Analytical Biochemistry 525 (2017): 89-91.

[75] Sajid, M., Kawde, A.-N. and Daud, M. Designs, formats and applications of lateral flow assay: A literature review. Journal of Saudi Chemical Society 19(6) (2015): 689-705.

[76] Zou, Z.X., Wang, J., Wang, H., Li, Y.Q. and Lin, Y. An integrated electrochemical device based on immunochromatographic test strip and enzyme labels for sensitive detection of disease-related biomarkers. Talanta 94 (2012): 58-64.

[77] Shu, Q., Wang, L., Ouyang, H., Wang, W., Liu, F. and Fu, Z. Multiplexed immunochromatographic test strip for time-resolved chemiluminescent detection of pesticide residues using a bifunctional antibody. Biosensors and Bioelectronics 87 (2017): 908-914.

[78] Samsonova, J.V., Safronova, V.A. and Osipov, A.P. Pretreatment-free lateral flow enzyme immunoassay for progesterone detection in whole cows' milk. Talanta 132 (2015): 685-689.

[79] Bahadır, E.B. and Sezgintürk, M.K. Lateral flow assays: Principles, designs and labels. TrAC Trends in Analytical Chemistry 82 (2016): 286-306.

[80] Hsu, C.K., Huang, H.Y., Chen, W.R., Nishie, W., Ujiie, H., Natsuga, K., Fan, S.T., Wang, H.K., Lee, J.Y.Y., Tsai, W.L., Shimizu, H. and Cheng, C.M. Paper-based ELISA for the detection of autoimmune antibodies in body fluid—The case of bullous pemphigoid. Analytical Chemistry 86(9) (2014): 4605-4610.

[81] Wang, S., Ge, L., Song, X., Yu, J., Ge, S., Huang, J. and Zeng, F. Paper-based chemiluminescence ELISA: Lab-on-paper based on chitosan modified paper device and wax-screen-printing. Biosensors and Bioelectronics 31(1) (2012): 212-218.

[82] Khan, M.S., Pande, T. and van de Ven, T.G. Qualitative and quantitative detection of T7 bacteriophages using paper based sandwich ELISA. Colloids and Surfaces B Biointerfaces 132 (2015): 264-70.

[83] Wu, D., Zhang, J., Xu, F., Wen, X., Li, P., Zhang, X., Qiao, S., Ge, S., Xia, N., Qian, S. and Qiu, X. A paper-based microfluidic Dot-ELISA system with smartphone for the detection of influenza A. Microfluidics and Nanofluidics 21(3) (2017): 43.

[84] Kim, H.S. and Pyun, J.C. Hyper Sensitive Strip Test with Chemi-luminescence Signal Band. Procedia Chemistry 1(1) (2009): 1043-1046.

[85] Wang, X., Liu, F., Shao, Q., Yin, Z., Wang, L. and Fu, Z. A novel chemiluminescent immunochromatographic assay strip for rapid detection of mercury ions. Analytical Methods 9(16) (2017): 2401-2406.

[86] Ozalp, V.C., Zeydanl, U.S., Lunding, A., Kavruk, M., Oz, M.T., Eyidogan, F., Olsen, L.F. and Oktem, H.A. Nanoparticle embedded enzymes for improved lateral flow sensors. Analyst 138(15) (2013): 4255-4259.

[87] Joung, H.A., Oh, Y.K. and Kim, M.G. An automatic enzyme immunoassay based on a chemiluminescent lateral flow immunosensor. Biosensors and Bioelectronics 53 (2014): 330-335.

[88] Carrilho, E., Martinez, A.W. and Whitesides, G.M. Understanding wax printing: A simple micropatterning process for paper-based microfluidics. Analytical Chemistry 81(16) (2009): 7091-7095.

[89] Ge, L., Yan, J., Song, X., Yan, M., Ge, S. and Yu, J. Three-dimensional paper-based electrochemiluminescence immunodevice for multiplexed measurement of biomarkers and point-of-care testing. Biomaterials 33(4) (2012): 1024-1031.

[90] Lu, Y., Shi, W., Qin, J. and Lin, B. Fabrication and characterization of paper-based microfluidics prepared in nitrocellulose membrane by wax printing. Analytical Chemistry 82(1) (2010): 329-335.

[91] Rivas, L., Medina-Sanchez, M., de la Escosura-Muniz, A. and Merkoci, A. Improving sensitivity of gold nanoparticle-based lateral flow assays by using wax-printed pillars as delay barriers of microfluidics. Lab on a Chip 14(22) (2014): 4406-4414.

[92] Han, K.N., Choi, J.S. and Kwon, J. Three-dimensional paper-based slip device for one-step point-of-care testing. Scientific Reports 6 (2016): 25710.

[93] Wang, T., Yang, Z., Lei, C., Lei, J. and Zhou, Y. An integrated giant magnetoimpedance biosensor for detection of biomarker. Biosensors and Bioelectronics 58 (2014): 338-344.

[94] Wang, H., Li, H., Zhang, Y., Wei, Q., Ma, H., Wu, D., Li, Y., Zhang, Y. and Du, B. Label-free immunosensor based on Pd nanoplates for amperometric immunoassay of alpha-fetoprotein. Biosensors and Bioelectronics 53 (2014): 305-309.

[95] Liu, J., Lin, G., Xiao, C., Xue, Y., Yang, A., Ren, H., Lu, W., Zhao, H., Li, X. and Yuan, Z. Sensitive electrochemical immunosensor for α-fetoprotein based on graphene/SnO2/Au nanocomposite. Biosensors and Bioelectronics 71 (2015): 82-87.

[96] Siegel, R.L., Miller, K.D. and Jemal, A. Cancer statistics, 2016. CA: A Cancer Journal for Clinicians 66(1) (2016): 7-30.

[97] Parolo, C., Medina-Sanchez, M., de la Escosura-Muniz, A. and Merkoci, A. Simple paper architecture modifications lead to enhanced sensitivity in nanoparticle based lateral flow immunoassays. Lab on a Chip 13(3) (2013): 386-390.

[98] Okda, F., Lawson, S., Liu, X., Singrey, A., Clement, T., Hain, K., Nelson, J., Christopher-Hennings, J. and Nelson, E.A. Development of monoclonal antibodies and serological assays including indirect ELISA and fluorescent microsphere immunoassays for diagnosis of porcine deltacoronavirus. BMC Veterinary Research 12(1) (2016): 95.

[99] Smejkal, G.B. and Kaul, C.A. Stability of nitroblue tetrazolium-based alkaline phosphatase substrates. Journal of Histochemistry & Cytochemistry 49(9) (2001): 1189-1190.

[100] Lee, S. and Kang, S.H. Wide-range quantification of human thyroid-stimulating hormone using gold-nanopatterned single-molecule sandwich immunoassay chip. Talanta 99 (2012): 1030-1034.

[101] Von Lode, P., Hagren, V., Palenius, T. and Lovgren, T. One-step quantitative thyrotropin assay for the detection of hypothyroidism in point-of-care conditions. Clinical Biochemistry 36(2) (2003): 121-128.

[102] You, D.J., Park, T.S. and Yoon, J.Y. Cell-phone-based measurement of TSH using Mie scatter optimized lateral flow assays. Biosensors and Bioelectronics 40(1) (2013): 180-185.

[103] Jung, W., Han, J., Kai, J., Lim, J.Y., Sul, D. and Ahn, C.H. An innovative sample-to-answer polymer lab-on-a-chip with on-chip reservoirs for the POCT of thyroid stimulating hormone (TSH). Lab on a Chip 13(23) (2013): 4653-4662.

[104] Zhang, B., Tang, D.P., Liu, B.Q., Cui, Y.L., Chen, H.F. and Chen, G.N. Nanogold-functionalized magnetic beads with redox activity for sensitive electrochemical immunoassay of thyroid-stimulating hormone. Analytica Chimica Acta 711 (2012): 17-23.

[105] Liao, J.Y. and Li, H. Lateral flow immunodipstick for visual detection of aflatoxin B-1 in food using immuno-nanoparticles composed of a silver core and a gold shell. Microchimica Acta 171(3-4) (2010): 289-295.

[106] Parolo, C., de la Escosura-Muniz, A. and Merkoci, A. Enhanced lateral flow immunoassay using gold nanoparticles loaded with enzymes. Biosensors and Bioelectronics 40(1) (2013): 412-416.

[107] Darwish, I.A. Immunoassay methods and their applications in pharmaceutical analysis: basic methodology and recent advances. International Journal of Biomedical Science : IJBS 2(3) (2006): 217-235.

[108] Choi, S., Hwang, J., Lee, S., Lim, D.W., Joo, H. and Choo, J. Quantitative analysis of thyroid-stimulating hormone (TSH) using SERS-based lateral flow immunoassay. Sensors and Actuators B: Chemical 240 (2017): 358-364.

[109] Yu, Z., Xu, Y. and Ip, M.P.C. An ultra-sensitive electrochemical enzyme immunoassay for thyroid stimulating hormone in human serum. Journal of Pharmaceutical and Biomedical Analysis 12(6) (1994): 787-793.

[110] Grasso, L., Bartalena, L., Mammoli, C., Martino, E., Kessler, A.-C. and Pinchera, A. Serum TSH measurements by a sensitive enzyme immunoassay discriminate euthyroid from hyperthyroid subjects and avoid the need for TRH test during suppressive therapy with L-thyroxine. Clinical Biochemistry 20(3) (1987): 197-200.

[111] Liu, Y.T., Zhang, Q.Q., Wang, H.J., Yuan, Y.L., Chai, Y.Q. and Yuan, R. An electrochemiluminescence immunosensor for thyroid stimulating hormone based on polyamidoamine-norfloxacin functionalized Pd-Au core-shell hexoctahedrons as signal enhancers. Biosensors and Bioelectronics 71 (2015): 164-170.

[112] Zhang, M., Ge, S., Li, W., Yan, M., Song, X., Yu, J., Xu, W. and Huang, J. Ultrasensitive electrochemiluminescence immunoassay for tumor marker detection using functionalized Ru-silica@nanoporous gold composite as labels. Analyst 137(3) (2012): 680-685.

[113] Li, Q., Lou, F. and Tang, D. Biofunctional nanogold microsphere doped with Prussian blue nanoparticles for sensitive electrochemical immunoassay of cancer marker. Analytical Methods 6(10) (2014): 3442-3448.

[114] Wang, X., Chen, L., Su, X. and Ai, S. Electrochemical immunosensor with graphene quantum dots and apoferritin-encapsulated Cu nanoparticles double-assisted signal amplification for detection of avian leukosis virus subgroup J. Biosensors and Bioelectronics 47 (2013): 171-177.

[115] Petrou, P.S., Georgiou, S., Christofidis, I. and Kakabakos, S.E. Increased sensitivity of heterogeneous fluoroimmunoassays employing fluorescein-labeled antibodies by simple treatment of the wells with glycerin solution. Journal of Immunological Methods 266(1–2) (2002): 175-179.

[116] Zhou, Y.L., Xia, X.H., Xu, Y., Ke, W., Yang, W. and Li, Q.G. Application of europium(III) chelates-bonded silica nanoparticle in time-resolved immunofluorometric detection assay for human thyroid stimulating hormone. Analytica Chimica Acta 722 (2012): 95-99.

[117] Ding, Y., Liu, J., Jin, X., Lu, H., Shen, G. and Yu, R. Poly-l-lysine/hydroxyapatite/carbon nanotube hybrid nanocomposite applied for piezoelectric immunoassay of carbohydrateantigen 19-9. Analyst 133(2) (2008): 184-190.

[118] Pang, Y., Rong, Z., Xiao, R. and Wang, S. "Turn on" and label-free core–shell Ag@SiO_2 nanoparticles-based metal-enhanced fluorescent (MEF) aptasensor for Hg^{2+}. Scientific Reports 5 (2015): 9451.

[119] Mayer, K.M. and Hafner, J.H. Localized surface plasmon resonance sensors. Chemical Reviews 111(6) (2011): 3828-3857.

[120] Xu, Y. and Li, Q. Multiple fluorescent labeling of silica nanoparticles with lanthanide chelates for highly sensitive time-resolved immunofluorometric assays. Clinical Chemistry 53(8) (2007): 1503-1510.

[121] Hagan, A.K. and Zuchner, T. Lanthanide-based time-resolved luminescence immunoassays. Analytical and Bioanalytical Chemistry 400(9) (2011): 2847-2864.

[122] Gao, J., Huang, X., Liu, H., Zan, F. and Ren, J. Colloidal stability of gold nanoparticles modified with thiol compounds: Bioconjugation and application in cancer cell imaging. Langmuir 28(9) (2012): 4464-4471.

[123] Wu, F.B. and Zhang, C. A new europium beta-diketone chelate for ultrasensitive time-resolved fluorescence immunoassays. Analytical Biochemistry 311(1) (2002): 57-67.

[124] Bagwe, R.P., Hilliard, L.R. and Tan, W. Surface modification of silica nanoparticles to reduce aggregation and non-specific binding. Langmuir : the ACS journal of surfaces and colloids 22(9) (2006): 4357-4362.

[125] Cheng, H., Wang, C., Xu, Z., Lin, H. and Zhang, C. Gold nanoparticle-enhanced near infrared fluorescent nanocomposites for targeted bio-imaging. RSC Advances 5(1) (2015): 20-26.

[126] Che, E., Wan, L., Zhang, Y., Zhao, Q., Han, X., Li, J., Liu, J. and Wang, S. Development of phosphonate-terminated magnetic mesoporous silica nanoparticles for pH-controlled release of doxorubicin and improved tumor accumulation. Asian Journal of Pharmaceutical Sciences 9(6) (2014): 317-323.

[127] Khreich, N., Lamourette, P., Boutal, H., Devilliers, K., Créminon, C. and Volland, H. Detection of *Staphylococcus enterotoxin* B using fluorescent immunoliposomes as label for immunochromatographic testing. Analytical Biochemistry 377(2) (2008): 182-188.

[128] Yao, Y., Guo, W., Zhang, J., Wu, Y., Fu, W., Liu, T., Wu, X., Wang, H., Gong, X., Liang, X. and Chang, J. Reverse fluorescence enhancement and colorimetric bimodal signal readout immunochromatography test strip for ultrasensitive large-scale screening and postoperative monitoring. ACS Applied Materials & Interfaces 8(35) (2016): 22963-22970.

APPENDIX

VITA

Miss Pattarachaya Preechakasedkit was born on April 26th, 1985 in Suphanburi, Thailand. She graduated with high school degree from Triamudom Suksa School, Major of Science-Mathematic in 2002. She received her Bachelor Degree of Science in Biotechnology from Thammasat University in 2006 and her Master Degree of Science in Biotechnology from Chulalongkorn University in 2010. She also received Certificate II in Spoken and Written English 91422NSW from Tasmanian Polytechnic, Australia in 2011. Then, she became a Ph.D. student of Program in Biotechnology as a member of Electrochemistry and Optical Spectroscopy Center of Excellence under the director of Professor Dr. Orawon Chailapakul. She received grants from the Thailand Research Fund (TRF) through the International Research Network (PHD58W0001) and the 90th Anniversary of Chulalongkorn University Fund (Ratchadaphiseksomphot Endowment Fund). She had an opportunity to do research in Biological Interface Lab, Sogang University, South Korea, under Professor Dr. Kwanwoo Shin for 4 months, and in Citterio Lab, Keio University, Japan, under Professor Dr. Daniel Citterio for 9 months. After she came back, she continuously did her researches and graduated with a Ph.D. Degree in Biotechnology of academic year 2017 from Chulalongkorn University.